

**SOLID-STATE MODIFICATION OF TAPIOCA STARCH  
USING NON-THERMAL PLASMA**



**Mr. Natchanon Srangsomjit**

จุฬาลงกรณ์มหาวิทยาลัย  
**CHULALONGKORN UNIVERSITY**

A Thesis Submitted in Partial Fulfillment of the Requirements  
for the Degree of Master of Science in Food Technology  
Department of Food Technology  
FACULTY OF SCIENCE  
Chulalongkorn University  
Academic Year 2021  
Copyright of Chulalongkorn University

การตัดแปรรสตา์ไขมันสำปะหลังในสถานะของแข็งด้วยพลาสติกที่ไม่ใช้ความร้อน



วิทยานิพนธ์นี้เป็นส่วนหนึ่งของการศึกษาตามหลักสูตรปริญญาวิทยาศาสตรมหาบัณฑิต

สาขาวิชาเทคโนโลยีทางอาหาร ภาควิชาเทคโนโลยีทางอาหาร

คณะวิทยาศาสตร์ จุฬาลงกรณ์มหาวิทยาลัย

ปีการศึกษา 2564

ลิขสิทธิ์ของจุฬาลงกรณ์มหาวิทยาลัย

Thesis Title	SOLID-STATE MODIFICATION OF TAPIOCA STARCH USING NON-THERMAL PLASMA
By	Mr. Natchanon Srangsomjit
Field of Study	Food Technology
Thesis Advisor	Associate Professor Jirarat Anuntagool, Ph.D.
Thesis Co Advisor	Associate Professor Thiti Bovornratanaraks, Ph.D.

---

Accepted by the FACULTY OF SCIENCE, Chulalongkorn  
University in Partial Fulfillment of the Requirement for the Master of  
Science

..... Dean of the FACULTY OF  
SCIENCE  
(Professor POLKIT SANGVANICH, Ph.D.)

#### THESIS COMMITTEE

..... Chairman  
(Assistant Professor DARIS KUAKPETOON,  
Ph.D.)

..... Thesis Advisor  
(Associate Professor Jirarat Anuntagool, Ph.D.)

..... Thesis Co-Advisor  
(Associate Professor Thiti Bovornratanaraks,  
Ph.D.)

..... Examiner  
(Associate Professor KANITHA  
TANANUWONG, Ph.D.)

..... External Examiner  
(Professor Vanna Tulyathan, Ph.D.)

ณัฐชนน สร้างสมจิตร : การตัดแปรสสารไขมันสำปะหลังในสถานะของแข็งด้วยพลาสมาที่ไม่ใช้ความร้อน. ( SOLID-STATE MODIFICATION OF TAPIOCA STARCH USING NON-THERMAL PLASMA) อ.ที่ปรึกษาหลัก : รศ. ดร.จิรรัตน์ อนันตกุล, อ.ที่ปรึกษาร่วม : รศ. ดร.ฉิติ บวรรัตนารักษ์

งานวิจัยนี้มีวัตถุประสงค์เพื่อศึกษาสมบัติทางกายภาพ เคมี และสมบัติเชิงหน้าที่ของการตัดแปรสสารไขมัน สำปะหลังในสถานะของแข็งด้วยพลาสมาแบบดิสซาร์จชนิดข้ามฉนวนโดยแปรชนิดของแก๊ส (ฮีเลียม และ อาร์กอน) แรงดันไฟฟ้า (10 และ 15 กิโลโวลต์) และเวลาตัดแปร (5, 10 และ 15 นาที) ภายหลังจากการตัดแปรพบว่าตัวอย่างมีค่า  $L^*$  เพิ่มขึ้น ขณะที่ค่า pH ลดลง ภาพจากเครื่องอิเล็กตรอนแบบส่องกราด (SEM) พบว่า พื้นผิวเม็ดสสารไขมันถูกทำลายแต่ยังพบ birefringence ที่ชัดเจน จากการวิเคราะห์โครงสร้างผลึกด้วยเทคนิคการเลี้ยวเบนของรังสีเอกซ์ (XRD) พบว่า ทุกตัวอย่างมีโครงสร้างผลึกเป็นแบบ C แต่พบการลดลงของปริมาณความเป็นผลึกภายหลังจากการตัดแปรด้วยพลาสมา สสารไขมันสำปะหลังมีคาร์โบไฮเดรต เส้นใยหยาบ ไขมัน เถ้า และโปรตีนเท่ากับร้อยละ 99.06, 0.18, 0.14 และ 0.46 โดยน้ำหนักแห้ง ตามลำดับ เมื่อตัดแปรตัวอย่างโดยใช้แก๊สอาร์กอนพบว่าปริมาณความชื้นไม่แตกต่างกันอย่างมีนัยสำคัญ ( $P \geq 0.05$ ) อย่างไรก็ตาม ตัวอย่างที่ตัดแปรโดยใช้แก๊สฮีเลียมส่งผลให้ปริมาณความชื้นลดลงอย่างมีนัยสำคัญ ( $P < 0.05$ ) ในการตัดแปรสสารไขมันด้วยพลาสมาส่งผลให้ปริมาณแอมิโลสและน้ำตาลรีดิวซ์สูงขึ้นเมื่อเพิ่มระดับแรงดันไฟฟ้า และเวลาตัดแปร อย่างไรก็ตามเมื่อเพิ่มเวลาตัดแปรตัวอย่างด้วยแก๊สฮีเลียมจาก 5 เป็น 15 นาที ที่ 15 กิโลโวลต์ พบว่าปริมาณแอมิโลสมีค่าลดลง จากการวิเคราะห์หมู่ฟังก์ชันด้วยเทคนิค Fourier transform infrared (FTIR) พบว่า การตัดแปรสสารไขมันด้วยพลาสมาไม่ทำให้เกิดการเปลี่ยนแปลงหมู่ฟังก์ชัน และไม่มีการเปลี่ยนแปลงอัตราส่วนเลขคลื่นที่ 1047 และ 1022  $\text{cm}^{-1}$  ( $P \geq 0.05$ ) ยกเว้นตัวอย่างที่ตัดแปรด้วยแก๊สอาร์กอนที่ 10 กิโลโวลต์ เวลาตัดแปร 5 นาที ( $P < 0.05$ ) ขนาดโมเลกุลเฉลี่ยโดยน้ำหนักของแอมิโลเพกตินที่ผ่านการตัดแปรด้วยพลาสมามีขนาดเล็กกว่าตัวอย่างที่ไม่ผ่านการตัดแปร นอกจากนี้ยังพบว่า ค่า peak viscosity, breakdown และ setback ลดลงภายหลังจากการตัดแปร ( $P < 0.05$ ) ขณะที่ค่า pasting temperature ของตัวอย่างตัดแปรไม่เปลี่ยนแปลงอย่างมีนัยสำคัญ ( $P \geq 0.05$ ) การตัดแปรตัวอย่างเป็นระยะเวลา 5 นาที ด้วยแก๊สอาร์กอนทำให้ค่าร้อยละ breakdown และ setback ลดลงอย่างมีนัยสำคัญ ( $P < 0.05$ ) ค่าการละลายและค่าความสามารถในการจับน้ำของตัวอย่างตัวอย่างที่ตัดแปรมีค่าเพิ่มขึ้น หลังจากเพิ่มระดับแรงดันไฟฟ้าและเวลาตัดแปร ขณะที่ค่าการพองตัวของตัวอย่างตัดแปรลดลง การทดสอบสมบัติวิทยากระแสแบบ frequency sweep พบว่า ตัวอย่างเพสต์สสารไขมัน (ร้อยละ 6) มีค่า  $G'$  สูงกว่า  $G''$  แสดงถึงความเป็นลักษณะของความ เป็นแข็งมากกว่าของเหลว การตัดแปรตัวอย่างที่เวลา 5 นาทีด้วยแก๊สอาร์กอนและฮีเลียมทำให้มีค่า  $G'$  สูงขึ้น ในทางกลับกัน หากเพิ่มเวลาตัดแปรและแรงดันไฟฟ้าส่งผลให้ค่า  $G'$  ลดลง ด้านสมบัติทางการไหลของตัวอย่างเพสต์สสารไขมันที่ผ่านการ เจลลาคีไนซ์ (ร้อยละ 6) พบว่าความเป็น thixotropy และ ค่า consistency index (K) ลดลง เมื่อเพิ่มระดับ แรงดันไฟฟ้า และเวลาตัดแปร ผลการทดลองยืนยันถึงประสิทธิภาพของการตัดแปรสมบัติสสารไขมันสำปะหลังด้วยพลาสมา แบบดิสซาร์จชนิดข้ามฉนวน

สาขาวิชา เทคโนโลยีทางอาหาร  
ปีการศึกษา 2564

ลายมือชื่อ นิสิต .....  
ลายมือชื่อ อ.ที่ปรึกษาหลัก .....  
ลายมือชื่อ อ.ที่ปรึกษาร่วม .....

# # 6270038323 : MAJOR FOOD TECHNOLOGY

KEYWORD: starch modification, solid-state modification, nonthermal plasma, tapioca starch  
 Natchanon Srangsomjit : SOLID-STATE MODIFICATION OF TAPIOCA STARCH  
 USING NON-THERMAL PLASMA. Advisor: Assoc. Prof. Jirarat Anuntagool, Ph.D.  
 Co-advisor: Assoc. Prof. Thiti Bovornratanaraks, Ph.D.

The objective of this research was to investigate the physical, chemical, and functional properties of tapioca starch subjected to solid-state modification by using nonthermal dielectric barrier discharge (DBD) plasma treatment using different gases (helium and argon), voltage levels (10 kV and 15 kV), and treatment times (5, 10, and 15 minutes). After treatment, an increase in  $L^*$  value and a marginal decrease in pH value of all treated samples were noted. Scanning electron micrographs showed dented starch granules after the plasma treatment but showed birefringence. From XRD measurement, all samples showed a characteristic C-type diffraction pattern but a reduction in the relative crystallinity after plasma treatment. Native tapioca starch contained 99.06% carbohydrate, 0.15% crude fiber, 0.18% fat, 0.14% ash, and 0.46% protein on a dry weight basis. There was no significant difference in the moisture content of argon plasma-treated samples ( $P \geq 0.05$ ), but a reduction in moisture content was found after using helium plasma treatment ( $P < 0.05$ ). The modified starch samples tended to have higher amylose content and reducing sugars with increasing voltage levels and times. However, increasing the treatment time from 5 to 15 minutes at 15 kV for helium plasma caused the amylose content to reduce ( $P < 0.05$ ). Fourier Transform Infrared (FTIR) spectra did not show the new formation of functional groups after treatments. No significant change in the intensity ratio of  $1047/1022 \text{ cm}^{-1}$  compared to native samples ( $P \geq 0.05$ ) except for the treatment at 10 kV for 5 min of argon plasma ( $P < 0.05$ ). After treatment, the weight-average molecular weight of amylopectin was smaller than that of native starch. A significant reduction in peak viscosity, breakdown, and setback was observed ( $P < 0.05$ ). However, no significant change in the pasting temperature of treated samples was found compared to the native sample. The samples with lower breakdown and setback percentages were found for 5 minutes treatment using argon plasma ( $P < 0.05$ ). After increasing voltage levels and times of modification, an increase in solubility and water binding capacity was observed, while swelling power was reduced. The frequency sweep rheological test revealed that 6% (w/w) starch paste samples had higher  $G'$  than  $G''$ , indicating dominant elastic behavior. The higher  $G'$  value of starch pastes was observed when using 5 minutes of argon and helium plasma treatment with lower  $\tan \delta$ . However,  $G'$  decreased with increasing treatment time due to depolymerization. Flow tests on 6% gelatinized modified starch pastes showed a lower thixotropy and consistency index (K) value after increasing both gas types' voltage levels and treatment time. The results confirmed the effectiveness of DBD plasma treatment in modifying tapioca starch properties.

CHULALONGKORN UNIVERSITY

Field of Study: Food Technology  
 Academic Year: 2021

Student's Signature .....  
 Advisor's Signature .....  
 Co-advisor's Signature .....

## ACKNOWLEDGEMENTS

This research would have been impossible without the financial support of graduate scholarship to the 90th anniversary of Chulalongkorn University's Ratchadaphiseksomphot Endowment Fund and Faculty of Science, Chulalongkorn University.

I would like to express my appreciation to Assoc. Prof. Dr. Jirarat Anuntagool and Assoc. Prof. Dr. Thiti Bovornratanaraks for their guidance, patience, and extraordinary support in this thesis process. I am most grateful for their teaching and advice, not just for the research techniques but also for many other approaches in life. I would not have achieved this far, and this thesis would not have been completed without all their support.

I would also like to appreciate Assistant Professor Dr. Daris Kuakpetoon, Associate Professor Dr. Kanitha Tananuwong, Dr. Sunee Chotineerarat, and Professor Dr. Vanna Tulyathan for their valuable suggestions.

I would like to thank all technicians, colleges, and friends in the Food Technology Department, Faculty of Science, Chulalongkorn University, Bangkok, for their support and wonderful collaboration. You all supported me greatly and were always willing to help.

Lastly and most importantly, I would like to sincerely thank my parents and family for their encouragement and support.

Natchanon Srangsomjit

## TABLE OF CONTENTS

	<b>Page</b>
.....	iii
ABSTRACT (THAI) .....	iii
.....	iv
ABSTRACT (ENGLISH) .....	iv
ACKNOWLEDGEMENTS .....	v
TABLE OF CONTENTS .....	vi
LIST OF TABLES .....	x
LIST OF FIGURES .....	xi
1. Chapter 1 Introduction.....	1
2. Chapter 2 A comprehensive review .....	2
2.1 Cassava .....	2
2.2 Tapioca starch .....	3
2.2.1 Amylose.....	3
2.2.2 Amylopectin .....	4
2.2.3 Starch granule.....	6
2.2.4 Semi-crystalline structure .....	7
2.2.5 Starch gelatinization and retrogradation.....	10
2.2.6 Rheological properties.....	12
2.2.6.1 Flow behavior .....	13
2.2.6.2 Dynamic Viscoelastic Behavior .....	14
2.3 Starch modification.....	16
2.3.1 Chemical modification .....	17
2.3.2 Physical modification .....	18

2.3.3 Biological modification .....	18
2.4 Non-thermal plasma technology .....	19
2.4.1 Plasma generation.....	20
2.4.2 Plasma sources .....	21
2.5 Nonthermal plasma modification.....	22
2.5.1 Mechanism of starch modification .....	22
2.5.1.1 Cross-linking .....	22
2.5.1.2 Depolymerization .....	23
2.5.1.3 Plasma etching .....	24
2.5.2 Effect of plasma treatment on starch properties .....	24
2.5.2.1 Physical properties.....	24
2.5.2.1.1 Molecular weight and chemical structure.....	24
2.5.2.1.2 Morphology .....	25
2.5.2.1.3 Starch crystalline structure .....	26
2.5.2.1.4 pH and color .....	26
2.5.2.2 Chemical properties.....	27
2.5.2.2.1 Chemical compositions.....	27
2.5.2.2.2 Amylose contents .....	27
2.5.2.3 Functional properties.....	28
2.5.2.3.1 Pasting properties .....	28
2.5.2.3.2 Swelling power and solubility .....	28
2.5.2.3.3 Rheological properties.....	29
3. Chapter 3 Materials and Methods.....	30
3.1 Materials .....	30
3.2 Methods .....	30
3.2.1 Sample preparation for nonthermal plasma treatment .....	30
3.2.2 Determination of physical properties .....	32
3.2.2.1 pH .....	32
3.2.2.2 Color.....	32



3.2.2.3	Surface morphology .....	32
3.2.2.4	Birefringence pattern .....	32
3.2.2.5	X-ray diffraction pattern.....	32
3.2.3	Determination of chemical properties .....	33
3.2.3.1	Chemical composition of native tapioca starch.....	33
3.2.3.2	Apparent amylose .....	33
3.2.3.3	Reducing sugar .....	33
3.2.3.4	Fourier transform infrared (FTIR) spectroscopy .....	33
3.2.3.5	Molecular weight analysis.....	33
3.2.4	Determination of functional properties .....	34
3.2.4.1	Pasting properties .....	34
3.2.4.2	Swelling power and solubility .....	34
3.2.4.3	Water binding capacity.....	34
3.2.4.4	Rheological properties.....	34
3.2.4.4.1	Viscoelastic properties.....	34
3.2.4.4.2	Flow properties .....	34
3.2.5	Statistical analysis .....	35
4.	Chapter 4 Results and Discussions.....	36
4.1	Effect of types of feed gas, voltage levels, and treatment time on physical properties of treated tapioca starch using nonthermal DBD plasma .....	36
4.1.1	pH .....	36
4.1.2	Color.....	37
4.1.3	Surface morphology .....	39
4.1.4	Birefringence pattern.....	41
4.1.5	X-ray diffraction pattern.....	43
4.2	Effect of types of the feed gas, voltage levels, and treatment time on chemical properties of treated tapioca starch using nonthermal DBD plasma .....	47
4.2.1	Chemical composition of native tapioca starch.....	47
4.2.2	Moisture content.....	47
4.2.3	Apparent amylose.....	48

4.2.4 Reducing sugar .....	49
4.2.5 Fourier transform infrared (FTIR) spectroscopy .....	51
4.2.6 Molecular weight analysis.....	53
4.3 Effect of types of the feed gas, voltage levels, and treatment time on functional properties of treated tapioca starch using nonthermal DBD plasma .....	57
4.3.1 Pasting properties .....	57
4.3.2 Swelling power and solubility.....	63
4.3.3 Water binding capacity.....	66
4.3.4 Rheological properties.....	67
4.3.4.1 Viscoelastic properties.....	67
4.3.4.2 Flow properties.....	74
5. Chapter 5 Conclusions.....	80
Suggestion.....	81
REFERENCES .....	82
6. Analytical methods.....	89
7. Additional Data .....	109
8. Analysis of Variance .....	110
VITA.....	155

## LIST OF TABLES

	<b>Page</b>
Table 2.1 Some methods for chemically starch modification.....	17
Table 2.2 Some methods for physically starch modification.....	18
Table 2.3 The processes of non-thermal plasma.....	20
Table 4.1 Color values ( $L^*$ , $a^*$ , $b^*$ ), whiteness index, and pH of native and DBD plasma-treated tapioca starch with various conditions. ....	38
Table 4.2 Relative crystallinity of native and treated starch granules by using plasma treatment with different conditions.....	45
Table 4.3 Chemical compositions of native tapioca starch.....	47
Table 4.4 Moisture content, apparent amylose contents, and reducing sugar of native and DBD plasma-treated tapioca starch with various conditions .....	49
Table 4.5 Ratio between 1047 and 1022 $\text{cm}^{-1}$ in the FTIR spectra of native and treated tapioca starch with different conditions.....	53
Table 4.6 Weight-average molecular weight ( $M_w$ ) of amylopectin before and after plasma modification.....	55
Table 4.7 Pasting properties of native and DBD plasma modified tapioca starch with various conditions .....	60
Table 4.8 Breakdown and Setback percentage of native and DBD plasma modified tapioca starch with different types of the feed gas, voltage levels, and treatment time .....	61
Table 4.9 Parameter of the Herschel-Bulkley model fitted to native and treated tapioca starch during steady shear rate and area of hysteresis .....	79
Table 6.1 Reaction mixture for standard amylose curve .....	96
Table 6.2 Molecular weight of standard dextran for construction standard curve ....	103
Table 6.3 Testing profile for RVA.....	104
Table 7.1 Swelling power of native and plasma modified tapioca starch with different conditions.....	109
Table 7.2 Solubility of native and plasma modified tapioca starch with different conditions.....	109

## LIST OF FIGURES

	<b>Page</b>
Figure 2.1 (a) Shapes of cassava roots; (b) cassava root cross-sectional view; and (c) components of cassava root in cross-section view. ....	2
Figure 2.2 Amylose structure.....	4
Figure 2.3 Amylopectin structure .....	4
Figure 2.4 Schematic models of amylopectin sub chains proposed by (a) French (1972), (b) Hizukuri (1986), and (c) Robin (1974).....	5
Figure 2.5 Scanning electron micrographs (SEM) of native tapioca starch at 1500x magnification .....	6
Figure 2.6 Native tapioca starch viewed by polarized microscopy at 40x magnification .....	7
Figure 2.7 A schematic drawing of a starch granule exhibiting the relationship between growth rings, amorphous and crystalline lamellae, and the structure of amylopectin.....	8
Figure 2.8 X-ray diffractograms of different starches that exhibit different crystalline patterns (A, B, C, and V).....	9
Figure 2.9 The alignment of double helices in the unit cells of crystalline A-starch amylopectin (left) and B-starch amylopectin (right) .....	10
Figure 2.10 Schematic drawing of starch gelatinization and retrogradation .....	11
Figure 2.11 Viscosity measurement of starch in an excess amount of water, applying a temperature profile including heating and cooling step.....	12
Figure 2.12 The stress relaxation curve of viscous, viscoelastic material elastic materials.....	13
Figure 2.13 The time-independent non-Newtonian behavior of thixotropic and rheopectic fluid.....	14
Figure 2.14 Typical response to strain or stress sweep presenting linear viscoelastic range region determined by the critical value of the amplitude sweep parameter.....	15
Figure 2.15 The viscoelastic behavior for an entangled polymer system is measured by frequency sweep test .....	16

Figure 2.16 The state of substances from solid state to plasma state by increasing the energy.....	19
Figure 2.17 Schematic model of nonthermal atmospheric pressure plasma generators with different methods .....	22
Figure 2.18 Cross-linking mechanism of two glycosidic chains of starch .....	23
Figure 2.19 Depolymerization of amylopectin side chains in starch granule.....	23
Figure 2.20 Plasma etching at starch granule by plasma species .....	24
Figure 3.1 Schematic diagram of nonthermal dielectric barrier discharge plasma system .....	31
Figure 3.2 A nonthermal dielectric barrier discharge (DBD) plasma machine (a) and solid-state modification of tapioca starch using DBD plasma machine (b).....	31
Figure 4.1 Scanning electron micrographs (SEM) of native and argon plasma modified tapioca starches. 1 and 2 represent images at 700x and 1500x magnification, respectively. A native starch, B 10 kV in 5 min, C 10 kV in 10 min, D 10 kV in 15 min, E 15 kV in 5 min, F 15kV 10 min, and G 15 kV 15min. Arrows indicate varying degrees of distortions after argon DBD plasma treatment.....	40
Figure 4.2 Scanning electron micrographs (SEM) of helium plasma modified tapioca starches. 1 and 2 represent images at 700x and 1500x magnification, respectively. A 10 kV in 5 min, B 10 kV in 10 min, C 10 kV in 15 min, D 15 kV in 5 min, E 15kV 10 min, and F 15 kV 15min. Arrows indicate varying degrees of distortions after helium DBD plasma treatment.....	41
Figure 4.3 Native, Ar10kV-5 min, Ar10kV-10 min, Ar10kV-15 min, Ar15kV-5 min, Ar15kV-10min, Ar15kV-15min of tapioca starch viewed by polarized light microscopy (A, B, C, D, E, F, and G respectively). 1 and 2 represent images at 400x and 1000x magnification, respectively. ....	42
Figure 4.4 He10kV-5min, He10kV-10min, He10kV-15min, He15kV-5min, He 15kV-10min, He15kV-15min of tapioca starch viewed by polarized light microscopy (A, B, C, D, E, and F respectively). 1 and 2 represent images at 400x and 1000x magnification, respectively .....	43
Figure 4.5 X-ray diffractogram of starch granule from native and treated tapioca starch by using plasma modification with different conditions. The arrows indicate the diffraction peak angles ( $2\theta$ ) of starch samples.....	46
Figure 4.6 Fourier-transform infrared spectroscopy (FTIR) spectra of native and treated tapioca starch with different conditions. ....	52

Figure 4.7 High-performance size exclusion chromatograph of native and plasma-treated tapioca starch with different conditions. (A and B) native and argon-plasma treated starch at 10 kV and 15 kV; (C and D) native and helium plasma-treated starch at 10 kV and 15 kV.....	56
Figure 4.8 Pasting curves of native, argon, and helium treated starch at different types of feed gas, voltage levels, and time.....	62
Figure 4.9 Swelling power of native and plasma modified tapioca starch at different temperatures (60, 70, 80, and 90 °C).....	65
Figure 4.10 Solubility of native and plasma-modified tapioca starch at different temperatures (60, 70, 80, and 90 °C).....	66
Figure 4.11 The water binding capacity of native and plasma modified tapioca starch under different conditions.....	67
Figure 4.12 Dynamic rheological behavior of native and argon treated tapioca starch at 10 kV levels and various treatment times (5, 10, 15 min). (A) Angular frequency on $G'$ (close symbol) and $G''$ (open symbol) for starch; (B) angular frequency of the loss tangent ( $\tan \delta$ ) at 25 °C for starch.....	70
Figure 4.13 Dynamic rheological behavior of native and argon treated tapioca starch at 15 kV levels and various treatment times (5, 10, 15 min). (A) Angular frequency on $G'$ (close symbol) and $G''$ (open symbol) for starch; (B) angular frequency of the loss tangent ( $\tan \delta$ ) at 25 °C for starch.....	71
Figure 4.14 Dynamic rheological behavior of native and helium treated tapioca starch at 10 kV levels and various treatment times (5, 10, 15 min). (A) Angular frequency on $G'$ (close symbol) and $G''$ (open symbol) for starch; (B) angular frequency of the loss tangent ( $\tan \delta$ ) at 25 °C for starch.....	72
Figure 4.15 Dynamic rheological behavior of native and helium treated tapioca starch at 15 kV levels and various treatment times (5, 10, 15 min). (A) Angular frequency on $G'$ (close symbol) and $G''$ (open symbol) for starch; (B) angular frequency of the loss tangent ( $\tan \delta$ ) at 25 °C for starch.....	73
Figure 4.16 Effect of shear rate on native and argon treated tapioca starch at 10 kV levels and various treatment times (5, 10, 15 min).....	77
Figure 4.17 Effect of shear rate on native and argon treated tapioca starch at 15 kV levels and various treatment times (5, 10, 15 min).....	77
Figure 4.18 Effect of shear rate on native and helium treated tapioca starch at 10 kV levels and various treatment times (5, 10, 15 min).....	78

Figure 4.19 Effect of shear rate on native and helium treated tapioca starch at 15 kV levels and various treatment times (5, 10, 15 min) .....	78
Figure 6.1 Standard curve for determining amylose content.....	97
Figure 6.2 Standard curve for determining reducing sugar content.....	100
Figure 6.3 Standard curve for calculating molecular weight of amylose and amylopectin.....	103



## Chapter 1 Introduction

Tapioca starch (*Manihot esculenta* Crantz) is produced from the roots of cassava, which consists of two chemical components: amylose and amylopectin. Currently, starch is used in food products as a thickening agent, a gelling agent, and a stabilizer. Nevertheless, many drawbacks of native tapioca starch, such as retrogradation tendency, poor solubility, reduced viscosity due to shearing, and thermal processing, have limited its application in the industry. Starch is modified either by chemical, biological or enzymatic, and physical means to enhance its structure and functions to overcome these disadvantages. The chemical modification provides high-quality starch and is an efficient technique because the operation is suitable for mass production. However, the method is time-consuming and yields chemical residues and wastewater. Even though enzymatic modification requires fewer chemicals than chemical modification and thus produces fewer chemical residues, wastewater is unavoidably produced. The current mainstream food trend called “Clean label” demands ingredients from minimal processes in which no chemical or artificial ingredients are added. Consequently, physically modified starch is preferred for green or clean labeled products. However, the traditional methods, including hydrothermal treatment and annealing, are time-consuming and generate wastewater. Nonthermal plasma has gained interest in food treatment, especially for heat-sensitive products. The technique has been used to improve the quality and safety of food. For starch modification, the plasma species are produced and allowed to interact with starch to cause the modification via three possible mechanisms: cross-linking, depolymerization, and plasma etching. The occurrence and extent of each mechanism depend on the type of feed gas, the voltage level, and the treatment time. Despite various reports, there has been no information on the application of high voltage nonthermal dielectric barrier discharge plasma for solid-state modification of tapioca starch with different types of feed gas.

The thesis objectives were to investigate the effect of voltage level and treatment time on the properties of modified tapioca starch using nonthermal dielectric barrier discharge plasma and to study the effect of types of feed gas on the properties of modified tapioca starch using nonthermal dielectric barrier discharge plasma.



## Chapter 2 A comprehensive review

### 2.1 Cassava

Cassava (*Manihot esculenta* Crantz) is a significant starch source for commercial production in tropical and subtropical regions (Sánchez et al., 2009). Cassava is a shrubby perennial crop that grows in various soil conditions. The roots, located under the soil layer, are collected 10-12 months after planting. Figure 2.1(a) shows various forms of roots, including conical, conical-cylindrical, cylindrical, and fusiform shapes. The cross-section of root tubers in Figure 2.1(b) reveals the peel and the center tuber. The peel is divided into two layers: the outer layer (referred to as the periderm) and the inner layer (referred to as the cortex), which is composed of sclerenchyma, cortical parenchyma, and phloem tissue, as depicted in Figure 2.1(c). The root's huge center pith is the starch-reserve flesh, which is composed of cambium and parenchyma tissue, as well as xylem vessels. Mature cassava roots have a 60–70% moisture content, a 30–35% carbohydrate content, and a 12–15% fat, fiber, and protein content with trace amounts of vitamins and minerals (Breuninger et al., 2009). Cassava roots have a range of sizes (3 to 15 cm in diameter), and the hue of the outer peel ranges from white to dark brown.

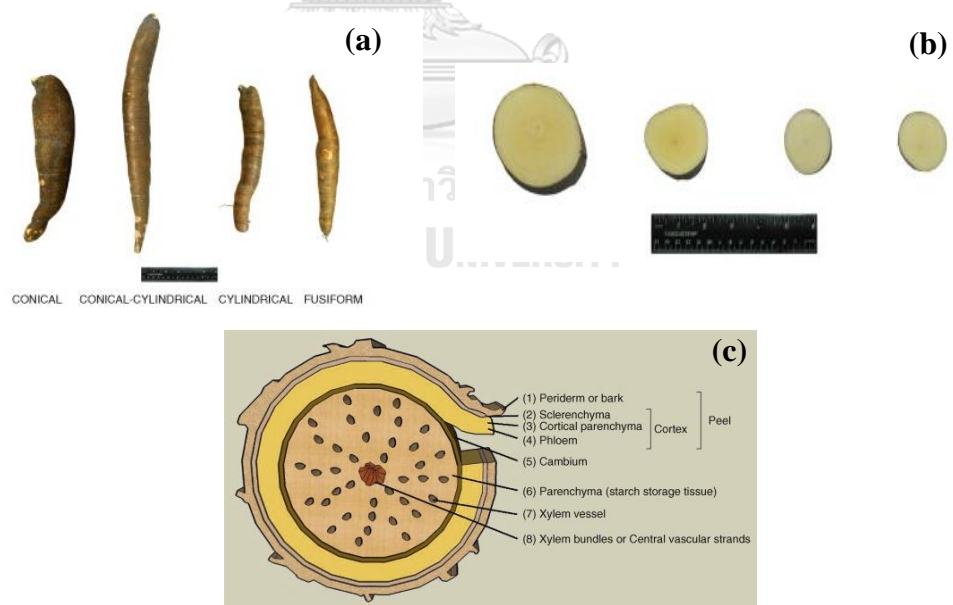


**Figure 2.1** (a) Shapes of cassava roots; (b) cassava root cross-sectional view; and (c) components of cassava root in cross-section view.

(Breuninger et al., 2009)

## 2.2 Tapioca starch

Tapioca starch, produced from cassava root milling, is applied in various food and non-food applications. The starch content in dry cassava root weight ranges from 73.7–84.39% (Rickard et al., 1991). Tapioca starch paste is odorless, clear, and sticky. Nonetheless, the limitations of native tapioca starch paste in food applications include sensitivity to heat, acid, and shear force (Wongsagonsup et al., 2014). Amylose and amylopectin are the two main chemical components of tapioca starch. These two polymers are organized to form semi-crystalline starch granules with diameters ranging from 1 to 100  $\mu\text{m}$  (Villa Zabala, 2020). The proportion of amylose and amylopectin in starches significantly impacts their physicochemical properties (Gayin et al., 2016).

### 2.2.1 Amylose

Amylose is a predominantly linear chain of glucose molecules linked by  $\alpha$ -(1,4)-D-glucopyranosyl units. However, it can be slightly branched with  $\alpha$ -(1,6) linkages. Amylose generally forms a left-handed-helical structure, with each twist of the helix containing six to eight anhydroglucose units, as shown in Figure 2.2. The hydrophilic region of the helix, which is the hydroxyl group of glucosyl residues, was located on the outer surface, while the hydrophobic region is in the internal cavity. The hydrophobic cavity of the amylose helix has also been linked to interactions with iodine, organic alcohols, and fatty acids by hydrophobic interactions, including hydrogen bonds, hydrophobic attractions, and van der Waals forces (Wang et al., 2020). The formation of a helical amylose complex with iodine can produce an intense blue color ( $\lambda_{\text{max}} = 620 \text{ nm}$ ) by spectrophotometer, which can determine the amylose content of starches (Luallen, 2018). Zhu (2015) reported that the amylose content of tapioca starch ranged from 0-30.3%, depending on sources and analytical techniques.

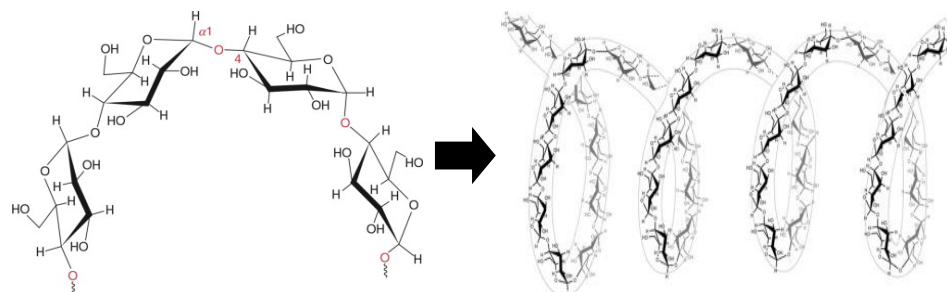


**Figure 2.2** Amylose structure  
(Bergthaller & Hollmann, 2014; Bonechi et al., 2017)

### 2.2.2 Amylopectin

Amylopectin, the major chemical composition in starches, has a highly branched molecular structure. Each linear chain is linked by  $\alpha$ -1,4 bonds, terminating in a non-reducing end. Branch chains are generated at the O-6 position of glucose units by  $\alpha$ -1,6 glycosidic linkages in a chain, which is then extended further by  $\alpha$ -1,4 glycosidic linkages (Figure 2.3). These branch points contain around 4 to 6% of all linkages.

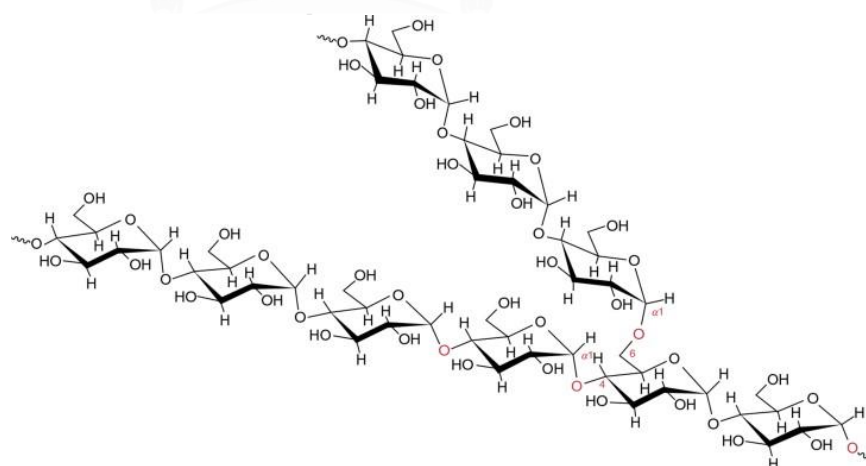


**Figure 2.3** Amylopectin structure  
(Bergthaller & Hollmann, 2014)

The cluster models of amylopectin were proposed by French (1972), Hizukuri (1986), and Robin (1974) (Figure 2.4). The crystalline regions are produced by clusters of short-branch chains of amylopectin molecules; these crystalline regions are interspersed with amorphous regions that represent amylopectin and amylose branching sites.

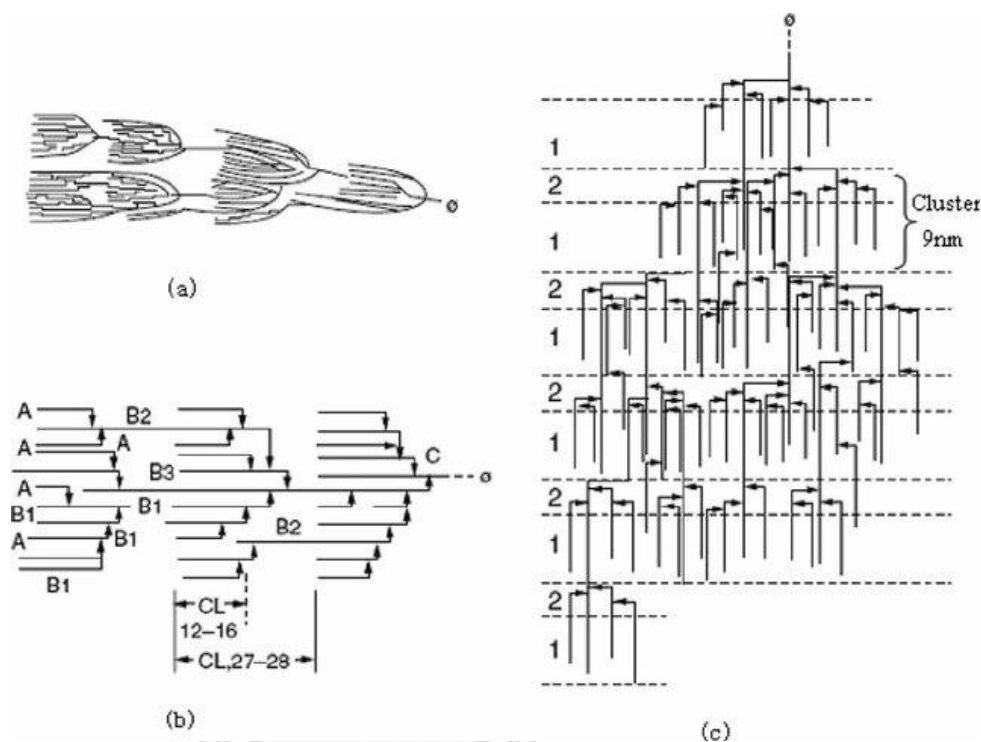


**Figure 2.4** Schematic models of amylopectin sub chains proposed by (a) French (1972), (b) Hizukuri (1986), and (c) Robin (1974) (Miao et al., 2015)

Hizukuri (1986) described the chain profiles of amylopectin that it could be classified into three chain profiles, including A, B, and C-chains. The shortest A-chains are unbranched and have a degree of polymerization (DP) ranging from 6 to 15 DP. The B chains (B1, B2, and B3) are connected by A chains or other B chains based on their lengths and the number of clusters they span. The chain lengths of B1, B2, and B3 chains are 13–24, 25–36, and 37–54 DP, respectively. The C-chain is identified by the presence of a single reducing terminal.

### 2.2.3 Starch granule

The shape and size of the starch granules may differ depending on the genus, plant sources, and the climatic conditions in which a crop was cultivated. The size of the granules varies among starches, ranging from 1 to 110  $\mu\text{m}$  (Hoover, 2001). The morphology of native tapioca starch was characterized using SEM at 1500 $\times$  magnification, as shown in Figure 2.5. Tapioca starch granules are smooth, irregular spheres, polygonal in shape with sizes of about 5  $\mu\text{m}$  to 10  $\mu\text{m}$ .

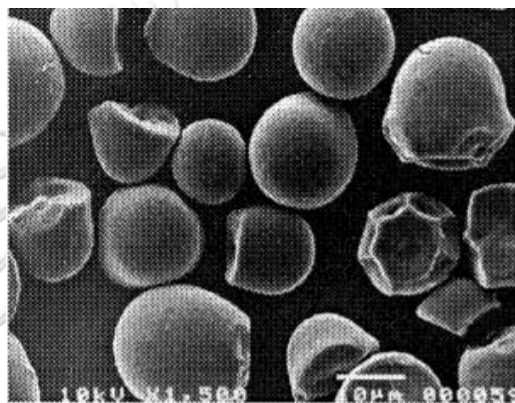


**Figure 2.5** Scanning electron micrographs (SEM) of native tapioca starch at 1500 $\times$  magnification (Sriroth et al., 1999)

When a starch granule is exposed to polarized light, a maltese cross or hilum can be observed, as shown in Figure 2.6. The capacity to refract polarized light twice is referred to as birefringence. Birefringence pattern in starch granules shows the radial organization of amylopectin molecules and their chains with the reduced ends directed toward the hilum (Alcázar-Alay & Meireles, 2015). A weak birefringence pattern indicates crystalline region disorder due to starch gelatinization or modification.

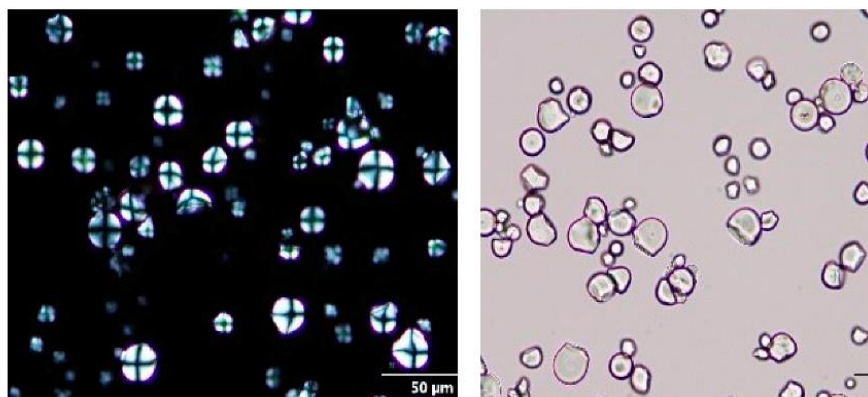


**Figure 2.6** Native tapioca starch viewed by polarized microscopy at 40x magnification (Grace & Jeyakumar Henry, 2020)

#### 2.2.4 Semi-crystalline structure

The starch granule is semicrystalline. The amorphous and crystalline regions of amylopectin are represented by the lamellae of a semi-crystalline growth ring identified by small-angle X-ray scattering, which is around 9–10 nm thick (Figure 2.7). The crystalline region contains amylopectin double helices, whereas the amorphous part comprises the amylose chain and amylopectin segments. Amylopectin chains are interlaced with amylose chains. The degree of structural organization in a solid body determines crystallinity. The crystallinity of native starches ranges between 14 and 45 % (Dome et al., 2020).

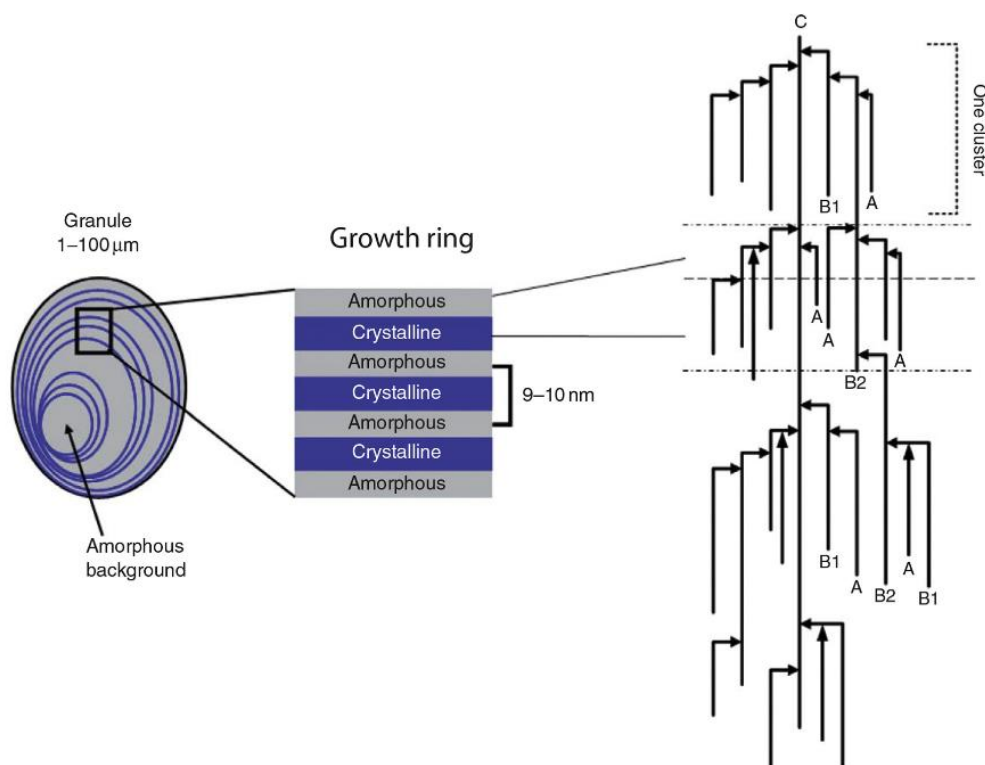


**Figure 2.7** A schematic drawing of a starch granule exhibiting the relationship between growth rings, amorphous and crystalline lamellae, and the structure of amylopectin (Bergthaller & Hollmann, 2014)

The X-ray Diffraction (XRD) method is used to classify the crystalline types of starch granules, as shown in Figure 2.8. The crystallinity patterns are classified into four types, which are A, B, C, and V type crystals. The A-type crystal is found in cereal starches (wheat, corn, rice). The B-type crystal starch is typically found in starch extracted from tubers and roots (potatoes and canna). C-type crystals, which are the combination of A-and B-type crystalline structures, can be found in root and seed starches (pea and cassava roots). In addition, starches can exhibit the V-type pattern when the amylose fraction complexes with lipid (a starch-lipid complex). Dome et al. (2020) reported that the A-type crystalline structure was shown by diffraction peaks ( $2\theta$ ) at  $15.0^\circ$ ,  $22.9^\circ$ , and a

doublet at  $17.0^\circ$  and  $17.9^\circ$  in the XRD pattern of maize starch. The diffraction peaks ( $2\theta$ ) of potato starch, which correspond to the B-type crystal, are at  $5.6^\circ$ ,  $15.1^\circ$ ,  $17.23^\circ$ ,  $19.67^\circ$ ,  $22.2^\circ$ ,  $24.0^\circ$ , and  $26.4^\circ$ . The diffraction peaks ( $2\theta$ ) of tapioca starch at  $5.0^\circ$ ,  $15.2^\circ$ ,  $22.8^\circ$ , and a doublet at  $17.1^\circ$  and  $18.2^\circ$  correspond to the C-type crystalline structure. The formation of the V-amylose complexes in legume starch-lipid complexes was verified by peaks observed at  $2\theta = 7.4^\circ$ ,  $12.7^\circ$ , and  $19.8^\circ$  (Exarhopoulos & Raphaelides, 2012).

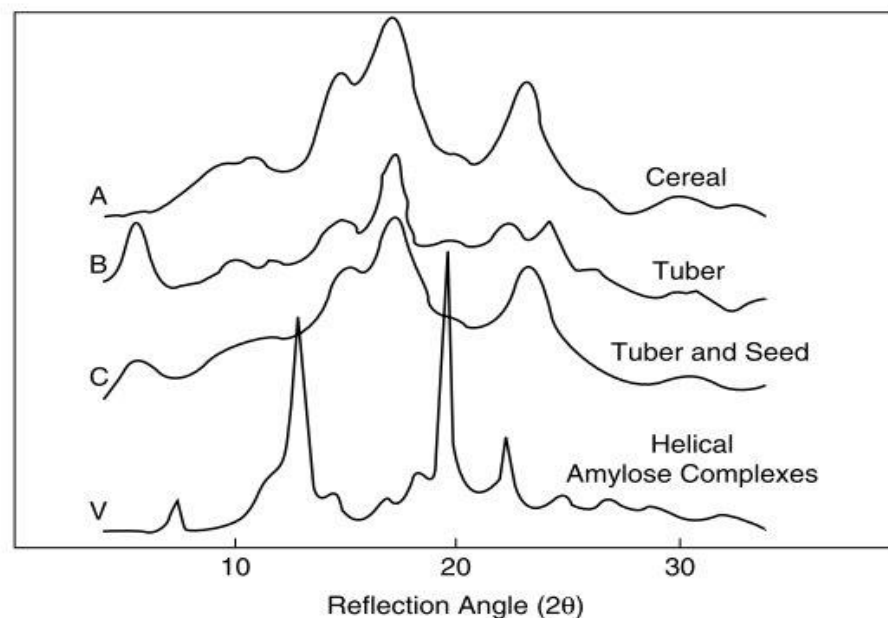


**Figure 2.8** X-ray diffractograms of different starches that exhibit different crystalline patterns (A, B, C, and V) (Cui, 2005)

Figure 2.9 shows the double helices' orientation in the unit cells of crystalline A-starch amylopectin and B-starch amylopectin. The double helices of A type-starches are formed in a monoclinic lattice unit cell. Each unit cell is packed in a parallel fashion and comprises four water molecules arranged in a tight circle. The B-type crystal is loosely packed into a hexagonal unit cell, which is packed in parallel as an array of left-handed parallel-stranded double helices. Thirty-six (36) water molecules are formed as a complex centered on the unit cell's sixfold screw axis.



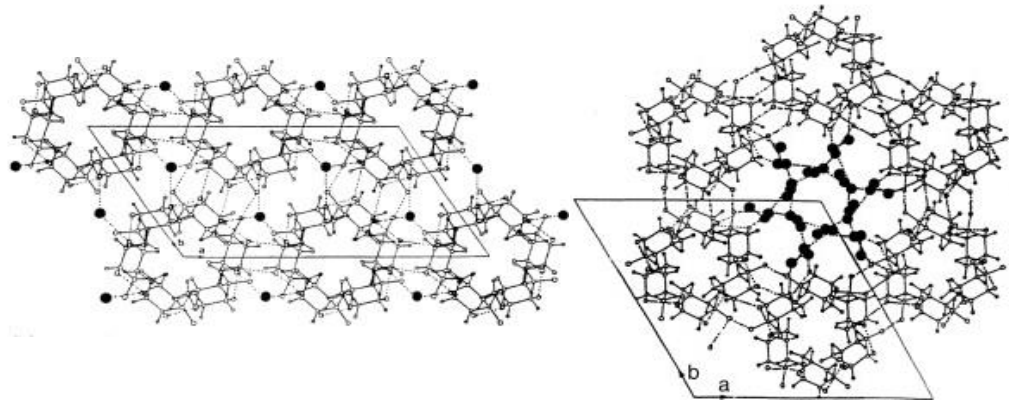


**Figure 2.9** The alignment of double helices in the unit cells of crystalline A-starch amylopectin (left) and B-starch amylopectin (right)

Modified from Pérez et al. (2009)

#### 2.2.5 Starch gelatinization and retrogradation

Starch changes during gelatinization and retrogradation are critical considerations of its functional properties in food processing. These properties affect the quality, acceptability, nutritional value, and shelf life of food products (Wang & Copeland, 2013). Starch gelatinization is the disruption of molecular orders inside the starch granule and the accompanying and irreversible changes in characteristics such as granular swelling, loss of birefringence, viscosity development, and starch solubilization (BeMiller, 2019). The degree of starch gelatinization depends on the types of starch, processing conditions, and water availability (Lund & Lorenz, 1984).

The amylose and amylopectin molecules in gelatinized starch can rearrange into more ordered structures after cooling and storage, a process known as retrogradation. Starch retrogradation is often associated with several physical changes, including increased paste viscosity and turbidity, gel formation, water exudation, and an increase in crystallinity with the formation of B-type crystal of retrograded starch (Hoover et al., 2010). These results impact the sensory and nutritional properties of the foods. The degree of retrogradation of starch is determined by the amylose content, storage time, and moisture

content (Wang & Copeland, 2013). The Schematic drawing of starch gelatinization and retrogradation is shown in Figure 2.10.

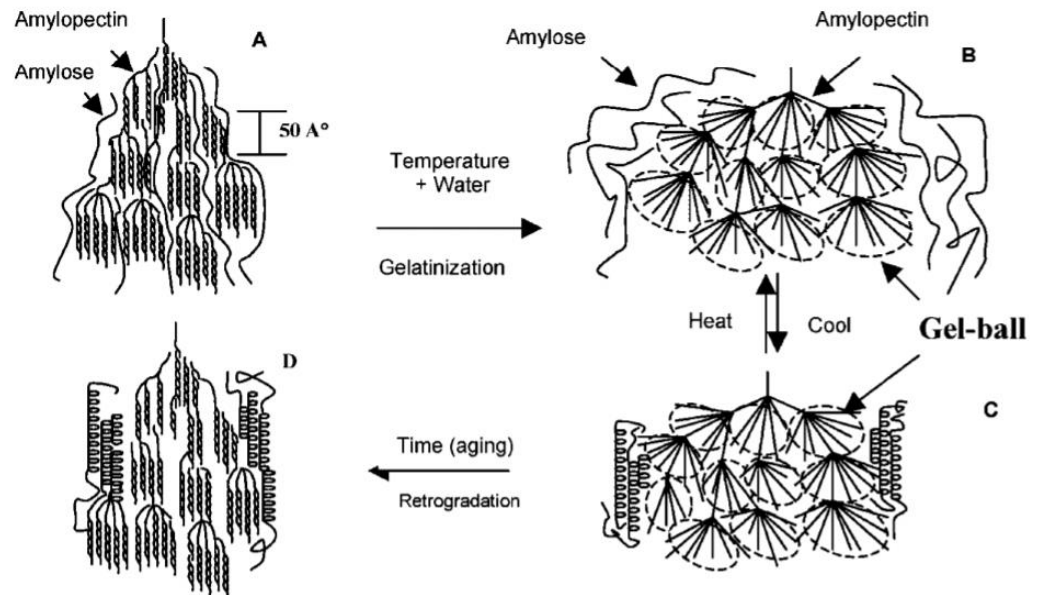


**Figure 2.10** Schematic drawing of starch gelatinization and retrogradation (Yu & Christie, 2005)

The Rapid Visco Analyzer (RVA) or visco-amylograph technique is used to analyze starch gelatinization and retrogradation with excess water under controlled temperature and shear conditions. The starch granule absorbs water and then swells; the crystalline structure melts (gelatinization) and forms a continuous gel. The viscosity changes caused by heating and cooling starch in water provide a characteristic pasting curve (Figure 2.11). Pasting temperature ( $T_p$ ), which indicates the minimum temperature necessary to gelatinize the starch, can have consequences for the stability of other components in a formula, as well as energy expenditures. Peak viscosity (PV) indicates the ability of starch to swell. PV is reached when the rate of granule swelling equals the rate of granule breakdown (Kumar & Khatkar, 2017). Setback viscosity (SV) refers to the reassociation or recrystallization of amylose and amylopectin in gelatinized starch under cooling (Schirmer et al., 2015).

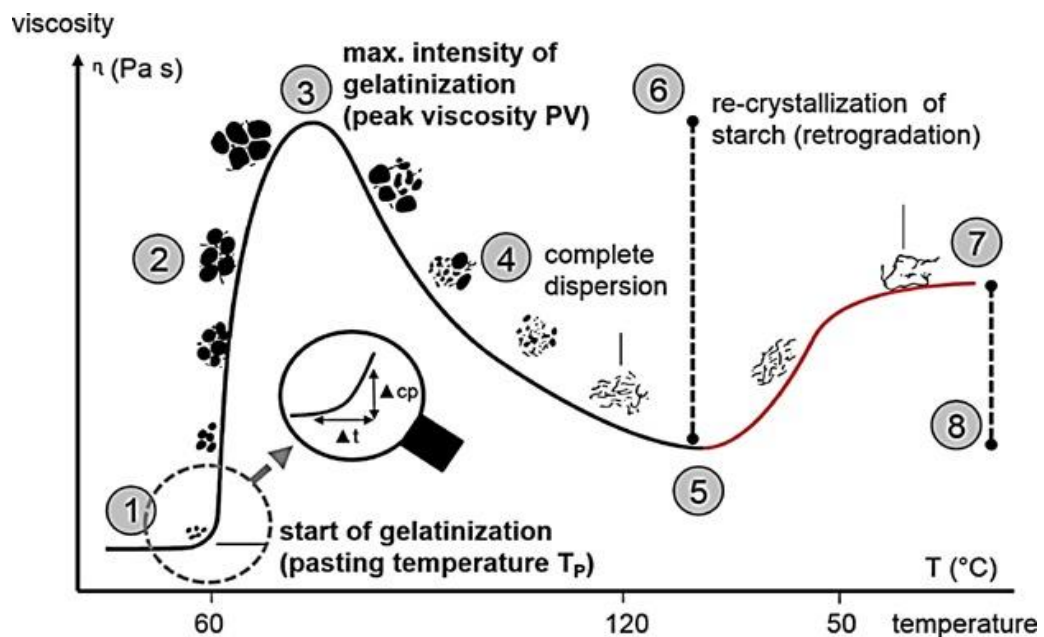


**Figure 2.11** Viscosity measurement of starch in an excess amount of water, applying a temperature profile including heating and cooling step

(Schirmer et al., 2015)

### 2.2.6 Rheological properties

Rheology is the study of materials deformation and flow. Food materials can be classified as viscous, viscoelastic, or elastic based on their rheological properties (Steffe, 1996). Stress ( $\sigma$ ) refers to the force applied to a unit area  $A$  and strain ( $\epsilon$ ) is a unit of relative displacement or deformation determined by the displacement gradient. Food materials generally show both viscous and elastic properties, called viscoelastic or viscoelastic food. When a fixed strain and the strain are held constant, the viscoelastic material exhibits a decrease in strain with increasing time (Figure 2.12).

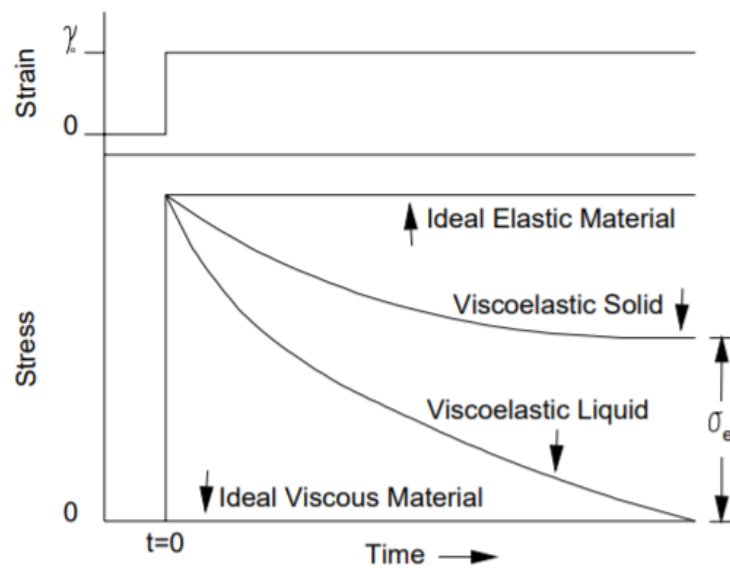


**Figure 2.12** The stress relaxation curve of viscous, viscoelastic material elastic materials (Steffe, 1996)

#### 2.2.6.1 Flow behavior

Flow behavior of gelatinized starch dispersion, having known as non-Newtonian, time-dependent, and viscoelastic behavior, is influenced by shear forces and gelatinization process, which affect its structure (Lagarrigue & Alvarez, 2001; Tattiyakul & Rao, 2000). At low concentration, the Herschel-Bulkley model with yield stress could be used to describe shear response with various shear rates (Chen & Ramaswamy, 1999). The Herschel-Bulkley model is a generic equation describing non-Newtonian fluids' behavior with yield stress (Equation 2.1).

$$\sigma = \sigma_0 + K(\dot{\gamma})^n \quad (2.1)$$

where

- $\sigma$  = shear stress
- $K$  = consistency index
- $\dot{\gamma}$  = shear rate
- $\sigma_0$  = yield stress
- $n$  = flow behavior index ( $n=1$  Newtonian,  $<1$  for shear-thinning, and  $>1$  for shear-thickening)

In the previous study, Tattiyakul and Rao (2000) reported that the gelatinized cross-linked waxy maize starch exhibited

both rheopexy and thixotropy. Thixotropy is a time-dependent shear thinning property, which reduces the apparent viscosity when increasing the shear rate. On the other hand, the rheopexy (anti-thixotropy) is a time-dependent shear-thickening that appears to have occurred from the formation of a shear-induced structure, resulting in an increase in viscosity. When the shear rate is increased from low to high and high to low, respectively. Both thixotropic and rheopectic behaviors show the different forms of hysteresis loop (Figure 2.13).

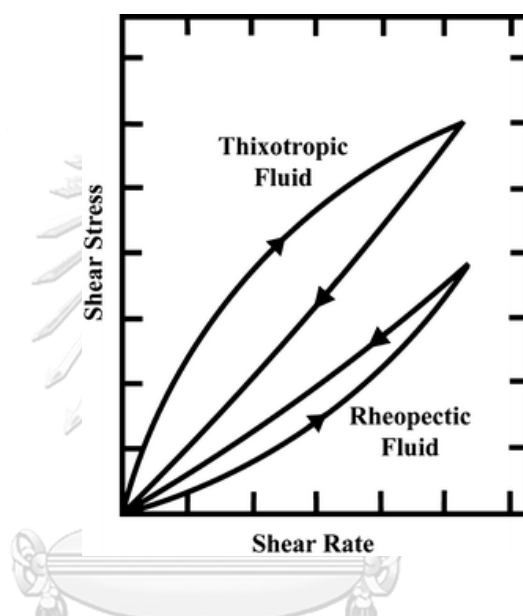


**Figure 2.13** The time-independent non-Newtonian behavior of thixotropic and rheopectic fluid (Chhabra, 2010)

#### 2.2.6.2 Dynamic Viscoelastic Behavior

Viscoelastic materials combine the properties of an elastic and viscous material. Their rheological characteristics are affected by the relative degrees of elasticity and viscosity and the time scale of the deformation. The amplitude sweep test is commonly used to determine the linear viscoelastic region (LVE region) of a material. The LVE region defines test ranges without destroying the material's structure when stress or strain is increased (Figure 2.14).

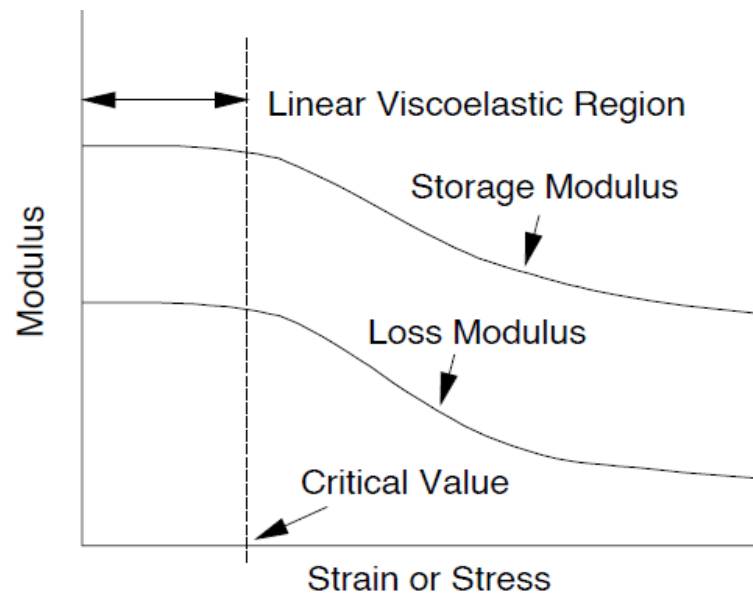


**Figure 2.14** Typical response to strain or stress sweep presenting linear viscoelastic range region determined by the critical value of the amplitude sweep parameter (Steffe, 1996)

The dynamic frequency sweep test is used to evaluate the viscoelastic properties of gelatinized starch dispersion. These investigations were carried out at strain values from inside the LVE region. The storage modulus ( $G'$ ), loss modulus ( $G''$ ), and loss tangent ( $\tan \delta$ ) of non-Newtonian fluids are measured. The  $G'$  expresses the material's ability to store energy elastically and represents the elastic behavior that dominates.  $G''$  is measured of the energy loss of the viscous (out of phase) component to the stress or represents liquid-like behavior (Liu et al., 2017). The viscoelastic properties of polymer solutions at various ranges of angular frequency are shown in Figure 2.15. When  $G''$  is much greater than  $G'$ ; the material behaves more like a liquid. Conversely, when  $G'$  is much greater than  $G''$ , the material behaves like a solid. The polymer has low moduli at low angular frequencies, which  $G''$  rises when the frequency is reduced. The polymer acts as a rubber or viscoelastic solid at a rubbery plateau. The polymer system is glassy with greater  $G'$  at high angular frequencies.

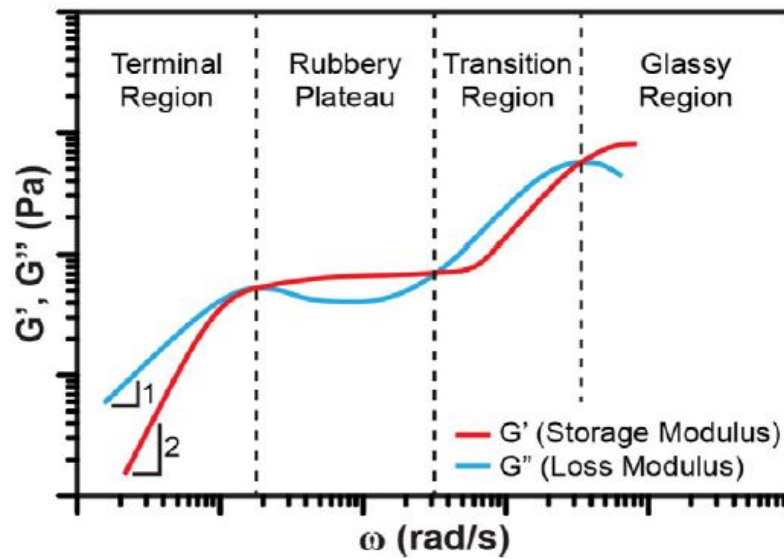


**Figure 2.15** The viscoelastic behavior for an entangled polymer system is measured by frequency sweep test (Liu et al., 2017)

$G'$  and  $G''$  are both frequency functions that may be described in terms of the amplitude ratio, as shown in Equations 2.2 and 2.3.

$$G' = \left(\frac{\sigma_0}{\gamma_0}\right)\cos(\delta) \quad (2.2)$$

and

$$G'' = \left(\frac{\sigma_0}{\gamma_0}\right)\sin(\delta) \quad (2.3)$$

When  $\sigma_0$  = The amplitude of the shear stress  
 $\gamma_0$  = Strain amplitude

Additionally, the tangent of the phase shift, which is also a function of frequency as shown in Equation 2.4

$$\tan(\delta) = \frac{G'}{G''} \quad (2.4)$$

### 2.3 Starch modification

Native starches have been widely used in food products. Nevertheless, drawbacks such as retrogradation tendency, poor

solubility, reduced viscosity due to shearing, and thermal processing reduces its properties (Tattiyakul et al., 2002). To conquer the disadvantages, starch is modified either by chemical, biological or enzymatic, and physical means to enhance its structure and functions.

### 2.3.1 Chemical modification

Chemical reagents are used to modify starch properties and are categorized according to their chemical characteristics as monofunctional or bifunctional reagents (Masina et al., 2017). The different methods and results of the chemical modification of starch are summarized in Table 2.1. The degree of starch modification is determined by the type of starch, the pH of the slurry, the reaction parameters (concentration, treatment time, and temperature), the existence of a catalyst, and the degree of substitution.

**Table 2.1** Some methods for chemically starch modification

Chemical modification	Key results	References
Acid treatment	Improved solubility, decreased in peak viscosity, retrogradation tendency	(Barretti et al., 2020)
Acetylation	Better stability after gelatinization, reduced pasting temperature and swelling power	(Trela et al., 2020)
Cross-linking	Increased in gel hardness, higher viscosity, and lower breakdown viscosity	(Shah et al., 2016)
Hydroxypropylation	Increased swelling power, freezing-thawing stability, higher viscosity, improved retrogradation tendency	(Schmitz et al., 2006)
Oxidation	Reduced the peak viscosity, breakdown, setback, and final viscosity	(Klein et al., 2014)



### 2.3.2 Physical modification

The current mainstream food trend called "Clean label" demands ingredients from minimal processes that add no chemical or artificial ingredients (Asioli et al., 2017). Consequently, physically modified starch is preferred for green or clean-labeled products. Physically starch modification (Table 2.2) involves the treatment of native starch granules under different temperature or moisture combinations, pressure, shear, and irradiation (Ashogbon & Akintayo, 2014). These methods do not require any chemical treatment that could be harmful for human use.

**Table 2.2** Some methods for physically starch modification

Physical modification	Key results	References
Heat-moisture treatment	Increased gelatinization temperature, reduced swelling power, peak viscosity, and breakdown viscosity	(Gunaratne & Hoover, 2002)
Annealing	Change pasting properties, surface morphology, crystalline region, and functional properties (depending on processing conditions)	(Zavareze & Dias, 2011)
Irradiation	Reduced amylose contents, swelling power, peak viscosity, and peak temperature.	(Dar et al., 2018)

### 2.3.3 Biological modification

Biological or enzymatic modification of starch is faster, environmentally safe, and can be performed under controllable conditions. Amylases are the most important enzymes, which are applied in the starch industry for modification (Thirumdas, Kadam, et al., 2017). Amylases hydrolyze starch by breaking  $\alpha$ -(1,4)-D-glucopyranosyl units between two glucose molecules, resulting in lower dextrose equivalency. Shariffa et al. (2009) found that hydrolyzed heat-modified sweet potato and tapioca

starch could enhance amylose content, swelling power, and solubility of starch.

#### 2.4 Non-thermal plasma technology

Plasma, the fourth state of matter, is a quasi-neutral ionized gas state that consists of ions, free electrons, atoms, and molecules in excited states with a net neutral charge that provides unique physical and chemical properties (Pankaj et al., 2018). The plasma state is achieved by increasing the energy level of matter. Energy levels increase from solid, liquid, gaseous, and plasma states, respectively, as shown in Figure 2.16.

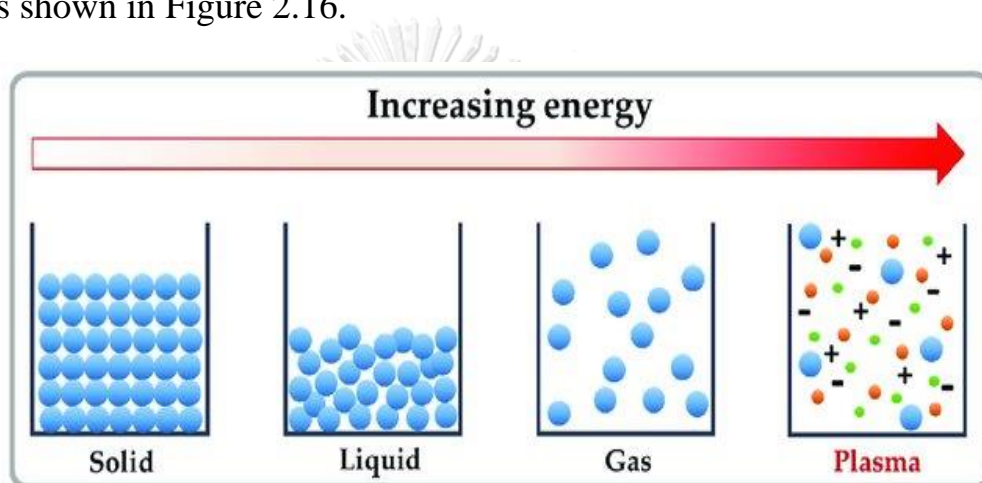


**Figure 2.16** The state of substances from solid state to plasma state by increasing the energy (Hojnik et al., 2017)

Plasma can be generated by energizing a neutral gas at different temperatures and pressures and is thus classified as thermal or non-thermal plasma (Chizoba Ekezie et al., 2017). Plasma has a net neutral charge and can exist on the ground or in an excited state. Thermal plasma needs extremely high pressures (105 Pa) and up to 50 MW of power to generate. Since the uniform gas temperature for all constituents is achieved, it is in a thermodynamic equilibrium state between the electrons and heavier species. Non-thermal plasma, on the other hand, is generated at low pressures and power levels without a localized thermodynamic equilibrium and is hence referred to as non-equilibrium plasma. Non-thermal plasma has a variety of applications in the food industry, including microbial decontamination of food products, packaging material

processing, and food component modification (Chizoba Ekezie et al., 2017).

### 2.4.1 Plasma generation

The ionization of gas is essential in plasma chemistry and other parameters such as collision patterns and electron energy distribution. Excitation, de-excitation, ionization, dissociations, fragmentations, and other gas-phase processes are typical during plasma generation (Thirumdas, Kadam, et al., 2017). This highly energetic electron collides with the atoms and molecules in the gas, causing them to be ionized, excited, or dissociated, as shown in Table 2.3. These processes are the primary processes that generate electrons, ions, and active atoms. Afterward, several active species recombine, creating the final products (Abd Allah, 2012). Schweigert et al. (2019) described that the metastable state of helium had higher energy than argon and caused helium plasma to generate more reactive species than argon plasma.

**Table 2.3** The processes of non-thermal plasma

Plasma process	Reaction
Excitation	$e^{-} + A \rightarrow A^{*} + e^{-}$
Ionization	$e^{-} + A \rightarrow A + e^{-} + e^{-}$
Dissociation	$e^{-} + A_2 \rightarrow 2A + e^{-}$
Attachment	$e^{-} + A_2 \rightarrow A_2^{-}$
Dissociative attachment	$e^{-} + A_2 \rightarrow A^{-} + A$
Dissociative ionization	$e^{-} + A_2 \rightarrow A^{-+} + A + 2e^{-}$
Electronic decomposition	$e^{-} + AB \rightarrow A + B + e^{-}$
Charge transfer	$A^{+} + B \rightarrow A + B^{+}$

(Abd Allah, 2012)

### 2.4.2 Plasma sources

Plasma can be produced by various methods, including dielectric barrier discharge (DBD), plasma jet, corona discharge, and gliding arc discharge (Figure 2.17). Air, oxygen, nitrogen, helium, argon, and their combinations are the most often used operating gases (Domonkos et al., 2021).

The dielectric barrier discharge (DBD) plasma is produced by applying a high voltage (kV) electric alternating current at a high frequency (kHz) across an adjustable small gap distance (up to 10 mm) between two electrodes separated by a dielectric barrier. Dielectric materials such as quartz, glass, ceramics, silicon rubber, and plastic are used to cover the electrodes.

The plasma jet generates a speedy stream of highly reactive active species with very weak light emitted. It comprises two concentric cylindrical electrodes. The inner electrode is linked to a radio frequency or microwave power generator that produces ionized gas. This gas exits through the nozzle, resulting in a "jet-like" appearance.

Corona discharges are created by a high voltage between two or more sharp electrodes. Typically, the colonizing electrode consists of a needle or a thin wire, and the ionization process creates a crown around this active electrode. The disadvantage of corona discharge is very weak discharge due to low electron and ion intensity.

Gliding arc discharge plasma reactors generate hot plasma, but they can also create cold plasma under certain conditions. Electrodes are located around gas flowing, and a high voltage is used to create the discharge at the spot, in which the distance between divergent electrodes is a minimum.

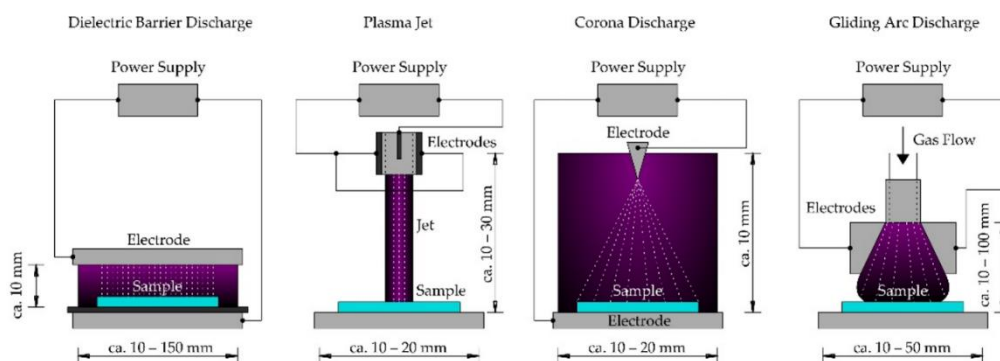


**Figure 2.17** Schematic model of nonthermal atmospheric pressure plasma generators with different methods (Domonkos et al., 2021)

## 2.5 Nonthermal plasma modification

Nonthermal plasma has gained interest in food treatment, especially for heat-sensitive products. The technique has been used to improve the quality and safety of food products and ingredients (Laroque et al., 2022). The advantages of nonthermal plasma are modification of the starch with a short reaction time and reduced wastewater in starch production.

### 2.5.1 Mechanism of starch modification

Thirumdas, Kadam, et al. (2017) reported that the plasma species were produced and allowed to interact with starch to cause the modification via three possible mechanisms, including cross-linking, depolymerization, and plasma etching. The occurrence and extent of each mechanism depend on the type of feed gas, the voltage level, and the reaction time.

#### 2.5.1.1 Cross-linking

During plasma treatment, free radicals and energetic electrons promoted the cross-linking mechanism between the polymeric chains of starch molecules. The mechanism of cross-linking is shown in Figure 2.18. The formation of a new C-O-C linkage occurs between the

reducing ends of two polymer chains (C-OH) with the removal of water molecules. Khorram et al. (2015) found that the argon plasma can induce the crosslinking of starch at the C-2 position.

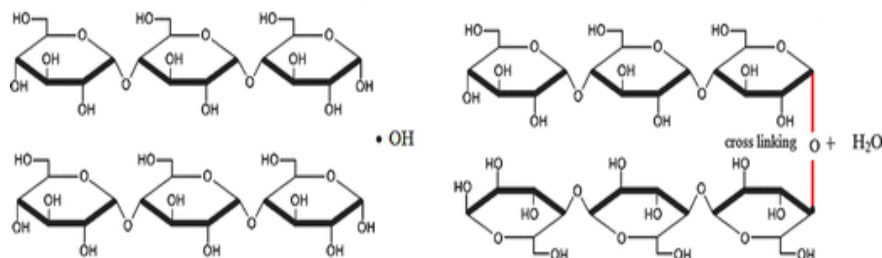


**Figure 2.18** Cross-linking mechanism of two glycosidic chains of starch  
(Thirumdas, Kadam, et al., 2017)

### 2.5.1.2 Depolymerization

The bombardment of the high-energy ions has induced depolymerization of amylose and amylopectin side chains, resulting in smaller fragments (Figure 2.20). The major products of starch depolymerization are maltose, maltotriose, and maltotetrose. Thirumdas, Kadam, et al. (2017). The acid group is formed due to the depolymerization of the amylopectin side chain (Abd-Allah et al., 1974). Wongsagonsup et al. (2014) studied the effect of input power to create an atmospheric jet argon plasma on tapioca starch suspension. The result showed increasing glycosidic linkages due to crosslinking of granular starch when the plasma was generated at 50 W. On the other hand, the depolymerization effect could result when increasing the power level to 100 W.

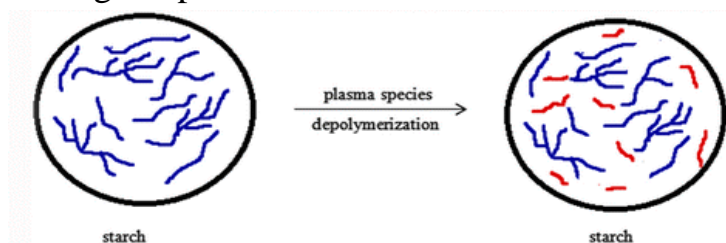


**Figure 2.19** Depolymerization of amylopectin side chains in starch granule  
(Thirumdas, Kadam, et al., 2017)

### 2.5.1.3 Plasma etching

Plasma etching is a surface modification that reactive plasma polishes and volatilizes the starch surface at a macro-to nano-scale level. This mechanism improves starch surface function. Plasma etching increases the material's surface energy, which is one of the main reasons for increased hydrophilicity. Chen et al. (2012) investigated the properties of brown rice—that were treated with glow discharge plasma (1 to 3 kV) for 30 minutes. The result showed that the water adsorption of the rice had increased due to plasma etching on the surface. It was observed that the hydrophilicity was enhanced, resulting in decreased cooking time.

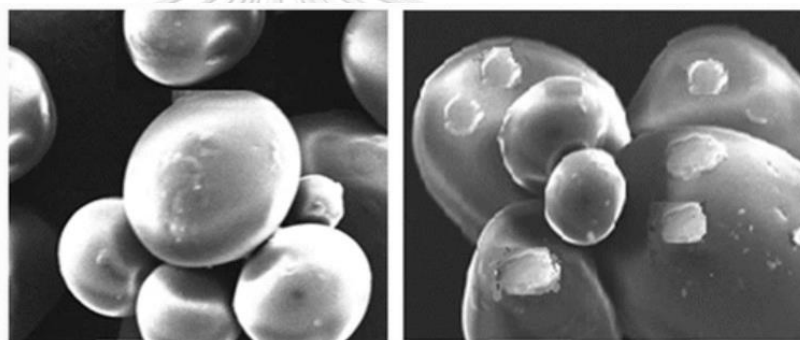


**Figure 2.20** Plasma etching at starch granule by plasma species (Thirumdas, Kadam, et al., 2017)

## 2.5.2 Effect of plasma treatment on starch properties

The starch properties are divided into physical, chemical, and physicochemical properties. The effect of plasma treatment on starch properties depends on the type of feed gas, voltage levels, and treatment time (Grgić et al., 2019).

### 2.5.2.1 Physical properties

#### 2.5.2.1.1 Molecular weight and chemical structure

Zhang et al. (2014) studied the effect of reaction time on the molecular size of oxygen plasma modified maize and potato starch using GPC-MALLS. A decrease in molecular weight and

the radius of gyration of starch was discovered after increasing treatment time from 30 to 60 min at 240V. The reduction in molecular weight implies that the polymeric side chains have been decomposed, resulting in lower molecular weight fragmentation and a change in the molecular mass distribution. Moreover, potato starch is more sensitive to plasma treatment than maize starch. Additionally, Bie et al. (2016) used air dielectric barrier discharge plasma (DBD) to characterize the molecular weight of maize starch. The result showed that plasma treatment significantly lowered the molecular weight of starch through molecular scission in a time-dependent manner.

Moreover, FTIR analysis revealed that as the plasma reaction time increased to 10 min at 70 W, the short-range order on the granule surface was reduced. The carboxyl peak (at  $1720\text{ cm}^{-1}$ ) was produced by plasma treatment with increasing power levels and time. Chaiwat et al. (2016) monitored the content of C-O-C linkage in argon plasma modified tapioca starch by FTIR analysis. The C-O-C peaks indicate the degree of cross-linking or depolymerization. A decrease in C-O-C peaks was found by increasing the production rate to 6 cycles at 60 W.

#### 2.5.2.1.2 Morphology

Plasma etching is the primary mechanism responsible for starch surface morphology. Thirumdas, Trimukhe, et al. (2017) discovered that plasma treatment at 60 W for 10 min resulted in the formation of fissures and cavities on the surface, whereas other treatments had no effect. This agrees with Lii et al. (2002), who found the fissures and holes in starch granules after plasma treatments. These findings point to the irregular shape of starch granules. Zou et al. (2004) described that high-energy electrons could react with argon atoms and turn them into the excited state ( $\text{Ar}^*$ ,  $\text{Ar}^{e-}$ ), which is



highly reactive. These reactive species can further interact with the hydroxyl groups on the helix structure of native starch, resulting in increasing starch hydrophilicity. Okyere et al. (2019) reported that the maltose cross pattern of the treated waxy starch was not changed when compared with native starch after using radio frequency nonthermal plasma.

#### 2.5.2.1.3 Starch crystalline structure

Thirumdas, Trimukhe, et al. (2017) followed the changes in relative crystallinity of rice starch after using cold air plasma modification by wide-angle X-ray scattering (WAXS) technique. They discovered that plasma treatment had no impact on the polymorph type but reduced crystallinity from 43% to 37% when applied plasma treatment at 40 W for 10 min. In support of previous research (Yan et al., 2020), a decrease in relative crystallinity of banana starch was discovered after modification using DBD plasma treatment with increasing voltage levels from 30 to 50V. This treatment induced partial disintegration of starch molecule chains on the surface layers of starch granules, resulting in a lower degree of crystallinity. Moreover, the plasma-treated banana starch tended to be more A-type than the B-type. It has been observed that the A-type crystalline starch amylopectin side chains are usually shorter than the B-type chains.

#### 2.5.2.1.4 pH and color

A decrease in pH of the sample after plasma treatment was described by Thirumdas, Trimukhe, et al. (2017). The oxidation of the molecules at the starch surface could induce the formation of an acidic group or acids such as carboxyl, carbonyl, and peroxide groups that cause pH reduction. This result was consistent with that reported by Lii et al. (2003). The pH reduction in potato starch after plasma treatment was found

when increasing treatment time. The increase in acidity can also be attributed to a rise in FTIR peak intensity at  $1710\text{ cm}^{-1}$  in plasma-treated samples. The functional group related to the stated wave numbers is a carboxylic acid, and the bond is C = O stretching.

Chaple et al. (2020) reported the effect of dielectric barrier discharge (DBD) plasma on the color of modified wheat flour. The  $L^*$  value of treated flour increased, while the  $a^*$  value decreased with increasing treatment time to 30 min at 80 kV. The increase in  $L^*$  and the reduction of  $a^*$  value could be related to the destruction of conjugated double bonds of carotenoids by ozone. This, in turn, increased the whiteness index of the samples.

## 2.5.2.2 Chemical properties

### 2.5.2.2.1 Chemical compositions

The effect of nonthermal plasma treatment on the chemical composition of wheat flour using nonthermal plasma was reported by Bahrami et al. (2016). The treatment did not influence the amount of total non-starch lipids and non-polar and glycolipids. However, lower total free fatty acids and phospholipids were found after plasma treatment. Additionally, the plasma treatment had no significant impact on the total proteins of wheat flour.

### 2.5.2.2.2 Amylose contents

Plasma treatment had a variable effect on the amylose content of starch, based on the type of starch and plasma generation. Higher amylose content of banana starch after plasma treatment was observed by Yan et al. (2020). An increase in the amylose content of treated samples might be resulted from partial destruction of the outer layer of banana starch granules by plasma etching and depolymerization. On the other hand, Banura et al.

(2018) discovered that the amylose content of corn starch was reduced after increasing the treatment time to 20 min at both power levels (40 and 60 W). The reduction in amylose content could be due to the conversion of amylose polymeric chains into simpler sugars such as glucose, maltose, and maltotriose (Thirumdas, Trimukhe, et al., 2017).

### 2.5.2.3 Functional properties

#### 2.5.2.3.1 Pasting properties

Peak viscosity (PV) of banana starch significantly decreased after DBD plasma treatment with increasing treatment time due to the decomposition of the amylopectin chain (Yan et al., 2020). Additionally, nitrogen and helium glow plasma treatment decreased peak viscosity (PV), breakdown (BD), and setback (SB) of potato starch. Chaiwat et al. (2016) reported that the lower breakdown after plasma treatment was due to the dominant effect of cross-linking of starch molecules on the surface of starch granules.

#### 2.5.2.3.2 Swelling power and solubility

Swelling power is a measure of the water holding capacity of starch and has traditionally been used to illustrate the difference between various types of starch (Crosbie, 1991). Solubility refers to the percentage of starch that is leached into the supernatant during the swelling volume determination (Singh et al., 2005). Yan et al. (2020) reported a decrease in swelling power after plasma treatment. The amylopectin in crystalline domains of starch granules might be decomposed, resulting in a decrease in swelling power. Moreover, the results showed higher solubility with increasing treatment times due to the depolymerization. The result was consistent with that reported by Thirumdas, Trimukhe, et al. (2017).

#### 2.5.2.3.3 Rheological properties

The flow behavior of native and treated tapioca starches was described by Chaiwat et al. (2016). After plasma treatment, the consistency index (K) of starch paste was higher than native tapioca starch. This could be explained by the induced cross-linking effect by plasma treatment. On the other hand, Wongsagonsup et al. (2014) found that increasing the power level to 100 W resulted in a lower K value for plasma-treated granular tapioca starch. They explained that the K value reduction could be because of depolymerization. The flow behavior index (n) was enhanced or decreased depending on the process condition. Wongsagonsup et al. (2014) investigated the dynamic viscoelastic properties of jet argon plasma treated tapioca starch. The result showed that plasma-treated samples at 50 W gave a stronger gel structure, with lower  $\tan \delta$ , than native tapioca starch (increased  $G'$  and  $G''$  of starch) due to a cross-linking mechanism.



## Chapter 3 Materials and Methods

### 3.1 Materials

The native tapioca starch used for the experiment was supported by Thanawat Quality Starch Co., Ltd. Chaiyaphum, Thailand. Argon gas (purity 99.999%) was purchased from Thai Inter Gas & Chemical Supply Co., Ltd. Samut Prakan, Thailand. Helium gas (purity 99.995%) was purchased from Thonburiwattana Ltd. Bangkok, Thailand. All other reagents and solvents were analytical grade and used as purchased.

### 3.2 Methods

#### 3.2.1 Sample preparation for nonthermal plasma treatment

A nonthermal dielectric barrier discharge (DBD) plasma system was used in this study (Figure 3.1). Argon (Ar) or helium (He) was used for plasma generation under atmospheric pressure. In this study, starch (approximately 5 g, 10.97% wb of moisture content) was placed in a sample holder in the reactor chamber. The samples were treated with the Argon (Ar) or helium (He) glow-plasma at two different high voltage levels (10 kV and 15 kV) for various treatment times (5, 10, and 15 min). Hantek DSO5102P Digital Storage Oscilloscope (Qingdao Hantek Electronic Co., Ltd. Shandong, China) was used to monitor the system's input current and voltage characteristics. The discharge distance was set at 1 cm. The samples were named native tapioca starch (NTS), Ar10 kV-5 min, Ar10kV-10 min, Ar10kV-15min, Ar15kV-5 min, Ar15kV-10 min, and Ar15kV-15 min, He10kV-5 min, He10kV-10 min, He10 kV-15min, He15 kV-5 min, He15 kV-10 min, and He15kV -15 min, respectively. The treated samples were filled in a laminated plastic bag (PET/AL/LDPE) and kept in a desiccator at ambient temperature for further analyses.

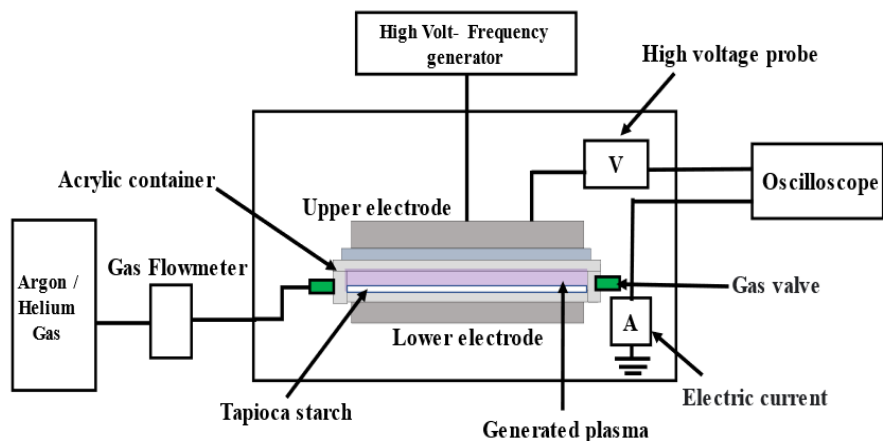


**Figure 3.1** Schematic diagram of nonthermal dielectric barrier discharge plasma system

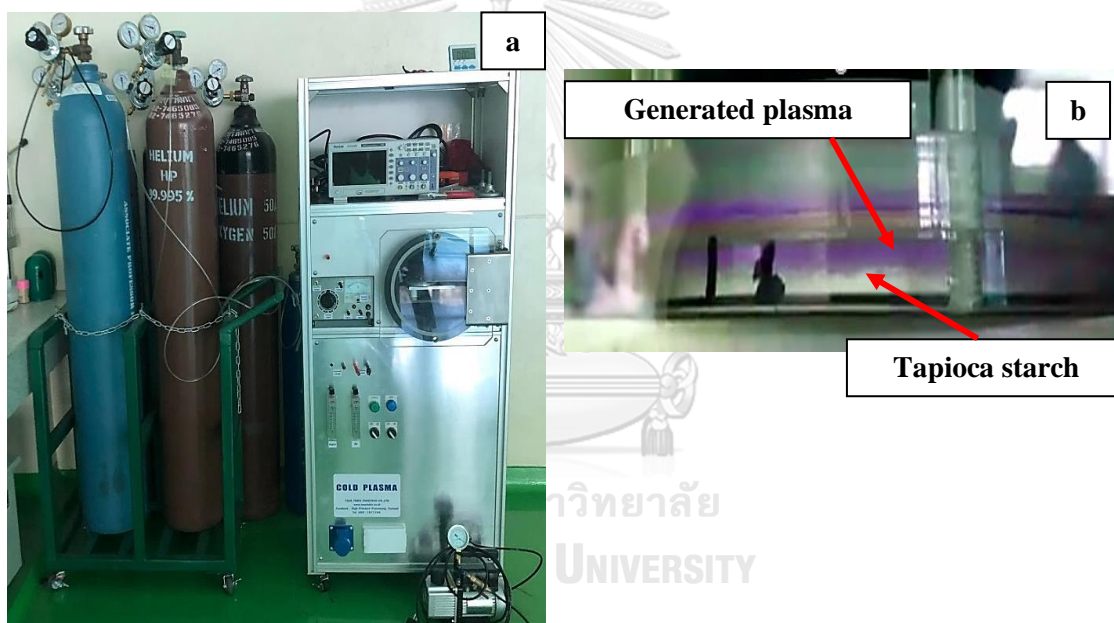


**Figure 3.2** A nonthermal dielectric barrier discharge (DBD) plasma machine (a) and solid-state modification of tapioca starch using DBD plasma machine (b)

### 3.2.2 Determination of physical properties

#### 3.2.2.1 pH

The pH value of 0.5% aqueous tapioca starch solution was measured by a pH meter (SevenCompact™ S220, Toledo, Malaysia).

#### 3.2.2.2 Color

A colorimeter (Konica Minolta model CR-400, Osaka, Japan) was used for measuring the color of samples. The values were expressed as  $L^*$  (lightness),  $a^*$  (redness to greenness), and  $b^*$  (yellowness to blueness) values (see appendix A1 for procedures). Whiteness index (WI) was calculated by equation 3.1 (Li & Lee, 1996).

$$WI = \sqrt{(100 - L^*)^2 + (a^*)^2 + (b^*)^2} \quad (3.1)$$

#### 3.2.2.3 Surface morphology

The morphology of starch granules was observed by a scanning electron microscope (Model IT5R, JEOL Co., Ltd. Japan) at 700x and 1500x magnification with the procedure of Scientific and Technological Research Equipment Centre (STREC), Chulalongkorn University, Thailand (see appendix A2).

#### 3.2.2.4 Birefringence pattern

The image of the starch samples under polarized light was obtained using the Olympus BX51 light microscope (Melville, NY., USA) connected to a digital camera at 400x and 1000x magnification (see appendix A3).

#### 3.2.2.5 X-ray diffraction pattern

The crystalline structure of native and treated starch was recorded using an X-ray diffractometer (Model D8 Discover, Bruker AXS, Germany), and the degree of crystallinity was calculated by TOPAS software (Bruker, USA) with the procedure of Scientific and Technological

Research Equipment Centre, Chulalongkorn University, Thailand (see appendix A4).

### 3.2.3 Determination of chemical properties

#### 3.2.3.1 Chemical composition of native tapioca starch

Native tapioca starch was prepared for proximate analyses following AOAC (2000) (see appendix A5-A10). Carbohydrate content was calculated following AOAC (2000)

#### 3.2.3.2 Apparent amylose

The amylose content of all samples was determined by the iodine colorimetry through the spectrophotometric detection following the method of Juliano (1971) with minor modification (see appendix A11)

#### 3.2.3.3 Reducing sugar

The reducing sugar of all samples was determined by the Nelson-Somogyi method, following the method of Trithavisup et al. (2019) as mentioned in appendix A12.

#### 3.2.3.4 Fourier transform infrared (FTIR) spectroscopy

The functional groups of all samples were analyzed by Fourier Transform Infrared Spectrometer (Thermo Scientific, model Nicolet 6700, USA) in the range 400 – 4000  $\text{cm}^{-1}$  using KBr as the ambient temperature following the method description of Yan et al. (2020) (see appendix A13).

#### 3.2.3.5 Molecular weight analysis

The mass molecular weight of amylose and amylopectin of native and modified tapioca starch was determined by a high-performance size-exclusion chromatography (Water e2695, Separations module, Waters Corporation, USA) equipped with multi-angle laser light scattering (MALLS, DAWN HELEOS, Wyatt Technology Corp., Santa Barbara, CA) and refractive index detector (Waters 2414, Waters Corporation, USA) (HPSEC-MALLS-RI system) following the method of Yoo and Jane (2002) with a slight modification as described in appendix A14.



### 3.2.4 Determination of functional properties

#### 3.2.4.1 Pasting properties

The native and treated starch suspensions (14%, wb of moisture content) were pasted under constant shearing and heating following the method described in AACC (2000) using the Rapid Visco Analyzer (series 4D, Newport Scientific, Australia) as described in appendix A15.

#### 3.2.4.2 Swelling power and solubility

Swelling power and solubility of all samples at constant temperatures (60°C, 70°C, 80°C, and 90°C) were measured according to (Schoch, 1964) (see appendix A16).

#### 3.2.4.3 Water binding capacity

Water binding capacity was measured following the method of Medcalf (1965) (see appendix A17).

#### 3.2.4.4 Rheological properties

##### 3.2.4.4.1 Viscoelastic properties

Viscoelastic properties of gelatinized starch pastes (6%, w/w) were determined by using MCR 102 rheometer (Anton Paar, Graz, Austria) with the method modified from Wongsagonsup et al. (2014) (see appendix A 18).

##### 3.2.4.4.2 Flow properties

Viscoelastic properties of gelatinized starch pastes (6%, w/w) were determined by using MCR 102 rheometer (Anton Paar, Graz, Austria) with the method modified from Chaiwat et al. (2016) (see appendix A19). The parallel plate geometry was programmed to ramp up and down in 2 cycles with shear rates of 1–500 s<sup>-1</sup> in each cycle. The data of shear stress and shear rate of the downward curve was used to characterize the flow behavior of the sample and was fitted to the Herschel-Bulkley model (Equation 3.2)

$$\sigma = \sigma_0 + K(\dot{\gamma})^n \quad (3.2)$$

Where  $\sigma$  is the shear stress (Pa),  $\sigma_0$  is yield stress,  $\dot{\gamma}$  is the shear rate ( $s^{-1}$ ),  $K$  is the consistency index ( $Pa.s^n$ ),  $n$  is the flow behavior index

### 3.2.5 Statistical analysis

A factorial experiment in a complete randomized design (CRD) was used in this study. The effect of plasma treatments on the properties of tapioca starch was analyzed by one-way analysis of variance (ANOVA) and Duncan's new multiple range tests (DNMRT) for comparing differences in the mean values at a 95% confidence interval. The effects of different feeding gases, voltage levels, and treatment times on the properties of tapioca starch were analyzed by Two-way ANOVA at a 95% confidence interval. All analyses were carried out using the IBM® SPSS® software (Version 19.0, SPSS Inc., Chicago, IL, USA). All measurements were done in triplicate, except for the molecular weight of amylose and amylopectin (duplicate), X-ray diffraction analysis (duplicate), and rheological properties (duplicate).

## Chapter 4 Results and Discussions

### 4.1 Effect of types of feed gas, voltage levels, and treatment time on physical properties of treated tapioca starch using nonthermal DBD plasma

#### 4.1.1 pH

The pH value of native and treated tapioca starch samples by plasma treatment is shown in Table 4.1. The data shows that the average pH value of native and treated samples was 4.54 to 5.75. The treated samples had a significant decrease in pH value compared to the native sample. ( $P < 0.05$ ). Increasing voltage levels and treatment time of helium plasma modified samples at 10 kV to 15 kV from 5 to 15 minutes produced samples with significantly lower pH values than the native sample ( $P < 0.05$ ). The lowest pH value was discovered in a treated sample with helium plasma at 15 kV for 15 minutes (He15kV-15min) ( $P < 0.05$ ). A decrease in pH of the sample after plasma treatment was described by Thirumdas, Kadam, et al. (2017). The amylopectin degradation after plasma treatment due to depolymerization could lead to formic acid. Moreover, the oxidation of the molecules at the starch surface could induce the formation of an acidic group or acids that cause pH reduction. This result was consistent with Lii et al. (2003), who found the pH reduction in potato starch after plasma treatment with increasing treatment time. It was found that helium plasma-treated samples had a lower pH value than argon plasma-treated samples. It might be due to the lower atomic number of helium gas, which produces plasma easily and gives higher energy of ion than argon gas. Moreover, Schweigert et al. (2019) described that the metastable state of helium had higher energy than argon and caused helium plasma to generate more reactive species than argon plasma.

The effects of types of the feed gas, voltage levels, and their interaction on pH value of plasma-treated samples using two-way ANOVA are shown in appendix C.67. Statistical analysis reveals that both types of feed gas, voltage levels, and their interactions significantly affected the pH value ( $P < 0.05$ ).

#### 4.1.2 Color

Table 4.1 presents the color parameters and whiteness index of native and modified starches under different conditions. All treated samples had a slight increase in  $L^*$  and  $b^*$  values. The  $L^*$  and  $b^*$  values of treated samples with helium plasma were significantly higher than those treated with argon plasma ( $P < 0.05$ ). For  $a^*$  values, the treated samples with argon plasma had a reduction in  $a^*$ , while the treated samples with helium plasma had an increase in  $a^*$ . There was no significant change in the calculated whiteness index after argon plasma treatment ( $P \geq 0.05$ ). A significant decrease in calculated whiteness was found in the treated samples with helium plasma ( $P < 0.05$ ). The sample treated with helium plasma at 15 kV for 15 minutes (He15kV-15min) showed the lowest whiteness index ( $P < 0.05$ ). This might be due to the plasma etching mechanism caused by active species on the starch surface that changed the light reflection ability of the treated starch granule, hence color change. Chaiwat et al. (2016) found a slight increase in  $L^*$  and  $b^*$  values after increasing the cycles in the plasma system, while a decrease in the  $a^*$  value was observed. In addition, Chaple et al. (2020) found that the  $L^*$  value of treated flour increased with increasing treatment time, while a decrease in the  $a^*$  value was discovered.

When comparing helium and argon plasma, it was found that helium plasma could reduce the whiteness index of treated samples. High-energy reactive species in the helium plasma could be generated. This causes more plasma etching on the surface of the starch granule. However, they did not show a negative effect in color after plasma treatment.

The effects of types of feed gas, voltage levels, and their interaction on the color and whiteness index of plasma-treated samples using two-way ANOVA are shown in appendixes C.63 to C.67. The result shows that the value of  $L^*$  was significantly influenced by different gas and treatment times ( $P < 0.05$ ). For  $a^*$  value, treatment times and their interaction between types of feed gas and voltage levels had no significant influence ( $P \geq 0.05$ ). Their interaction of types of feed gas, voltage levels, and treatment times had no significant influence on  $b^*$  values and whiteness index ( $P \geq 0.05$ ).

**Table 4.1** Color values ( $L^*$ ,  $a^*$ ,  $b^*$ ), whiteness index, and pH of native and DBD plasma-treated tapioca starch with various conditions.

Samples	Color values			Whiteness index	pH
	$L^*$	$a^*$	$b^*$		
NTS	98.51 <sup>e</sup> ± 0.06	0.20 <sup>cd</sup> ± 0.01	1.36 <sup>f</sup> ± 0.03	97.94 <sup>a</sup> ± 0.11	5.75 <sup>a</sup> ± 0.03
Ar10kV-5min	99.07 <sup>cd</sup> ± 0.15	0.12 <sup>f</sup> ± 0.02	1.73 <sup>de</sup> ± 0.01	98.05 <sup>a</sup> ± 0.14	5.49 <sup>c</sup> ± 0.02
Ar10kV-10min	98.55 <sup>de</sup> ± 0.42	0.13 <sup>ef</sup> ± 0.01	1.96 <sup>d</sup> ± 0.03	96.97 <sup>a</sup> ± 0.63	5.04 <sup>e</sup> ± 0.04
Ar10kV-15min	99.20 <sup>c</sup> ± 0.08	0.15 <sup>de</sup> ± 0.01	1.71 <sup>de</sup> ± 0.03	98.21 <sup>a</sup> ± 0.11	5.23 <sup>d</sup> ± 0.04
Ar15kV-5min	99.15 <sup>a</sup> ± 0.13	0.16 <sup>def</sup> ± 0.01	1.65 <sup>e</sup> ± 0.04	98.26 <sup>a</sup> ± 0.13	5.25 <sup>d</sup> ± 0.02
Ar15kV-10min	99.05 <sup>cde</sup> ± 0.69	0.18 <sup>cd</sup> ± 0.01	1.65 <sup>e</sup> ± 0.02	98.01 <sup>a</sup> ± 0.77	5.20 <sup>d</sup> ± 0.05
Ar15kV-15min	99.31 <sup>c</sup> ± 0.10	0.18 <sup>cd</sup> ± 0.01	1.78 <sup>de</sup> ± 0.07	98.16 <sup>a</sup> ± 0.08	5.62 <sup>b</sup> ± 0.03
He10kV-5min	102.52 <sup>b</sup> ± 0.57	0.22 <sup>bc</sup> ± 0.03	2.46 <sup>c</sup> ± 0.06	93.66 <sup>b</sup> ± 1.50	5.30 <sup>d</sup> ± 0.08
He10kV-10min	103.13 <sup>a</sup> ± 0.21	0.20 <sup>cd</sup> ± 0.02	2.60 <sup>bc</sup> ± 0.14	91.70 <sup>c</sup> ± 0.81	5.07 <sup>e</sup> ± 0.14
He10kV-15min	103.11 <sup>a</sup> ± 0.04	0.26 <sup>b</sup> ± 0.07	2.65 <sup>bc</sup> ± 0.33	91.57 <sup>c</sup> ± 0.74	4.74 <sup>f</sup> ± 0.04
He15kV-5min	102.89 <sup>ab</sup> ± 0.25	0.34 <sup>a</sup> ± 0.06	2.64 <sup>bc</sup> ± 0.21	92.25 <sup>c</sup> ± 0.67	5.08 <sup>e</sup> ± 0.06
He15kV-10min	102.85 <sup>ab</sup> ± 0.30	0.31 <sup>a</sup> ± 0.03	2.78 <sup>b</sup> ± 0.17	91.98 <sup>c</sup> ± 0.89	4.85 <sup>f</sup> ± 0.05
He15kV-15min	103.17 <sup>a</sup> ± 0.11	0.16 <sup>def</sup> ± 0.01	3.25 <sup>a</sup> ± 0.21	89.64 <sup>d</sup> ± 0.56	4.54 <sup>g</sup> ± 0.15

Means ± standard deviation (n=3) with different letters within a column are significantly different (P<0.05).  $L^*$  as 0 and 100 corresponded to black and white,  $a^*$  values- +a (reddish) and -a\* (greenish) and  $b^*$  values - +b\* (yellowish) and -b\* (bluish).

### 4.1.3 Surface morphology

The morphology of native tapioca starch before and after DBD plasma treatment was characterized using a scanning electron microscope at 700x and 1500x magnification (Figures 4.1 to 4.2). From Figure 4.1, the native and modified tapioca starch granules treated using plasma at 10 kV for 5 minutes are smooth-surfaced with truncated globular shape with 5  $\mu\text{m}$  – 10  $\mu\text{m}$  of size ranging. After argon plasma treatments at 10 kV for 10 minutes to 15 kV for 15 minutes (Figures 4.1 C1 to G2), the granules' surface is clearly dented, possibly due to plasma etching. In the same way, the damaged starch granules were observed after modification with helium plasma at 10 kV for 5 minutes and beyond (Figures 4.2 A1 to F2).

This result indicated that helium plasma could more severely damage starch granules than argon plasma. Higher energy and reactive species from helium plasma can interact with starch granules effectively through depolymerization and plasma etching, resulting in dented granules from the beginning of the 5-minute treatment time.

Zou et al. (2004) reported that during the treatment, high-energy electrons could react with gas atoms and turn them to the excited state, which is highly reactive. These reactive species can further interact with the hydroxyl groups on the helix structure of native starch, resulting in an increase in starch hydrophilicity. Crosslinking of the hydroxyl group between two glucose units could also be promoted. This result was consistent with Lii et al. (2003), who stated that the starch granule was changed remarkably after plasma treatments. Similarly, Guo et al. (2022) found cracks and pores on the starch surface due to plasma etching. The effect of plasma etching on the pasting properties of tapioca starch was noted in our study and is to be discussed later in the following section.

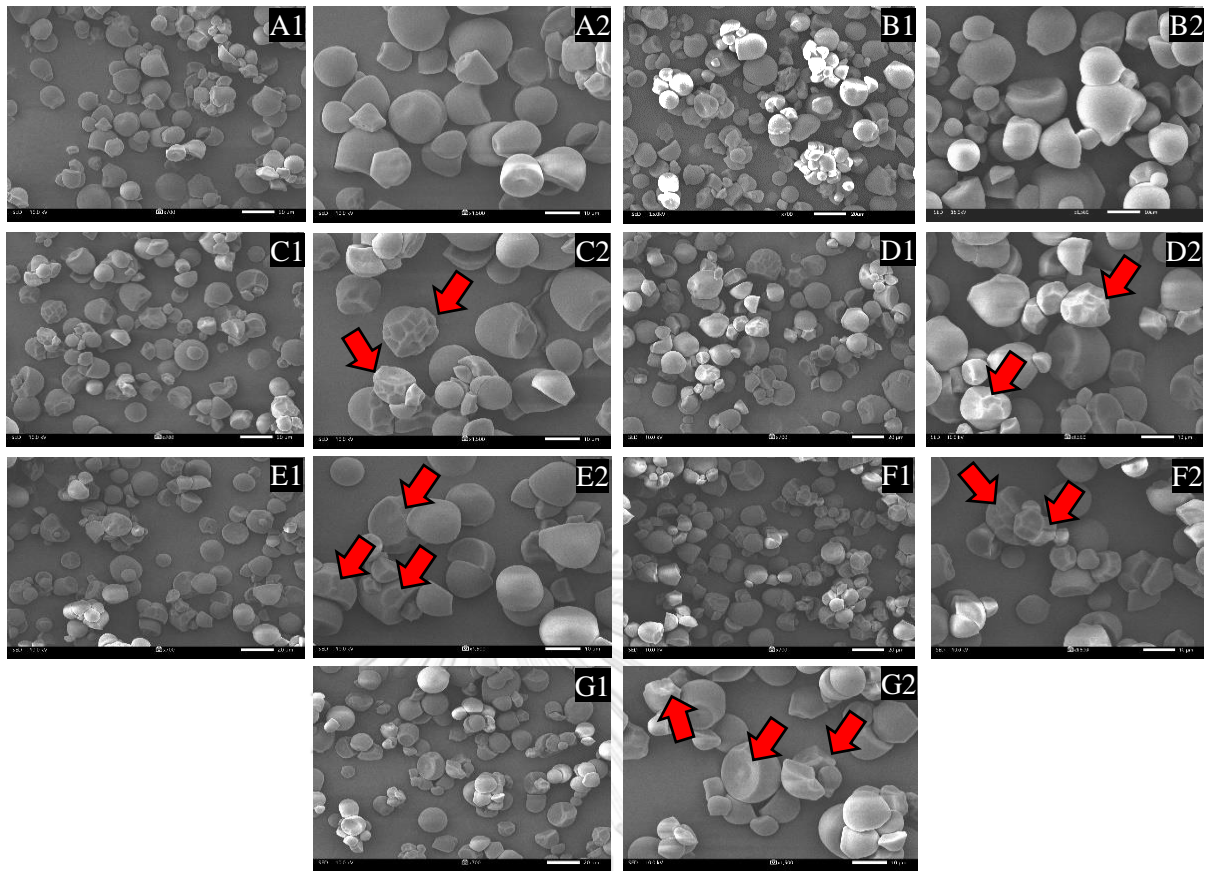


**Figure 4.1** Scanning electron micrographs (SEM) of native and argon plasma modified tapioca starches. **1** and **2** represent images at 700x and 1500x magnification, respectively. **A** native starch, **B** 10 kV in 5 min, **C** 10 kV in 10 min, **D** 10 kV in 15 min, **E** 15 kV in 5 min, **F** 15kV 10 min, and **G** 15 kV 15min. Arrows indicate varying degrees of distortions after argon DBD plasma treatment.

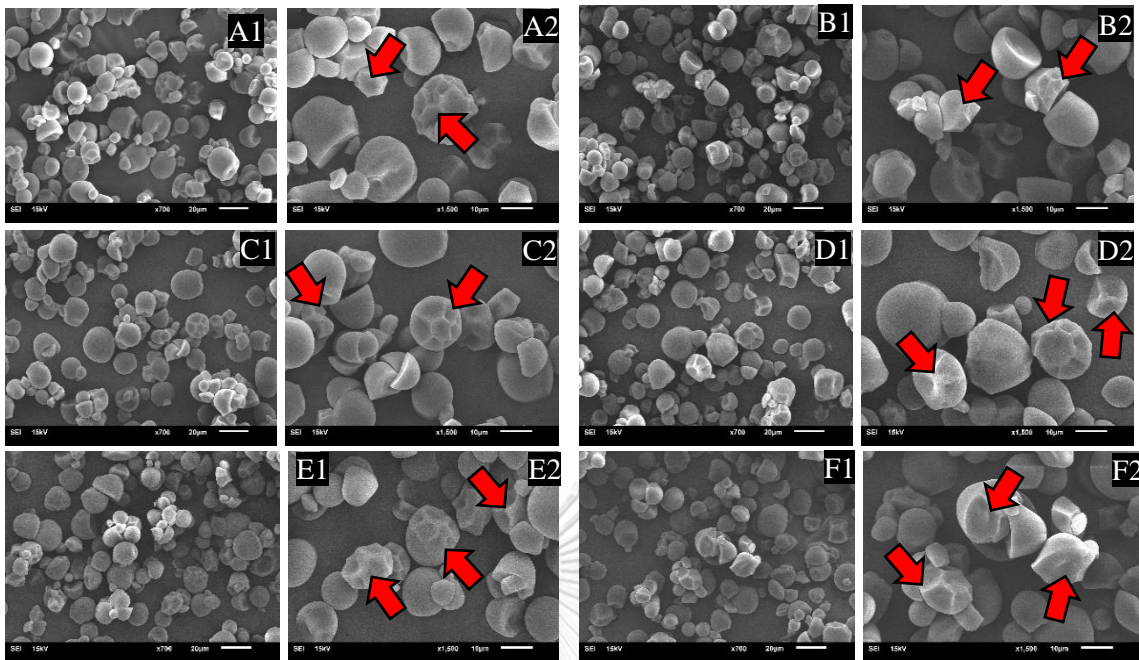


**Figure 4.2** Scanning electron micrographs (SEM) of helium plasma modified tapioca starches. **1** and **2** represent images at 700x and 1500x magnification, respectively. **A** 10 kV in 5 min, **B** 10 kV in 10 min, **C** 10 kV in 15 min, **D** 15 kV in 5 min, **E** 15kV 10 min, and **F** 15 kV 15min. Arrows indicate varying degrees of distortions after helium DBD plasma treatment.

#### 4.1.4 Birefringence pattern

Figures 4.3 and 4.4 display polarized light micrographs of native starch and treated tapioca starch granules. A maltese cross can be observed when starch granules are exposed under polarized light since starch granules are semi-crystalline, i.e., they contain both crystalline and amorphous parts (Alcázar-Alay & Meireles, 2015). The maltese cross pattern of the treated samples with plasma (Figure 4.3 B1 to G2) and helium plasma (Figure 4.4 A1 to F2) was not changed compared with native starch. This result is in reasonable agreement with a previous study (Guo et al., 2022), which improved the properties of potato starch using DBD plasma treatment. The result confirms that the samples did not undergo significant gelatinization and crystalline region breakdown from nonthermal DBD plasma modification.



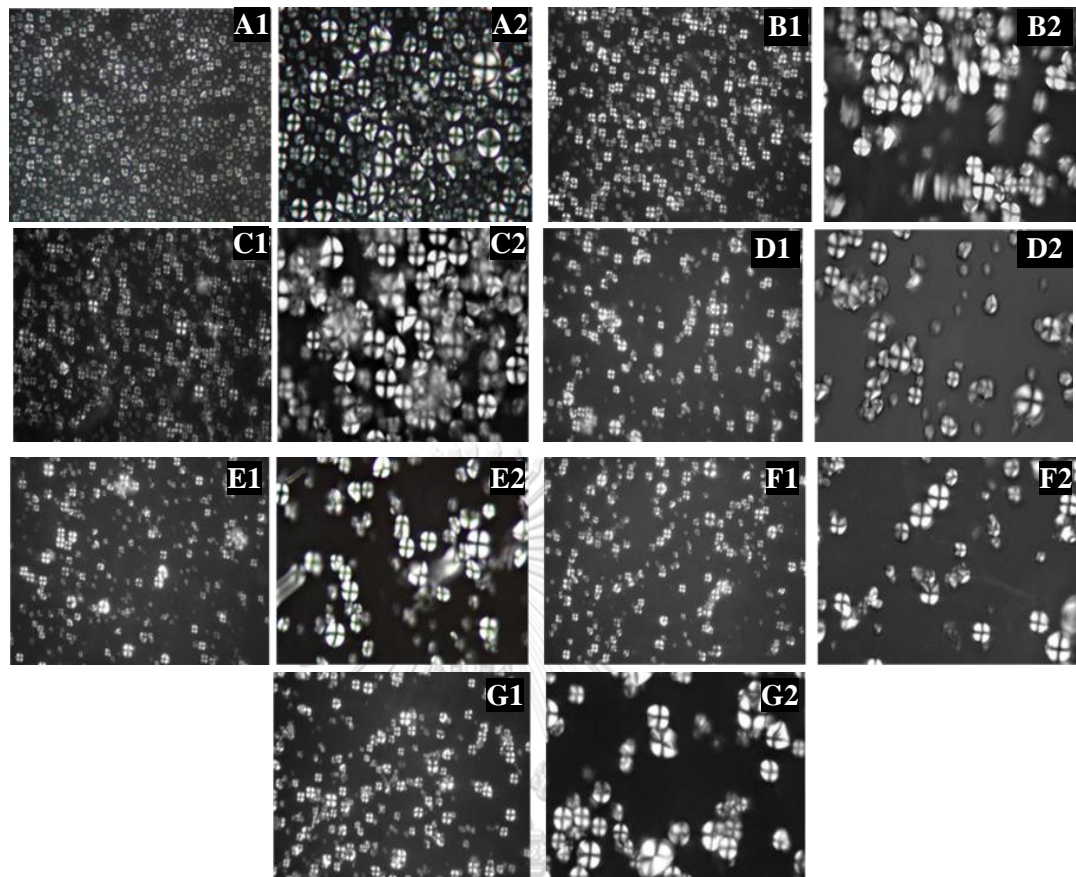


**Figure 4.3** Native, Ar10kV-5 min, Ar10kV-10 min, Ar10kV-15 min, Ar15kV-5 min, Ar15kV-10min, Ar15kV-15min of tapioca starch viewed by polarized light microscopy (A, B, C, D, E, F, and G respectively). 1 and 2 represent images at 400x and 1000x magnification, respectively.

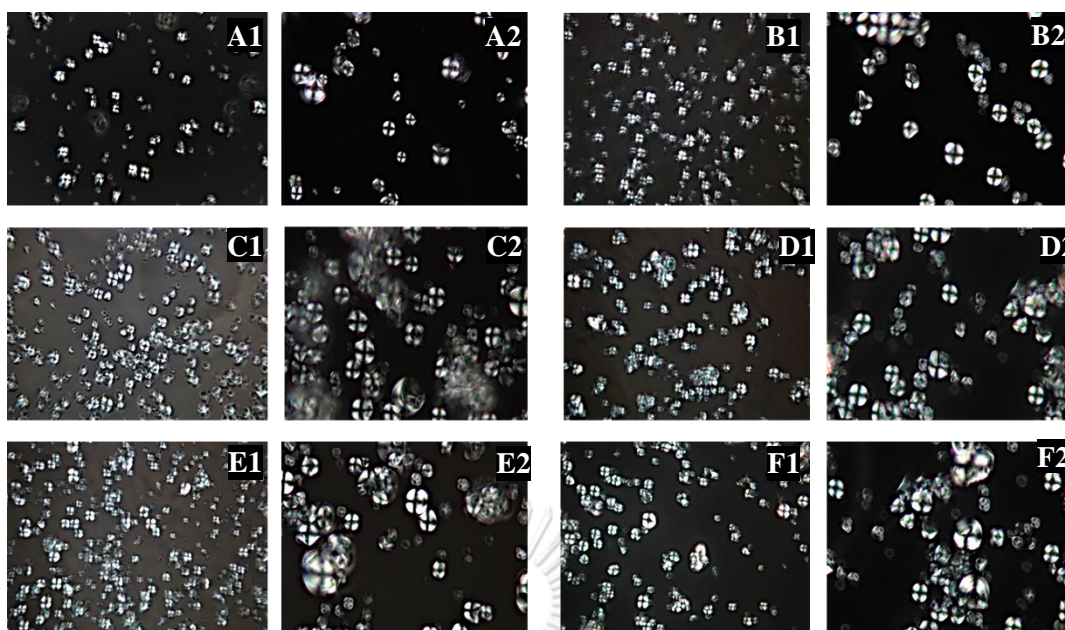


**Figure 4.4** He10kV-5min, He10kV-10min, He10kV-15min, He15kV-5min, He 15kV-10min, He15kV-15min of tapioca starch viewed by polarized light microscopy (A, B, C, D, E, and F respectively). 1 and 2 represent images at 400x and 1000x magnification, respectively

#### 4.1.5 X-ray diffraction pattern

The X-ray diffraction pattern (XRD) of tapioca starch with and without plasma modification is shown in Figure 4.5. All samples showed a characteristic C-type diffraction pattern that is a combination of the A and B-type polymorphs. The result agrees with previous research by Dome et al. (2020). The XRD pattern of native and modified showed strong peaks ( $2\theta$ ) at  $3.67^\circ$ ,  $9.95^\circ$ ,  $11.35^\circ$ ,  $15.19^\circ$ ,  $17.16^\circ$ ,  $17.19^\circ$ ,  $23.01^\circ$ , and  $26.39^\circ$ , respectively. After plasma modification, the C-type pattern of starch samples remained unchanged, indicating that the damage to the crystalline structure of starch granules was insufficient. This result is consistent with the birefringence of treated samples observed after argon and helium-plasma modification (Figures 4.3-4.4).

The relative crystallinity of samples calculated from the ratio of the area of all crystalline peaks to the total area is displayed in Table 4.2. The degree of crystallinity in native and treated starch ranged from 27.30 to 34.50%. The native sample had the highest relative crystallinity ( $P < 0.05$ ). In comparison to native starch, the treated samples had a significantly lower relative crystallinity ( $P < 0.05$ ).

Depolymerization and plasma etching of the starch surface by reactive argon and helium plasma species resulted in a decrease in relative crystallinity. Moreover, a longer period of mechanical activation causes amorphization of the starch crystalline structure of A-, B-, and C-type polymorphs, resulting in a lower relative crystallinity (Dome et al., 2020). A similar result was found in Yan et al. (2020). After argon plasma modification, there was no significant difference in relative crystallinity ( $P \geq 0.05$ ), while the reduction in relative crystallinity was discovered after using helium plasma ( $P < 0.05$ ). The metastable state of helium had higher energy than argon and caused helium plasma to generate more reactive species than argon plasma (Schweigert et al., 2019). This presumption confirms that the crystalline region of the starch granule can be more damaged by higher energy and reactive species from helium plasma by depolymerization and plasma etching.

Appendix C.68 shows a two-way ANOVA analysis for the relative crystallinity of plasma-treated starch. The result revealed that the interaction of gas types and voltage levels had no significant influence on the relative crystallinity of treated samples ( $P \geq 0.05$ ). Similarly, their interaction of gas types and treatment times showed an insignificant influence on relative crystallinity ( $P \geq 0.05$ ).

**Table 4.2** Relative crystallinity of native and treated starch granules by using plasma treatment with different conditions

Samples	Relative crystallinity (%)
NTS	34.50 <sup>a</sup> ± 0.14
Ar10kV-5min	33.00 <sup>b</sup> ± 0.85
Ar10kV-10min	33.25 <sup>b</sup> ± 0.64
Ar10kV-15min	32.75 <sup>b</sup> ± 0.35
Ar15kV-5min	32.15 <sup>b</sup> ± 1.06
Ar15kV-10min	32.95 <sup>b</sup> ± 0.64
Ar15kV-15min	32.25 <sup>b</sup> ± 0.64
He10kV-5min	27.45 <sup>de</sup> ± 0.07
He10kV-10min	28.70 <sup>cd</sup> ± 0.28
He10kV-15min	27.30 <sup>e</sup> ± 0.28
He15kV-5min	27.95 <sup>cde</sup> ± 0.64
He15kV-10min	27.30 <sup>e</sup> ± 0.14
He15kV-15min	29.20 <sup>c</sup> ± 0.71

Means ± standard deviation (n=2) with different letters within a column are significantly different (P<0.05).

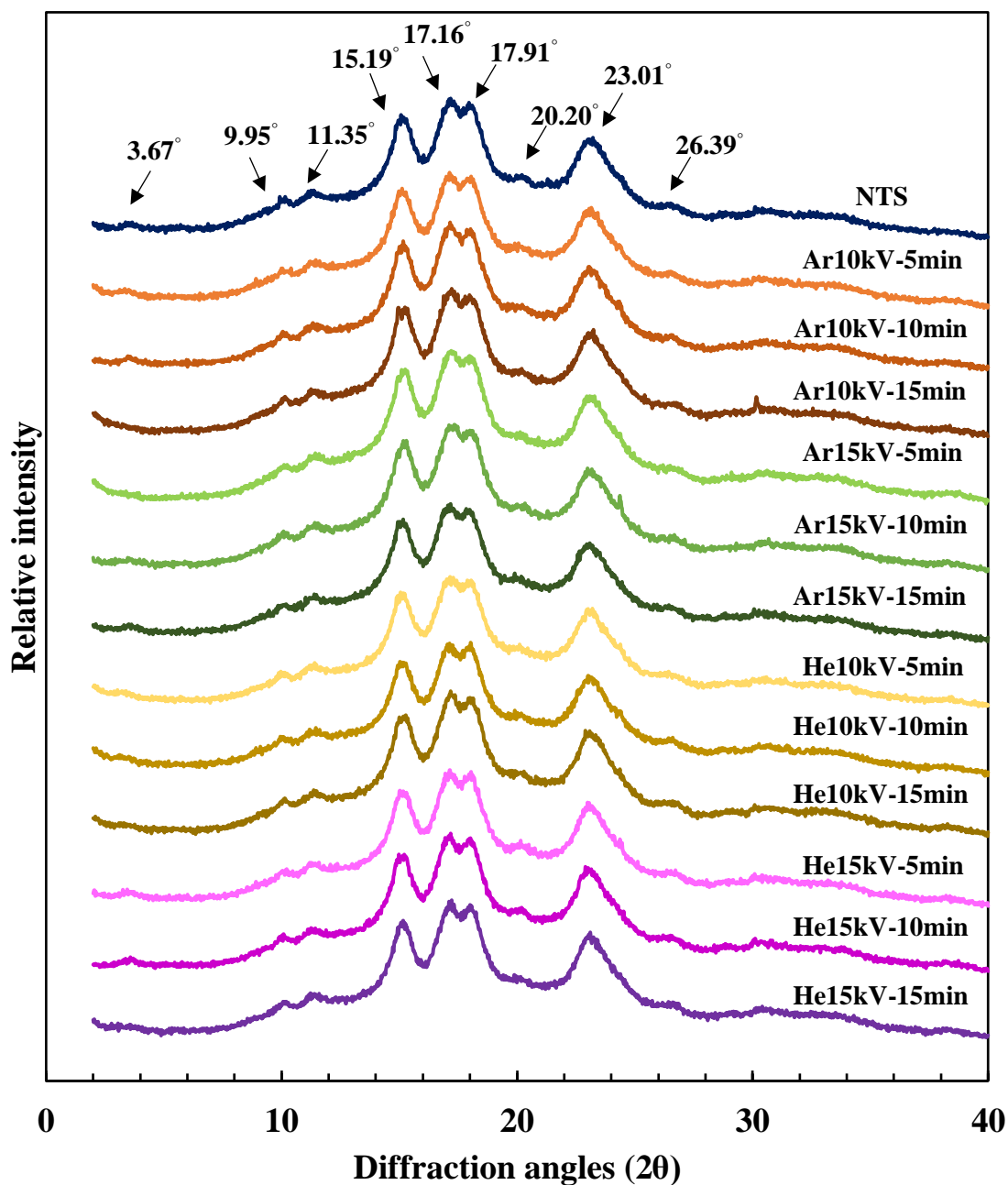


**Figure 4.5** X-ray diffractogram of starch granule from native and treated tapioca starch by using plasma modification with different conditions. The arrows indicate the diffraction peak angles ( $2\theta$ ) of starch samples.

## 4.2 Effect of types of the feed gas, voltage levels, and treatment time on chemical properties of treated tapioca starch using nonthermal DBD plasma

### 4.2.1 Chemical composition of native tapioca starch

Native tapioca starch consists of moisture, protein, fat, ash, crude fiber, and carbohydrates, as shown in Figure 4.3. The native tapioca starch showed the highest carbohydrate content (99.06% db), followed by moisture (10.97% wb), protein (0.46% db), fat (0.18% db) %, crude fiber (0.15% db), and ash content (0.14% db).

**Table 4.3** Chemical compositions of native tapioca starch

Composition	Native tapioca starch
Moisture content (% , wb)	10.97 ± 0.19
Protein (% , db)	0.46 ± 0.04
Fat (% , db)	0.18 ± 0.02
Ash (% , db)	0.14 ± 0.02
Crude fiber (% , db)	0.15 ± 0.02
Carbohydrate (% , db)	99.06 ± 0.05

Mean (±standard deviation) of triplicate analysis.

### 4.2.2 Moisture content

Table 4.4 shows the moisture content of starch before and after plasma modification. The moisture contents of native and treated samples were in the range of 8.67 to 10.97% wb. The data obtained showed no significant change in the sample's moisture content when treating the sample using argon plasma at an increasing voltage level and treatment time ( $P \geq 0.05$ ). This could be due to the short reaction time of argon plasma-treated tapioca starch without vacuum applied during the treatment. On the other hand, a significant reduction in moisture content was discovered when treating the sample using helium plasma ( $P < 0.05$ ). A helium plasma gave a higher electron temperature and a lower electron density than an argon plasma under atmospheric pressure (Jonkers, 2002). This reason is probably due to the interaction of high energy of reactive species and water in the starch molecule, resulting in released water from the starch molecule. Chaiwat et al. (2016) reported that the

moisture content was reduced by the effect of energy generated by plasma reaction combined with the applied vacuum.

Appendix C.69 displays the effects of the types of feed gas, voltage levels, treatment times, and their interaction on the moisture content of plasma-treated samples using two-way ANOVA. This result revealed that the moisture content of the treated sample was significantly affected by gas types and voltage levels ( $P < 0.05$ ). Moreover, the interaction of the gas type and the voltage level had a significant effect on moisture content ( $P < 0.05$ ).

#### 4.2.3 Apparent amylose

The apparent amylose content of native and the plasma modified tapioca starch is displayed in Table 4.4. The native and modified samples contained 22.63% to 28.24% apparent amylose. Zhu (2015) reported that the amylose content of tapioca starch ranged from 0-30.3%, depending on sources and analytical techniques. This study found that modified samples using argon plasma were significantly different from the native sample ( $P < 0.05$ ). Increasing treatment time from 5 to 15 minutes at 10 kV of argon plasma caused the amylose content to increase from 24.35% to 28.16% ( $P < 0.05$ ). The same pattern was observed at a higher voltage of 15 kV, with amylose content increasing from 24.58% to 28.24% ( $P < 0.05$ ). Nevertheless, there was no significant difference between the starch samples modified with 10 kV and 15 kV at the same treatment time ( $P < 0.05$ ).

The modified samples at 10 kV had higher apparent amylose than native ( $P < 0.05$ ) for helium plasma treatment. There were no significant differences between the samples modified for 10 and 15 minutes ( $P < 0.05$ ). The increase in amylose content could be related to the depolymerization of amylopectin side chains and plasma etching at the starch granule surface, resulting in smaller amylose fragments. These findings are similar to those reported by Banura et al. (2018) and Yan et al. (2020). Banura et al. (2018) reported that the high amylopectin content could contribute to the higher amylose content after plasma treatment.

In contrast, increasing treatment time from 5 to 15 minutes at 15 kV of helium plasma could reduce the apparent amylose content from 25.36% to 23.01%. This could be due to the depolymerization

of the amylose chains caused by reactive species bombardment in the helium plasma. The decomposition of starch granule surface after plasma treatment was strongly consistent with changes in the surface morphology of granules in Figures 4.1 and 4.2.

The effects of the types of feed gas, voltage levels, and their interactions on the apparent amylose content of plasma-treated samples using two-way ANOVA are shown in appendix C.70. The apparent amylose of the treated sample was significantly affected by the types of feed gas and treatment time ( $P < 0.05$ ). Nevertheless, the voltage level and the interaction of gas types and voltage levels had no significant influence on the plasma-treated samples ( $P \geq 0.05$ ).

**Table 4.4** Moisture content, apparent amylose contents, and reducing sugar of native and DBD plasma-treated tapioca starch with various conditions

Samples	Moisture content (% , wb)	Apparent amylose content (% of starch)	Reducing sugar ( $\mu\text{g/g}$ dry starch)
NTS	10.97 <sup>a</sup> $\pm$ 0.19	22.63 <sup>f</sup> $\pm$ 0.47	26.34 <sup>ij</sup> $\pm$ 0.86
Ar10kV-5min	10.78 <sup>a</sup> $\pm$ 0.57	24.37 <sup>cd</sup> $\pm$ 0.42	35.22 <sup>ij</sup> $\pm$ 0.93
Ar10kV-10min	10.62 <sup>a</sup> $\pm$ 0.50	25.25 <sup>bc</sup> $\pm$ 0.33	63.32 <sup>gh</sup> $\pm$ 1.33
Ar10kV-15min	10.73 <sup>a</sup> $\pm$ 0.43	28.65 <sup>a</sup> $\pm$ 0.51	143.17 <sup>e</sup> $\pm$ 3.75
Ar15kV-5min	10.81 <sup>a</sup> $\pm$ 0.02	24.60 <sup>bcd</sup> $\pm$ 0.53	51.85 <sup>hi</sup> $\pm$ 2.92
Ar15kV-10min	10.61 <sup>a</sup> $\pm$ 0.72	25.41 <sup>b</sup> $\pm$ 0.74	74.14 <sup>fg</sup> $\pm$ 1.97
Ar15kV-15min	10.89 <sup>a</sup> $\pm$ 0.42	28.24 <sup>a</sup> $\pm$ 0.72	194.10 <sup>d</sup> $\pm$ 7.99
He10kV-5min	9.73 <sup>b</sup> $\pm$ 0.21	23.74 <sup>de</sup> $\pm$ 0.28	34.95 <sup>ij</sup> $\pm$ 1.43
He10kV-10min	9.21 <sup>bc</sup> $\pm$ 0.24	24.89 <sup>bc</sup> $\pm$ 0.53	139.07 <sup>e</sup> $\pm$ 5.09
He10kV-15min	9.41 <sup>b</sup> $\pm$ 0.11	25.07 <sup>bc</sup> $\pm$ 0.39	241.69 <sup>c</sup> $\pm$ 5.31
He15kV-5min	9.05 <sup>bc</sup> $\pm$ 0.33	25.36 <sup>bc</sup> $\pm$ 0.79	85.21 <sup>f</sup> $\pm$ 6.28
He15kV-10min	8.59 <sup>c</sup> $\pm$ 0.43	24.64 <sup>bcd</sup> $\pm$ 0.44	1214.89 <sup>b</sup> $\pm$ 22.98
He15kV-15min	8.67 <sup>c</sup> $\pm$ 0.70	23.01 <sup>ef</sup> $\pm$ 0.25	1636.28 <sup>a</sup> $\pm$ 32.23

Means  $\pm$  standard deviation (n = 3) with different letters within a column are significantly different ( $P < 0.05$ ).

#### 4.2.4 Reducing sugar

Reducing sugar content of native and treated tapioca starch using argon and helium plasma under various conditions is shown in



Table 4.4. From the data obtained, it was found that the native sample had the lowest reducing sugar content ( $P < 0.05$ ). Increasing treatment time from 5 to 15 minutes at 10 kV of argon plasma caused the reducing sugar to increase from 35.22 to 143.17  $\mu\text{g/g}$  dry starch. The same trend was observed at a higher voltage of 15 kV, that was, reducing sugar increased from 51.85 to 194.10  $\mu\text{g/g}$  dry starch, respectively. At 15 minutes of treatment times, the reducing sugar of samples treated with 15 kV of argon plasma (194.10  $\mu\text{g/g}$  dry starch) was significantly higher than the sample treated with 10 kV (143.17  $\mu\text{g/g}$  dry starch) ( $P < 0.05$ ).

An increase in reducing sugar of helium plasma-modified samples was resulted when increasing treatment time from 5 to 15 minutes at 10 kV (34.95 – 241.69  $\mu\text{g/g}$  dry starch). The treated samples at 15 kV rapidly increased after treating for 10 minutes and beyond. The reducing sugar was observed to be the highest for the treated sample at 15 kV for 15 minutes (1636.28  $\mu\text{g/g}$  dry starch) ( $P < 0.05$ ). This result suggested that the depolymerization induced by DBD plasma treatment could lead to the formation of small fragments which convert starch to more reducing ends. An increase in reducing sugar could be due to the conversion of amylose polymeric chains or amylopectin side chains into smaller molecules with more free hydroxyl groups (reducing end) after plasma treatments. In support of previous research (Prasertsung et al., 2017), this study found that the plasma process could enhance the reducing sugar content of cellulose solution due to cellulose degradation.

It was found that the reducing sugar of helium plasma-modified samples was higher than argon plasma-modified samples when modified at 10 kV for 10 minutes and beyond ( $P < 0.05$ ). A higher electron temperature and lower electron density of helium plasma could produce several small fragments of starch molecules, resulting in higher reducing sugar.

Appendix C.71 shows the effects of the types of feed gas, voltage levels, treatment times, and their interactions on the reducing sugar of plasma-treated samples using two-way ANOVA. All the main factors and their interactions significantly influenced the

reducing sugar content of the treated sample using nonthermal plasma ( $P < 0.05$ ).

#### 4.2.5 Fourier transform infrared (FTIR) spectroscopy

The functional groups of tapioca starch before and after plasma modification with different conditions were investigated by FTIR analysis (Figure 4.6). The native tapioca starch shows the absorption bands related to O-H stretching ( $3424 \text{ cm}^{-1}$ ), CH and  $\text{CH}_2$  stretching ( $2932 \text{ cm}^{-1}$ ), tightness of bond water ( $1648 \text{ cm}^{-1}$ ), C-O-C asymmetric stretching glycosidic bond ( $1158 \text{ cm}^{-1}$ ), and C-O-C skeletal mode of  $\alpha$ -glycosidic linkage ( $929 \text{ cm}^{-1}$ ). After plasma modification, similar bands were discovered in all starch samples, suggesting that the treatment did not introduce any functional groups into the starch structure. Moreover, the FTIR spectrum showed no change in the FTIR peak at  $1700 \text{ cm}^{-1}$ , corresponding to the functional carboxylic acid group. This result might be due to the formation of other acidic groups or acids without producing carboxylic groups during plasma treatment. This study agrees with the previous research by Thirumdas, Trimukhe, et al. (2017) and Lii et al. (2002), who described that the reduction in pH could not consist of the formation of an acid functional group in the IR peak ( $P < 0.05$ ).

The intensity ratio of bands at  $1047 \text{ cm}^{-1}$  and  $1022 \text{ cm}^{-1}$  ( $R_{1047/1022}$ ) in the FTIR spectra of native and treated tapioca starch are presented in Table 4.5.  $R_{1047/1022}$  indicates the degree of short-range ordering and the ratio of crystalline to amorphous regions on the starch granule surface (Shen et al., 2021). The result showed that the  $R_{1047/1022}$  value of a treated sample using helium plasma tended to increase. This might be due to the decomposition of starch chain by depolymerization and plasma etching, which increased the ratio of crystalline and amorphous regions on the starch surface layers. As a result, the  $R_{1047/1022}$  value of treated starch increased (Yan et al., 2020). This presumption was consistent with that of the lower crystallinity after using helium plasma treatment. From two-way ANOVA analysis (appendix C.72), the types of feed gas had a significant effect on the  $R_{1047/1022}$  value of the treated samples ( $P < 0.05$ ).

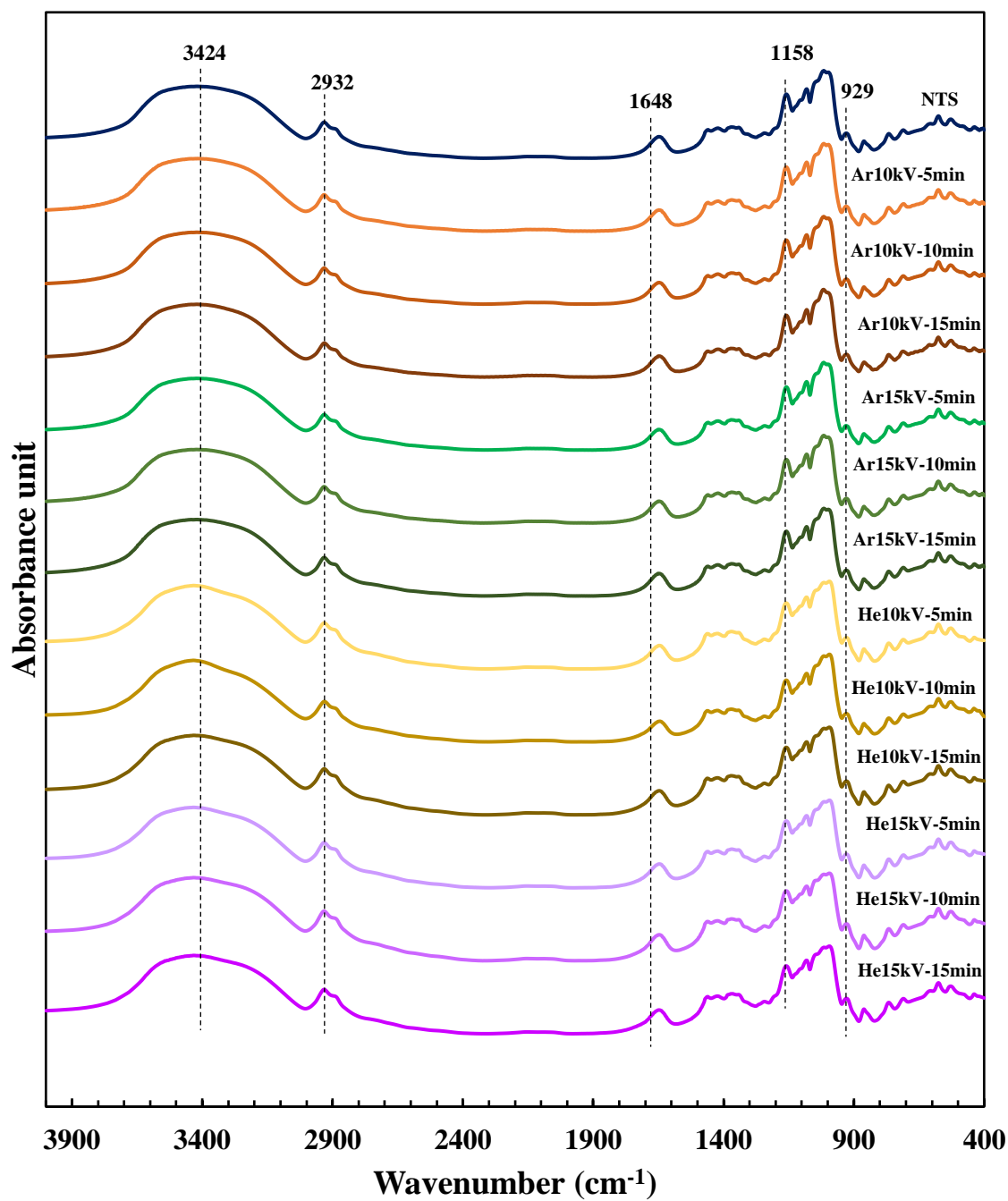


**Figure 4.6** Fourier-transform infrared spectroscopy (FTIR) spectra of native and treated tapioca starch with different conditions.

**Table 4.5** Ratio between 1047 and 1022  $\text{cm}^{-1}$  in the FTIR spectra of native and treated tapioca starch with different conditions.

Samples	Ratio at 1047/1022 $\text{cm}^{-1}$
NTS	0.90 <sup>ab</sup> $\pm$ 0.00
Ar10kV-5min	0.91 <sup>ab</sup> $\pm$ 0.00
Ar10kV-10min	0.90 <sup>ab</sup> $\pm$ 0.01
Ar10kV-15min	0.89 <sup>b</sup> $\pm$ 0.01
Ar15kV-5min	0.90 <sup>ab</sup> $\pm$ 0.00
Ar15kV-10min	0.90 <sup>ab</sup> $\pm$ 0.00
Ar15kV-15min	0.91 <sup>ab</sup> $\pm$ 0.00
He10kV-5min	0.92 <sup>ab</sup> $\pm$ 0.02
He10kV-10min	0.96 <sup>a</sup> $\pm$ 0.09
He10kV-15min	0.93 <sup>ab</sup> $\pm$ 0.02
He15kV-5min	0.92 <sup>ab</sup> $\pm$ 0.00
He15kV-10min	0.94 <sup>ab</sup> $\pm$ 0.03
He15kV-15min	0.92 <sup>ab</sup> $\pm$ 0.01

The assay was performed in triplicate. Mean  $\pm$  SD values in the same column with different superscript letters are significantly different ( $P \leq 0.05$ ).

#### 4.2.6 Molecular weight analysis

The molecular weight distribution of native and treated tapioca starch was measured by using the HPSEC-MALLS-RI system, as shown in Figure 4.7. Due to the difference in molecular size, all starch sample fractions were classified as amylopectin, intermediate material, and amylose based on their retention time. The results showed that the amylopectin, intermediate material, and amylose content of modified samples were changed compared with native samples. The lower molecular weight molecules of treated samples were discovered after increasing voltage levels and treatment times of both gas types. This finding is probably due to depolymerization of amylopectin branch side chains and plasma etching at the starch granule surface, resulting in small fragmented linear chains.

Weight-average molecular weight ( $\overline{M}_w$ ) of amylopectin of native starch before and after plasma modification are shown in Table 4.6. The result showed that the sample treated with argon plasma at 15 kV for 5 minutes had a high variance in  $\overline{M}_w$  of

amylopectin. It might be due to the nonuniformity of solid-state modification achieved using plasma treatment. The presumption could be supported by the surface morphology of samples that showed nonuniformity after plasma modification. The samples tended to have a reduced  $\overline{M}_w$  compared with native samples. Increasing voltage levels and treatment times of argon plasma caused a decrease in  $\overline{M}_w$ . A similar trend was observed after using helium plasma at 10 kV. This result is consistent with a previous study by Zhang et al. (2015). This study showed that long-term plasma treatment caused starch molecules to break down, which led to more starch molecules with smaller molecular weights. The destruction of starch molecules could be confirmed by the lower relative crystallinity and higher reducing sugar of samples after plasma treatment in the previous section.

On the other hand, the sample treated at 15 kV of helium plasma had a lower  $\overline{M}_w$  than that of 10 kV. This could be due to the smaller atomic mass of helium than argon, which causes easier plasma generation with high voltage power. The presumption could induce helium plasma at a high voltage level to deviate from the Maxwellian distribution. The Maxwellian distribution describes the distribution of speeds of molecules in thermal equilibrium as given by statistical mechanics. According to Jae Koo et al. (2004), a high voltage level causes a deviation from the Maxwellian distribution that can decrease the electron temperature. This might cause a decrease in the energy of active species that interact with starch surface granules. As a result, the effect of high voltage plasma on molecular weight reduction was less pronounced.

**Table 4.6** Weight-average molecular weight ( $\overline{M}_w$ ) of amylopectin before and after plasma modification

Samples	$\overline{M}_w \times 10^7$ (g/mol)	
	Replicate	
	1	2
NTS	22.73	21.65
Ar10kV-5min	21.70	11.96
Ar10kV-10min	13.36	7.09
Ar10kV-15min	5.21	2.28
Ar15kV-5min	50.35	5.94
Ar15kV-10min	2.40	3.19
Ar15kV-15min	3.64	1.45
He10kV-5min	4.40	5.46
He10kV-10min	2.47	3.44
He10kV-15min	2.97	3.20
He15kV-5min	15.20	9.28
He15kV-10min	12.4	11.9
He15kV-15min	18.0	18.8

The assay was performed in duplicate.

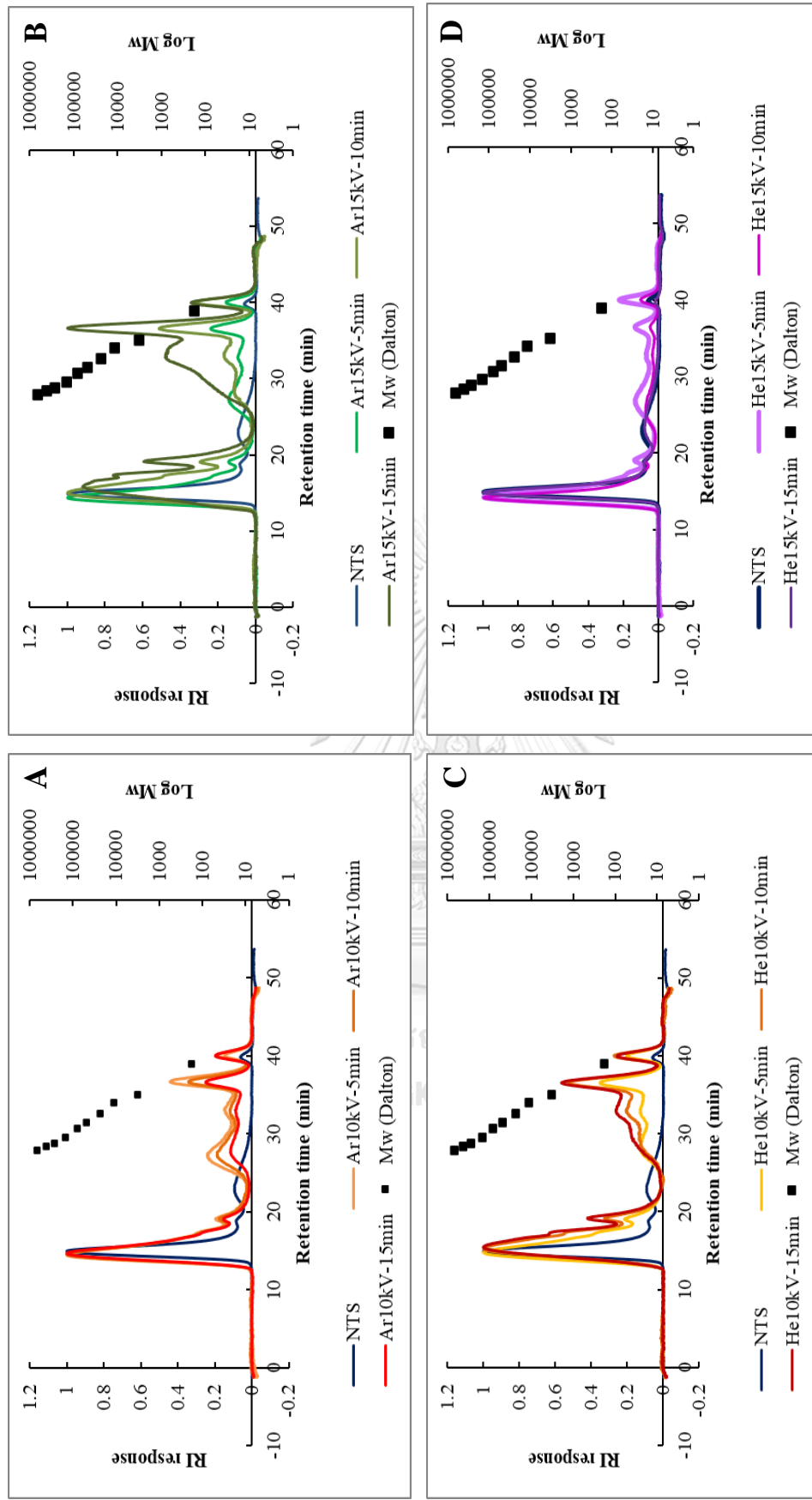


**Figure 4.7** High-performance size exclusion chromatograph of native and plasma-treated tapioca starch with different conditions. (A and B) native and argon-plasma treated starch at 10 kV and 15 kV; (C and D) native and helium plasma-treated starch at 10 kV and 15 kV.

### **4.3 Effect of types of the feed gas, voltage levels, and treatment time on functional properties of treated tapioca starch using nonthermal DBD plasma**

#### **4.3.1 Pasting properties**

Table 4.7 and Figure 4.8 show the pasting properties of native and plasma-modified tapioca starches. The pasting temperature (PT) is used for determining the temperature requirements in the production of starch-based food products. All the treated samples were not different in PT compared to the native sample ( $P \geq 0.05$ ). There was no significant difference in PT with increasing voltage levels and the treatment time for both argon and helium plasma-treated samples ( $P \geq 0.05$ ). Compared with gas types at the same voltage power, the treated sample with helium plasma for 15 minutes had a significantly higher PT than the treated sample with argon for 15 minutes ( $P < 0.05$ ). High PT of starches indicates a higher gelatinization temperature. The peak viscosity (PV) of modified tapioca starch through argon and helium plasma treatment decreased significantly ( $P < 0.05$ ) as compared with native tapioca starch (NTS). Increasing treatment time from 5 to 15 minutes at 10 kV of argon plasma caused the PV to reduce from 4,106 cP to 1,823 cP. The same trend was observed at a higher voltage of 15 kV; that is, PV reduced from 3,202.3 cP to 1,667.7 cP when increasing the treatment time from 5 to 15 minutes, respectively. The reduction in PV was discovered in helium plasma by increasing the voltage powers (10–15 kV) and time (5–15 minutes) from 3871.3 cP to 340.7 cP. At the same condition, helium plasma-modified samples had a significantly lower PV than argon plasma-modified samples ( $P < 0.05$ ). The PV is a measure of starch granule swelling. A lower PV of treated starch samples indicates a low ability of starch swelling since the surface of the starch granules was damaged by plasma etching, resulting in lower PV. This finding could be confirmed by surface morphology (Figure 4.1) and swelling power of plasma modified tapioca starch in the following section. Starch's breakdown viscosity (BV) indicates starch paste stability to heat and shear forces. A lower BV is generally associated with better stability after gelatinization. The sample subjected to plasma treatment had significantly lower BV, which decreased with increasing treatment time and power level ( $P < 0.05$ ).



The lowest BV was discovered in the sample treated with helium plasma using 15 kV for 5 minutes (320.0 cP). The reassociation or recrystallization of amylose and amylopectin in gelatinized starch undercooling is called starch retrogradation and can be related to setback viscosity (SV). Starches with low SV have low tendencies towards retrogradation, which causes staling (Zhang et al., 2015). A significant reduction in SV was observed in the plasma-treated tapioca starch ( $P < 0.05$ ). An increase in treatment time and power level resulted in a significant decrease in SV of the treated tapioca starch samples ( $P < 0.05$ ). The SV of argon plasma-treated samples was higher than that of helium plasma-treated samples under the same conditions.

The breakdown and setback percentage of native and DBD plasma modified tapioca starch under various conditions is displayed in Table 4.8. The breakdown percentage is calculated from the proportion between breakdown viscosity and peak viscosity. A reduction in breakdown percentage was observed in the samples treated using argon plasma with 10 kV for 5 minutes and 15 kV for 5 minutes (54.80% and 52.20%, respectively) ( $P < 0.05$ ). Chaiwat et al. (2016) reported that the lower BV after plasma treatment was due to the dominant effect of crosslinking of starch molecules at the surface of the tapioca starch granule. This result indicated that the starch paste was more stable to heat and shear force during cooking due to the crosslinking mechanism. On the other hand, the breakdown percentage was raised with increasing treatment time. This could be due to the plasma etching and depolymerization. These mechanisms could lead to lower starch paste stability.

The result showed that when applied voltage powers at 10 kV and 15 kV for 5 minutes of helium plasma, the breakdown percentage did not differ significantly from the native sample ( $P \geq 0.05$ ). However, increasing the treatment time to 15 minutes caused the breakdown percentage to increase. The highest breakdown percentage was found when the sample was treated by helium plasma at 15 kV for 15 minutes (93.85%) ( $P < 0.05$ ). The same trend was found in the setback percentage, calculated from the proportion between setback viscosity and trough viscosity. A reduction in the setback percentage was observed compared to the native starch sample ( $P < 0.05$ ).

Increasing treatment time at both voltage levels in argon plasma resulted in an increase in setback percentage from 39.34% to 55.50% at 10 kV and from 39.48% to 59.77%, respectively. Furthermore, there was no significant setback percentage difference between helium-plasma samples at 10 kV for 5 to 15 minutes ( $P \geq 0.05$ ). Increasing the treatment time from 5 to 15 minutes at 15 kV of helium plasma caused the setback percentage to increase from 55.04 to 216.33 cP. The reduction in setback percentage compared with the native tapioca starch indicated that the plasma-treated samples tend to have lower retrogradation potential.

Two-way ANOVA tests on the effects of gas types, voltage levels, treatment time, and their interactions on pasting temperature, peak viscosity, breakdown percentage, and setback percentage are shown in appendices C.73 to C.76. The result showed that pasting temperatures of modified tapioca starch were significantly affected by the gas types ( $P < 0.05$ ). For peak viscosity, the interaction effect of gas types and voltage levels had no significant influence on peak viscosity. A similar result was found in the interaction effect of voltage levels and treatment time ( $P \geq 0.05$ ). All main effects (gas types, voltage levels, and treatment times) and their interactions had a significant influence on the breakdown and setback percentage of plasma-modified samples ( $P < 0.05$ ).

**Table 4.7** Pasting properties of native and DBD plasma modified tapioca starch with various conditions

Samples	Peak Viscosity (cP)	Trough Viscosity (cP)	Final Viscosity (cP)	Break Down (cP)	Setback (cP)	Pasting temperature (°C)
NTS	4442.3 <sup>a</sup> ± 43.1	1722.3 <sup>b</sup> ± 25.9	2940.7 <sup>a</sup> ± 72.7	2720.0 <sup>a</sup> ± 68.8	1218.3 <sup>a</sup> ± 75.2	71.1 <sup>abc</sup> ± 0.5
Ar10kV-5min	4106.0 <sup>b</sup> ± 356.6	1850.3 <sup>a</sup> ± 71.5	2577.0 <sup>b</sup> ± 68.0	2255.7 <sup>b</sup> ± 286.0	726.7 <sup>b</sup> ± 49.1	70.9 <sup>bc</sup> ± 0.6
Ar10kV-10min	2731.3 <sup>d</sup> ± 91.6	1085.3 <sup>d</sup> ± 5.1	1581.3 <sup>d</sup> ± 24.09	1646.0 <sup>c</sup> ± 91	496.0 <sup>d</sup> ± 25.2	71.1 <sup>abc</sup> ± 0.4
Ar10kV-15min	1823.0 <sup>e</sup> ± 10.4	600.0 <sup>f</sup> ± 2.0	933.0 <sup>e</sup> ± 1.0	1223.0 <sup>ef</sup> ± 10.8	333.0 <sup>efg</sup> ± 3.0	70.4 <sup>c</sup> ± 0.4
Ar15kV-5min	3202.3 <sup>c</sup> ± 292.7	1530.3 <sup>c</sup> ± 141.8	2130.7 <sup>c</sup> ± 145.4	1672.0 <sup>c</sup> ± 155.3	600.3 <sup>c</sup> ± 51.3	70.8 <sup>bc</sup> ± 0.4
Ar15kV-10min	2248.3 <sup>ef</sup> ± 11.0	843.7 <sup>e</sup> ± 35.8	1308.3 <sup>e</sup> ± 40.5	1404.7 <sup>de</sup> ± 20.9	464.7 <sup>d</sup> ± 5.13	70.5 <sup>c</sup> ± 0.1
Ar15kV-15min	1677.7 <sup>g</sup> ± 50.8	532.3 <sup>f</sup> ± 41.3	849.7 <sup>g</sup> ± 48.9	1145.3 <sup>f</sup> ± 10.6	317.3 <sup>fg</sup> ± 7.8	70.8 <sup>bc</sup> ± 0.2
He10kV-5min	3871.3 <sup>b</sup> ± 41.3	1535.3 <sup>c</sup> ± 50.5	2121.3 <sup>c</sup> ± 28.1	2336.0 <sup>b</sup> ± 40.7	586.0 <sup>bc</sup> ± 45.9	71.1 <sup>abc</sup> ± 0.3
He10kV-10min	2687.7 <sup>d</sup> ± 220.9	984.3 <sup>d</sup> ± 99.3	1360.0 <sup>e</sup> ± 137.2	1703.3 <sup>c</sup> ± 96.7	375.7 <sup>ef</sup> ± 38.0	71.2 <sup>abc</sup> ± 0.6
He10kV-15min	2329.0 <sup>e</sup> ± 253.1	783.7 <sup>e</sup> ± 68.9	1085.7 <sup>f</sup> ± 85.0	1545.3 <sup>cd</sup> ± 194.3	302.0 <sup>g</sup> ± 17.1	71.4 <sup>ab</sup> ± 0.5
He15kV-5min	1979.3 <sup>fg</sup> ± 185.2	727.0 <sup>e</sup> ± 94.3	1126.7 <sup>f</sup> ± 142.1	1252.3 <sup>ef</sup> ± 95.7	399.7 <sup>e</sup> ± 53.7	71.1 <sup>abc</sup> ± 0.3
He15kV-10min	787.7 <sup>h</sup> ± 155.5	157.0 <sup>g</sup> ± 46.3	278.7 <sup>h</sup> ± 74.1	630.7 <sup>g</sup> ± 110.5	121.7 <sup>h</sup> ± 28.0	71.6 <sup>ab</sup> ± 0.3
He15kV-15min	340.7 <sup>i</sup> ± 17.9	21.0 <sup>h</sup> ± 4.0	65.7 <sup>i</sup> ± 6.8	320.0 <sup>h</sup> ± 15.52	44.7 <sup>i</sup> ± 3.21	71.8 <sup>a</sup> ± 0.2

The assay was performed in triplicate. Mean ± SD values in the same column with different superscript letters are significantly different ( $P \leq 0.05$ ). cP, centipoise.

**Table 4.8** Breakdown and Setback percentage of native and DBD plasma modified tapioca starch with different types of the feed gas, voltage levels, and treatment time

Samples	Breakdown percentage* (%)	Setback percentage** (%)
NTS	61.22 <sup>de</sup> ± 0.95	70.76 <sup>bc</sup> ± 4.73
Ar10kV-5min	54.80 <sup>f</sup> ± 2.32	39.34 <sup>ef</sup> ± 3.59
Ar10kV-10min	62.48 <sup>de</sup> ± 1.42	45.70 <sup>def</sup> ± 2.40
Ar10kV-15min	67.09 <sup>c</sup> ± 2.23	55.50 <sup>cde</sup> ± 0.69
Ar15kV-5min	52.20 <sup>g</sup> ± 0.84	39.48 <sup>ef</sup> ± 5.38
Ar15kV-10min	60.23 <sup>e</sup> ± 1.30	55.13 <sup>cdef</sup> ± 1.77
Ar15kV-15min	68.30 <sup>c</sup> ± 1.48	59.77 <sup>cd</sup> ± 3.09
He10kV-5min	60.34 <sup>e</sup> ± 1.09	38.25 <sup>f</sup> ± 4.04
He10kV-10min	63.40 <sup>d</sup> ± 1.05	38.17 <sup>f</sup> ± 0.44
He10kV-15min	66.28 <sup>c</sup> ± 1.62	38.62 <sup>ef</sup> ± 1.63
He15kV-5min	63.34 <sup>d</sup> ± 1.61	55.04 <sup>cdef</sup> ± 4.40
He15kV-10min	80.33 <sup>b</sup> ± 2.42	78.76 <sup>b</sup> ± 7.18
He15kV-15min	93.85 <sup>a</sup> ± 1.00	216.33 <sup>a</sup> ± 29.31

Means ± standard deviation (n = 3) with different letters within a column are significantly different (P≤0.05). \*The breakdown percentage was calculated from the proportion between breakdown viscosity and peak viscosity. \*\*The setback percentage was calculated from the proportion between setback viscosity and trough viscosity.

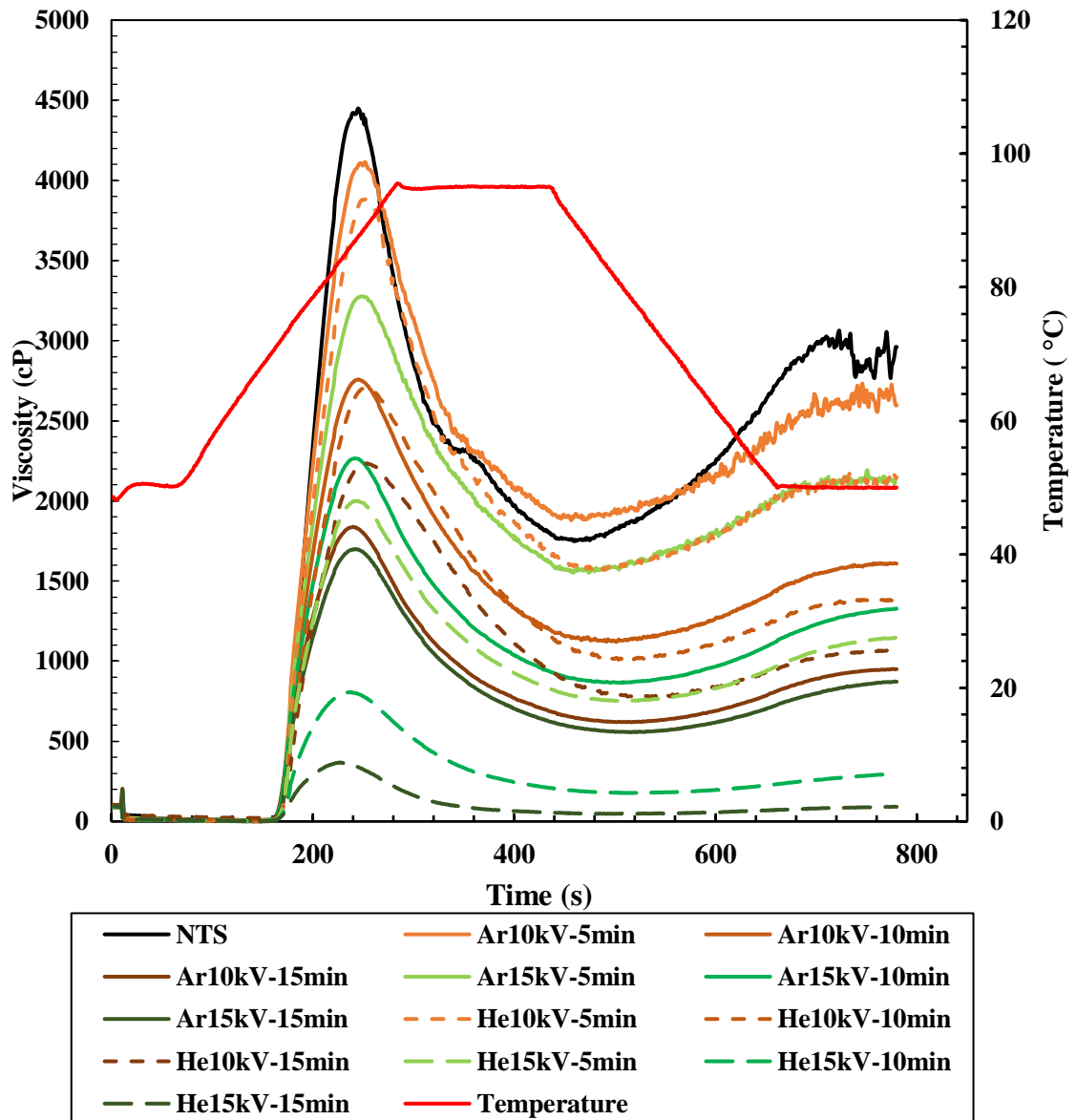


**Figure 4.8** Pasting curves of native, argon, and helium treated starch at different types of feed gas, voltage levels, and time.

### 4.3.2 Swelling power and solubility

The swelling power of native and modified samples at different temperatures (60, 70, 80, and 90°C) is shown in Figure 4.9 and appendix B.1. An increase in swelling power was observed after increasing the temperature. After increasing the temperature, the molecular structure of starch granules was disrupted, resulting in higher starch swelling. This reason could be supported by the pasting temperature of samples (Table 4.7), which indicated that samples tended to gelatinize after increasing the heating temperature up to 70°C and beyond. The increase in swelling power of the native sample was 3.86 to 11.29 g/g at 60°C to 90°C.

There was no significant difference in swelling power at 60°C and 70°C between native and argon-plasma treated samples, except for the treated sample at 10 kV for 10 minutes (60°C) ( $P < 0.05$ ). The reduction trend was observed after increasing the modification time of helium-plasma treated samples at 60°C and 70°C when compared with native and argon-plasma treated samples. The swelling power of helium at 60°C decreased from 2.99 to 2.38 g/g and from 2.74 to 2.17 g/g with an increase in modification time at 10 kV and 15 kV, respectively. The swelling power of helium-plasma treated samples at 70°C was reduced from 6.55 to 4.70 g/g and from 5.27 to 3.29 g/g at 10 kV and 15 kV, respectively. At 80°C and 90°C, the swelling power of both samples treated with argon and helium plasma was reduced as the treatment time increased. After increasing the treatment time (5 to 15 minutes), the swelling power of treated samples with argon and helium plasma at 80°C was 8.16 to 6.33 g/g (10 kV), 7.99 to 6.39 g/g (15 kV), 7.87 to 5.12 g/g (10 kV), and 6.47 to 3.66 g/g (15 kV), respectively. At 90°C, the swelling power of argon and helium-plasma treated samples followed the same pattern. An increase in treatment time of treated samples caused the swelling power to reduce from 11.07 to 8.86 g/g (10 kV, argon), from 10.64 to 8.64 g/g (15 kV, argon), from 6.70 to 5.38 g/g (10 kV, helium), and from 5.84 to 3.88 g/g (15 kV, argon), respectively. It could be noticed that the treated samples with helium plasma had statistically lower swelling power than argon-plasma treated samples at the same voltage level and time.

The decrease in swelling power of plasma-treated samples was consistent with that of dented starch granules (Figure 4.1 – 4.2), lower crystallinity (Table 4.2), and lower peak viscosity (Table 4.7). The disruption of amylopectin in crystalline regions of the starch granule surface is induced by depolymerization and plasma etching. This finding agrees with a previous study by Yan et al. (2020), who reported that the degradation of amylopectin induced by DBD treatment significantly decreased the strength of the three-dimensional structure produced by starch granules during the swelling process.

Figure 4.10 and appendix B.2. depict the solubility of native and modified starches at 60, 70, 80, and 90°C. The result showed that the solubility at five temperature levels of plasma-treated samples was significantly higher than the native sample as the treatment time increased from 5 to 15 minutes ( $P < 0.05$ ). Increasing the treatment time of argon-plasma treated starch from 5 to 15 minutes at 10 kV and 15 kV resulted in increasing solubility from 0.97 to 1.87 % and 1.05 to 1.83%, respectively. For helium plasma treatment, the solubility at 60°C was significantly higher than modified samples with argon plasma at 10 kV and 15 kV for 15 minutes ( $P < 0.05$ ). The voltage level at 15 kV for 15 minutes of helium plasma showed the lowest solubility (7.48%) at 70°C. Helium plasma treatments had significantly higher solubility at 80°C and 90°C than argon plasma treatments at the same voltage level and treatment time ( $P < 0.05$ ). The highest solubility at 80 and 90°C was found in the sample treated with helium plasma at 15 kV for 15 minutes (12.08% and 25.19%). These results indicate that plasma treatment could partially break down starch granules by depolymerization and plasma etching, resulting in several water-soluble starch fragments and a loose surface structure of starch granules. The presumption is consistent with higher reducing sugar and amylose content, enhancing the hydroxyl group and hydrophilicity of starch. Moreover, in agreement with recent studies (Thirumdas, Trimukhe, et al., 2017; Yan et al., 2020), who reported that active plasma species cause partial depolymerization of starch, resulting in the formation of smaller fragments.

Two-way ANOVA analysis showed that the swelling power at 70°C to 90°C of plasma modified starch was significantly influenced by gas types, voltage levels, treatment time, and their interaction (see appendices C.77 to C.80) ( $P < 0.05$ ), but only the swelling power at 60°C was influenced by gas types, treatment time, and their interaction (see appendix C.73) ( $P < 0.05$ ). At 60°C to 90°C, two-way ANOVA tests were performed to determine the effects of gas types, voltage levels, treatment time, and their interaction on solubility (see appendices C.81–C.84). The result showed that voltage levels and their interaction had no significant influence on solubility at 60°C, except for the interaction effect of voltage levels and time ( $P \geq 0.05$ ). However, the solubility at 70 to 90°C was significantly influenced by gas types, voltage levels, treatment time, and their interactions ( $P < 0.05$ ).

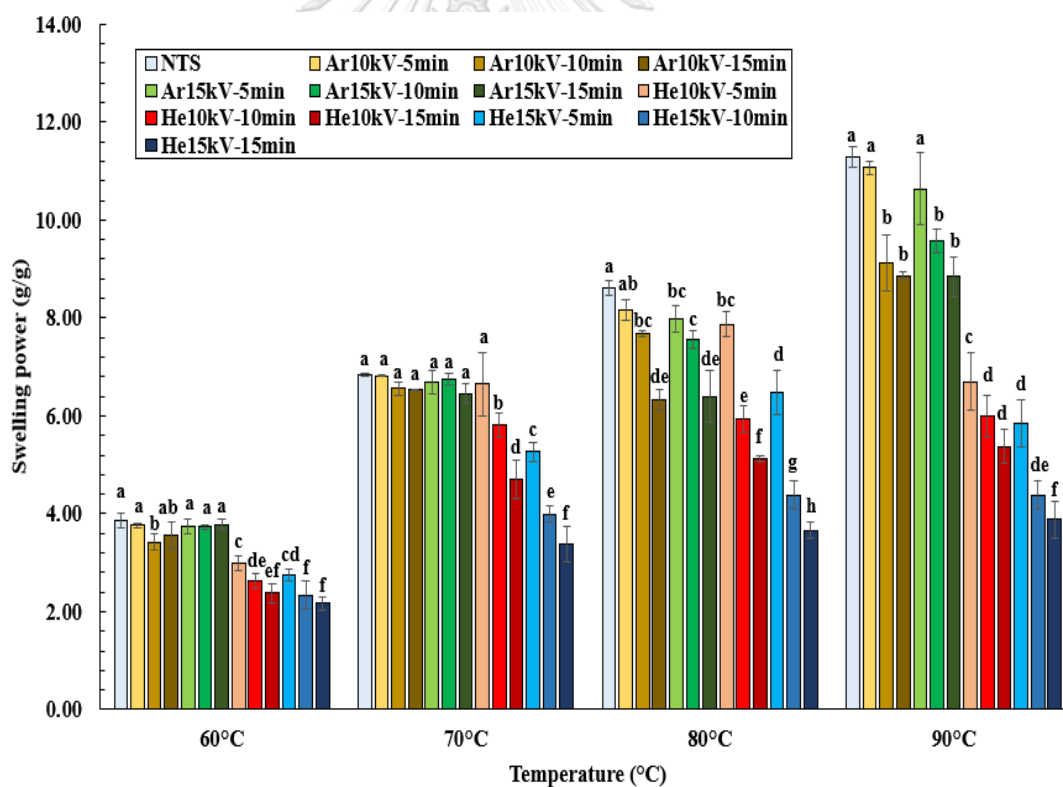


**Figure 4.9** Swelling power of native and plasma modified tapioca starch at different temperatures (60, 70, 80, and 90°C)



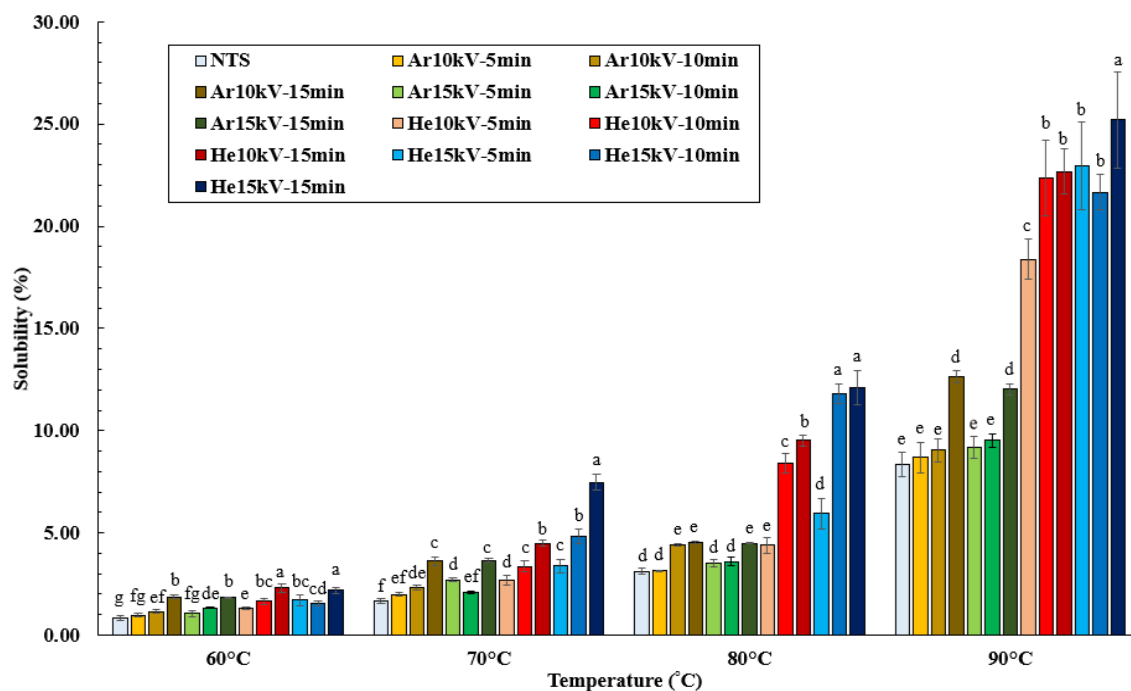


**Figure 4.10** Solubility of native and plasma-modified tapioca starch at different temperatures (60, 70, 80, and 90 °C)

### 4.3.3 Water binding capacity

The water-binding capacity of native tapioca starch before and after plasma modification was in the range of 0.73 to 0.89 g water/g sample (Figure 4.11). All treated samples had a significant increase in the water-binding capacity compared to the native sample ( $P < 0.05$ ). However, there was no significant difference in all treated samples ( $P \geq 0.05$ ). The plasma etching, which is the mechanical damage of starch granules, caused the absence of a network structure and an increase in free hydroxyl groups. This reason can increase the hydrophilicity of starch surface granules. This presumption is confirmed by scanning electron micrographs, which showed dented starch granules after plasma modification in the previous sections.

Appendix C.85 shows the effects of types of the feed gas, voltage levels, and their interactions on the water-binding capacity of plasma-treated samples using two-way ANOVA. All the main factors and their interactions did not significantly influence the water-binding capacity of the treated sample using nonthermal plasma ( $P \geq 0.05$ )

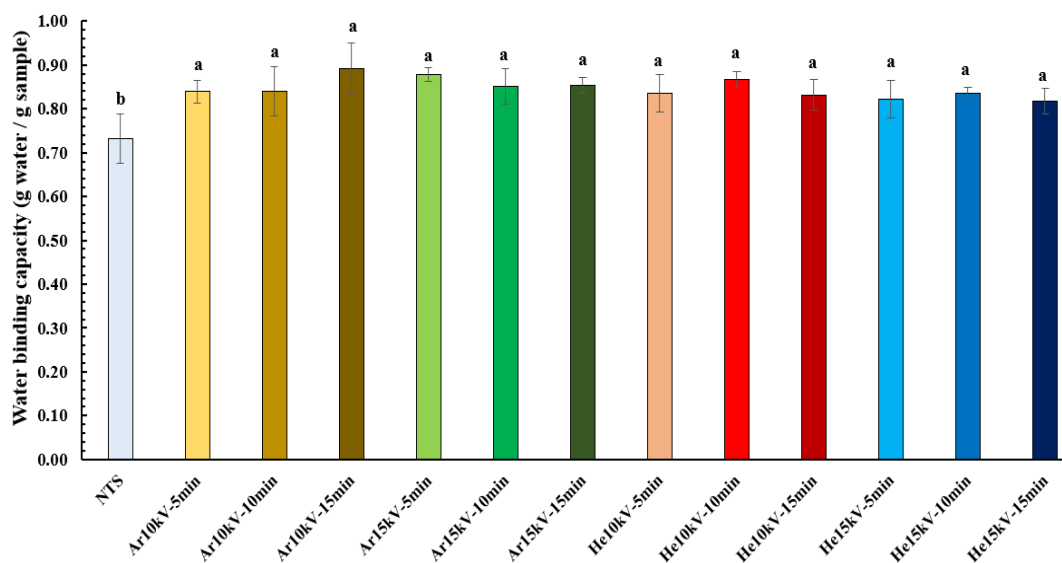


**Figure 4.11** The water binding capacity of native and plasma modified tapioca starch under different conditions.

### 4.3.4 Rheological properties

#### 4.3.4.1 Viscoelastic properties

Dynamic rheological behavior of native and treated tapioca starch using argon and helium plasma at 10 and 15 kV at various treatment times (5–15 minutes) is shown in Figures 4.12 to 4.15, respectively. The storage modulus ( $G'$ ) represents the deformation energy stored in a sample during shear. On the other hand, the loss modulus ( $G''$ ) is related to the amount of deformation energy used during shear and thus the sample's viscosity (Liu et al., 2017). 6% (w/w) starch paste samples had higher  $G'$  than  $G''$ , indicating dominated elastic behavior. Both argon-treated tapioca starch at 10 kV and 15 kV for 5 minutes had a higher  $G'$  than the native sample, whereas increasing the treatment time from 5 to 15 minutes had a lower  $G'$ .

Furthermore, both voltage powers for 10 minutes and beyond resulted in a lower  $G''$ . The same pattern was found when helium plasma was used at 10 kV. In contrast, increasing the voltage to 15 kV causes  $G'$  to decrease compared to the native sample. At both voltage levels, increasing the treatment time reduced the  $G''$  of the helium-treated sample.

These findings revealed that the argon-treated samples with 10 kV and 15 kV for 5 minutes and the helium-treated samples with 10 kV for 5 minutes had a stronger and more stable starch paste structure. According to Chaiwat et al. (2016) and Wongsagonsup et al. (2014), crosslinked tapioca starch by argon plasma treatment had a higher  $G'$  than native starch. Recent findings confirmed these results in terms of a reduced setback viscosity (Table 4.7) of the argon plasma treated sample under 10 kV and 15 kV for 5 minutes treatment. Crosslinking is the major mechanism by which a new linkage can be formed between the reducing ends of two polymer amylose chains (C-OH), resulting in a decrease in setback viscosity. On the other hand, increasing treatment time from 5 to 15 minutes at both voltage power levels could result in a weaker starch paste structure. This could be due to depolymerization and plasma etching at the glycosidic bond of starch molecules. Furthermore, higher reducing sugar content after plasma treatment could reduce  $G'$  because of its antiplasticizing effect. This reason could decrease granule swelling and amylose leaching. This presumption was supported by the lower setback viscosity and swelling power of treated samples after increasing treatment time, which indicated the dominant mechanism of depolymerization and plasma etching.

The lower  $G''$  of treated samples could be attributed to particle size variation and the distribution of starch granules after solid-state modification, which produced smaller particles. Moreover, depolymerized fragments by plasma treatment could reduce viscous parts. This presumption is consistent with SEM images of dented starch granules and higher apparent amylose content after plasma modification (Figure 4.2).

The loss tangent ( $\tan \delta$ ) is a ratio of  $G''$  and  $G'$  that can be used to calculate a gel's viscoelastic properties. All the samples had a  $\tan \delta$  of less than one, indicating that they are elastic and exhibit a typical gel network. The  $\tan \delta$  of argon-treated samples gradually decreased compared to the native sample. The same trend was discovered when the samples were modified using helium plasma. The lower  $\tan \delta$  might be due to a decrease in the fraction of  $G''$  and  $G'$ . However, the  $\tan \delta$  of treated samples was almost the same as the high-frequency ranges (50 rad/s beyond).



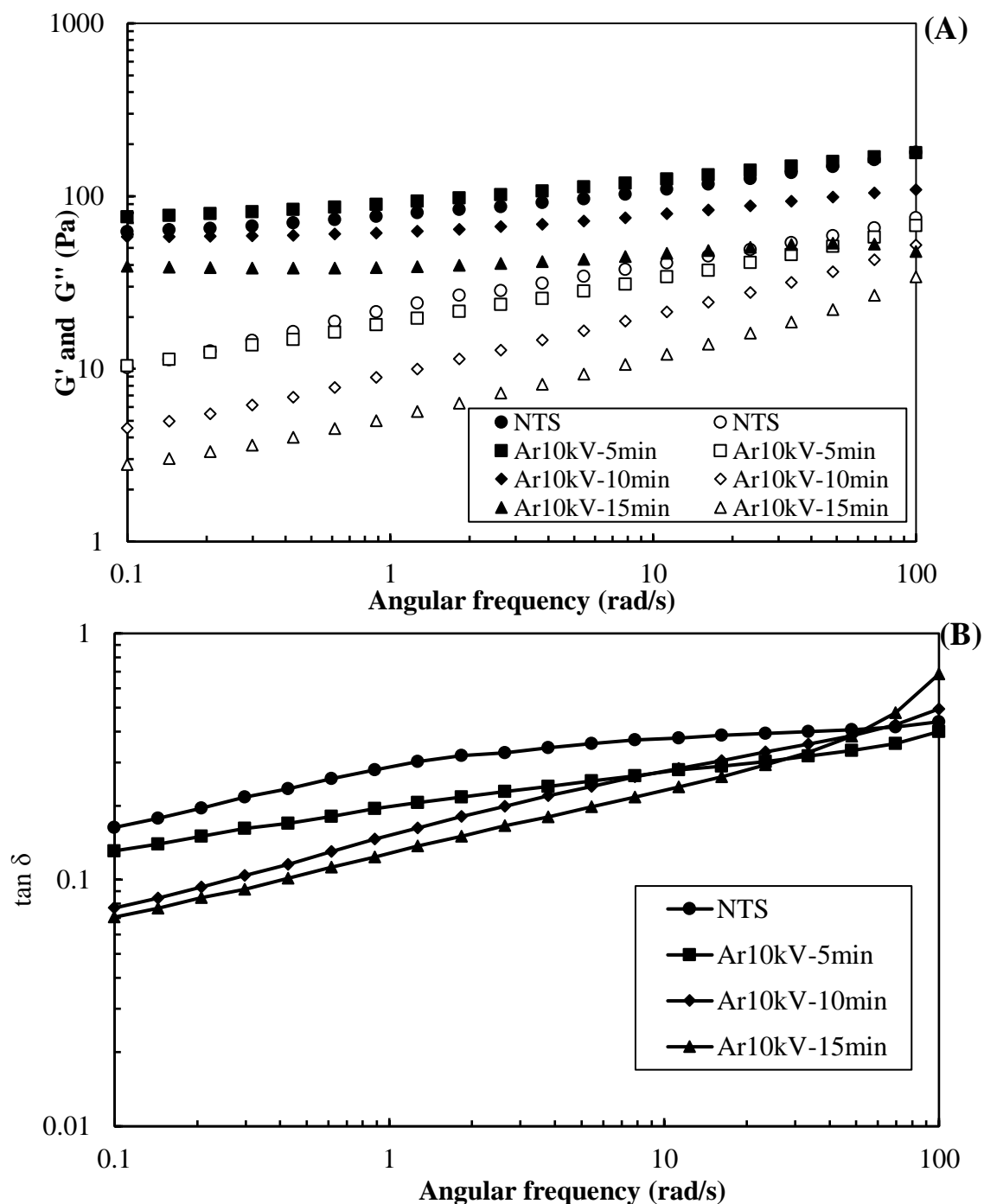


**Figure 4.12** Dynamic rheological behavior of native and argon treated tapioca starch at 10 kV levels and various treatment times (5, 10, 15 min). (A) Angular frequency on  $G'$  (close symbol) and  $G''$  (open symbol) for starch; (B) angular frequency of the loss tangent ( $\tan \delta$ ) at 25°C for starch

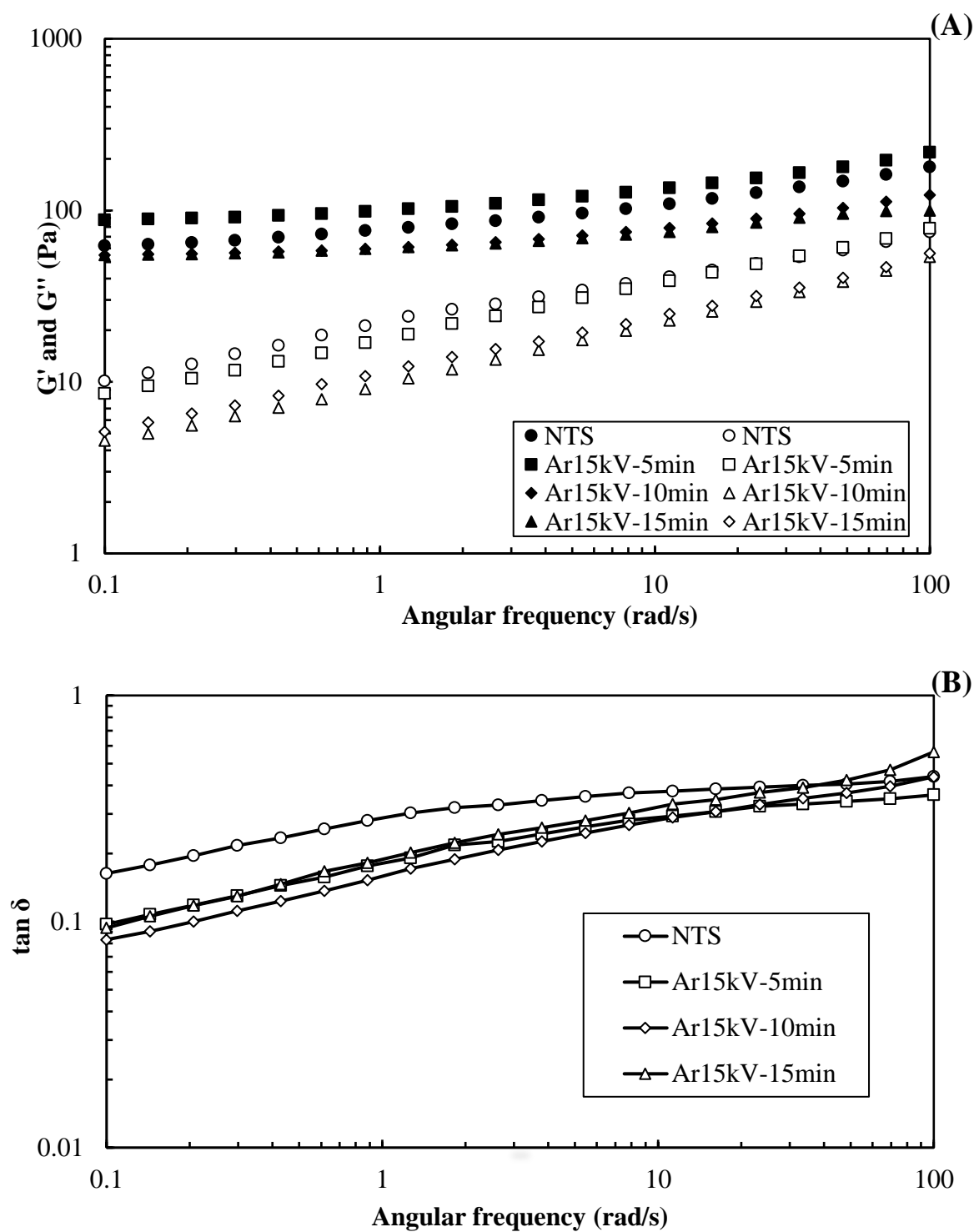


**Figure 4.13** Dynamic rheological behavior of native and argon treated tapioca starch at 15 kV levels and various treatment times (5, 10, 15 min). (A) Angular frequency on  $G'$  (close symbol) and  $G''$  (open symbol) for starch; (B) angular frequency of the loss tangent ( $\tan \delta$ ) at 25°C for starch

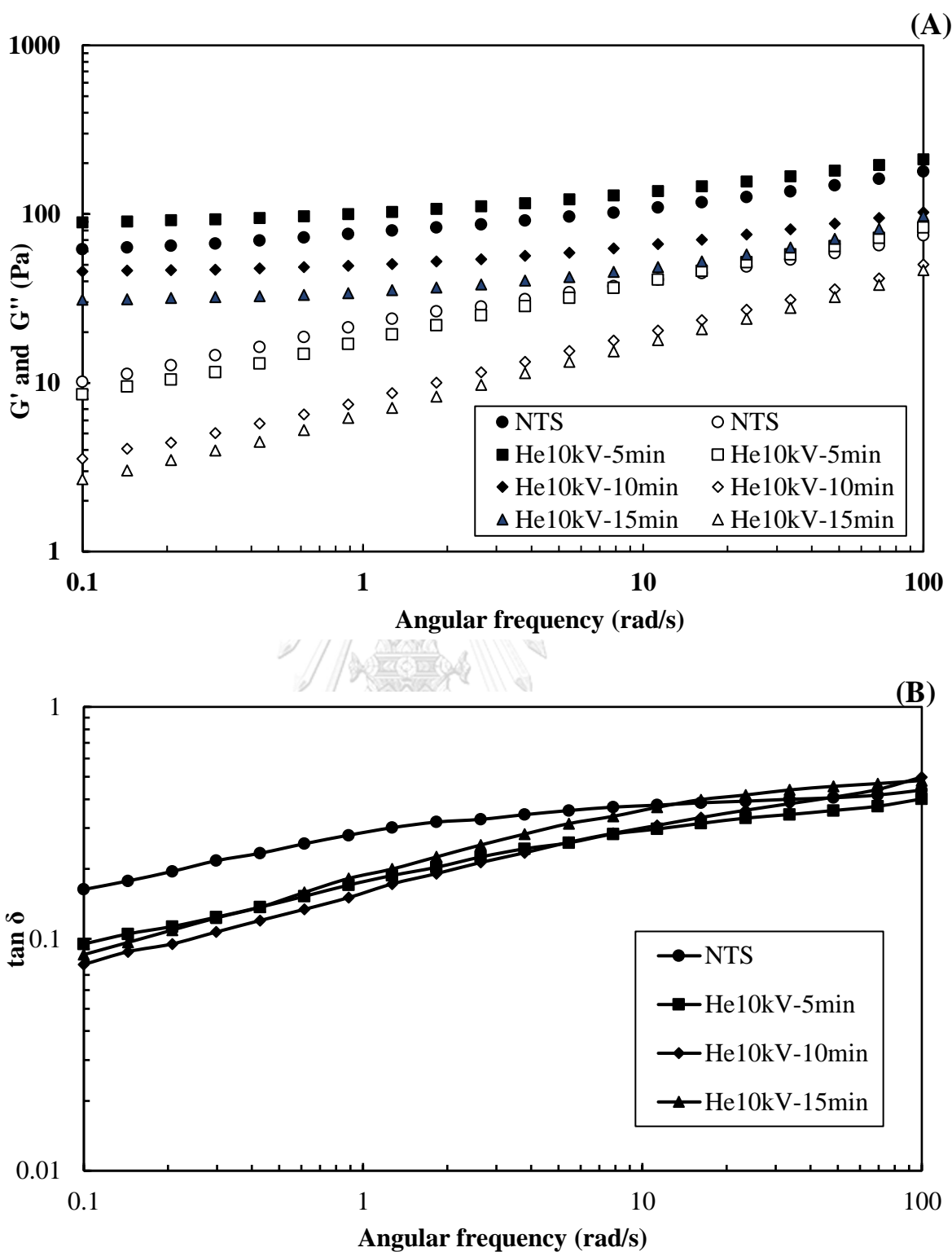


**Figure 4.14** Dynamic rheological behavior of native and helium treated tapioca starch at 10 kV levels and various treatment times (5, 10, 15 min). (A) Angular frequency on  $G'$  (close symbol) and  $G''$  (open symbol) for starch; (B) angular frequency of the loss tangent ( $\tan \delta$ ) at 25°C for starch

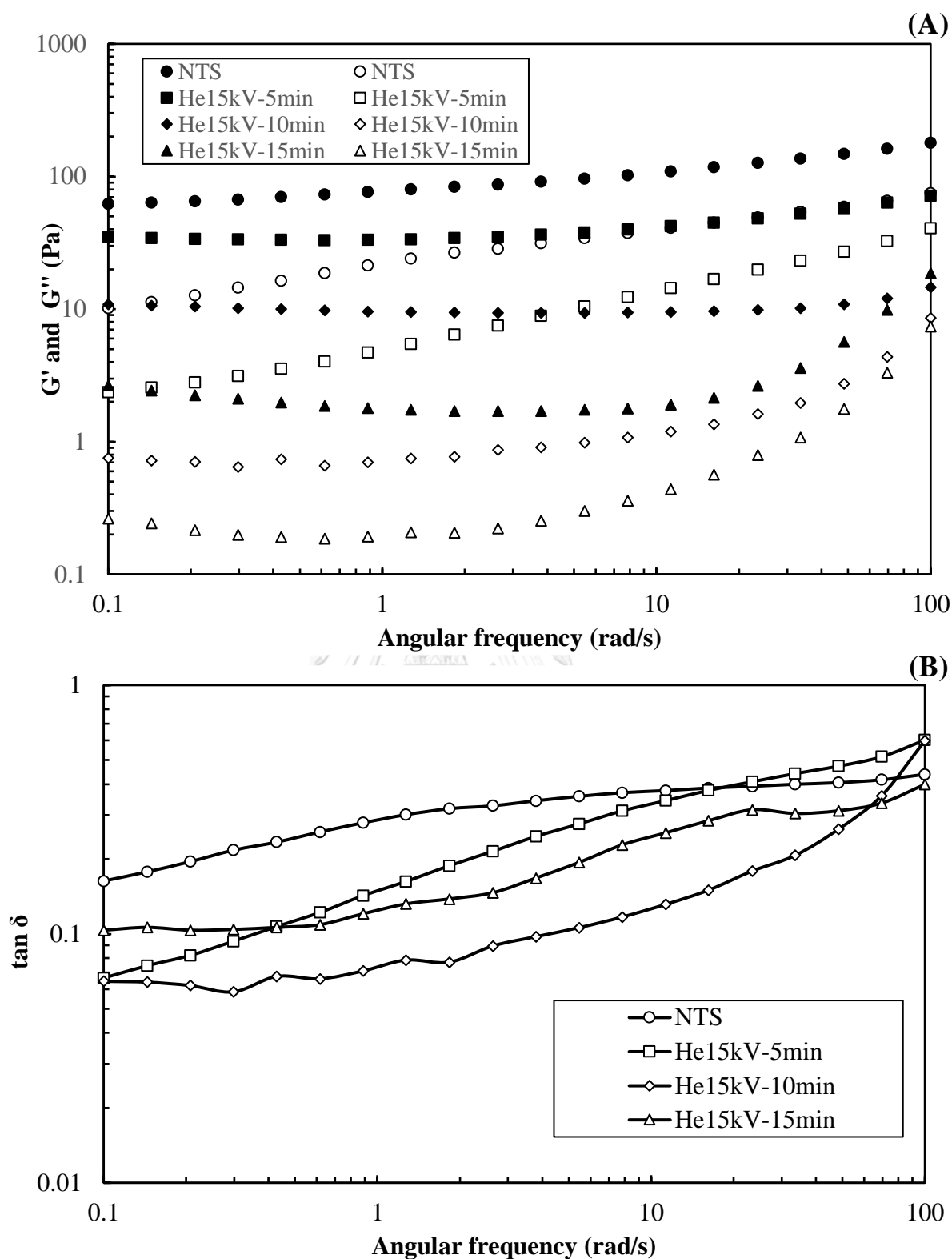


**Figure 4.15** Dynamic rheological behavior of native and helium treated tapioca starch at 15 kV levels and various treatment times (5, 10, 15 min). (A) Angular frequency on  $G'$  (close symbol) and  $G''$  (open symbol) for starch; (B) angular frequency of the loss tangent ( $\tan \delta$ ) at 25°C for starch



#### 4.3.4.2 Flow properties

6% (w/w) native and treated starch paste samples using argon and helium plasma exhibited clockwise hysteresis loops of thixotropic behavior when shear stress ( $\sigma$ ) versus shear ( $\dot{\gamma}$ ) rate data from both increasing-order (up curve) and decreasing-order (down curve) shear cycles were plotted (Figure 4.16 to Figure 4.19), except for helium plasma at 15 kV for 10 and 15 minutes. The parameters of the Herschel-Bulkley model and yield stress fitted to native and treated tapioca starch and the area of hysteresis used for describing the flow curve are shown in Table 4.9. The model well described the steady shear properties with high determination coefficients ( $R^2 = 0.992$  to  $1.000$ ). When sheared at the same shear rate range ( $0.1$ – $500$   $s^{-1}$ ), all treated samples exhibited less thixotropy after increasing treatment time from 5 to 5 minutes at both voltage levels.

The yield stress ( $\sigma_0$ ), which is the required minimal stress to begin the flow of native and plasma-treated starch paste, ranged from  $0.00$  to  $3.16$  Pa. When compared with the native sample, A higher  $\sigma_0$  value was observed at 15 kV for 5 minutes of argon plasma ( $3.16$  Pa), followed by treatment of helium plasma at 10 kV for 10 minutes ( $2.92$  Pa) and the treatment at 15 kV for 10 minutes of argon plasma ( $2.35$  Pa) ( $P < 0.05$ ). The lowest  $\sigma_0$  value was observed after using helium plasma at 15 kV for 15 minutes ( $0.00$  Pa). An increase  $\sigma_0$  value might be due to the rapid aggregation between polymer chains of small fragments of depolymerized starch granules by depolymerization. This presumption is consistent with higher amylose contents (Table 4.4) and lower setback viscosity (Table 4.7) after plasma treatment.

The consistency index (K) value of native and treated tapioca starch was shown in Table 4.9. This result showed that there was no significant change in K value between native and helium-plasma-treated samples at 10 kV for 5 minutes ( $P \geq 0.05$ ). Increasing treatment time from 5 to 15 minutes at 10 kV and 15 kV of both gas types caused the K value to decrease ( $P < 0.05$ ). At 15 kV, the samples treated with helium

plasma had a lower K value than those treated with argon plasma at the same treatment time ( $P < 0.05$ ). In agreement with Bie et al. (2016), the viscosity decreased because of starch molecule disintegration, resulting in a lower K value of modified samples after increasing treatment time. However, the treated samples' lower swelling power and lower peak viscosity could also support this presumption.

Flow behavior index value ( $n$ ) is commonly used to characterize fluid, and semi-fluid behavior was displayed in Figure 4.9 ( $n = 1$  Newtonian,  $< 1$  for shear-thinning, and  $> 1$  for shear-thickening). From the data obtained, it was found that there was no difference between native and treated samples at 10 kV ( $P \geq 0.05$ ). A significant increase in  $n$  value was observed when increasing the treatment time from 5 to 15 minutes at 15 kV of helium plasma modification ( $P < 0.05$ ). The helium-plasma treated sample at 15 kV for 15 minutes had the highest  $n$  value (0.97) ( $P < 0.05$ ), indicating a tendency to be a Newtonian fluid. This finding is probably due to the high energy of helium plasma species that causes etched lead to damage starch surface granules.

Compared to native tapioca starch, the hysteresis area of modified tapioca starch treated with argon and helium plasma decreased significantly ( $P < 0.05$ ). Increasing treatment time from 5 to 15 minutes at 10 kV and 15 kV of argon plasma modification caused the hysteresis area to reduce from 1,689.90 to 267.03 Pa / (s·cm<sup>3</sup>) and 1581.60 to 165.15 Pa / (s·cm<sup>3</sup>), respectively. The same trend was observed for helium plasma modification, in which the hysteresis area reduced from 1716.50 to 788.15 Pa / (s·cm<sup>3</sup>) at 10 kV and 221.31 to 20.60 Pa / (s·cm<sup>3</sup>) at 15 kV. Moreover, the 15 kV helium plasma-treated starch showed a lower hysteresis area than the argon-plasma treated starch under the same condition. A reduction in the hysteresis area is possibly due to the lower weight-average molecular weight ( $\overline{M}_w$ ) of amylopectin, lower swelling power, and higher solubility after plasma treatment. This could reduce the molecular interaction of starch molecules, resulting in lower resistance to shear force.

Thixotropy exhibits a decrease in the flow resistance of starch molecular structures (particle aggregation, polymer entanglement, etc.) that can be organized by applying shear force. As a result of the degraded structure of starch granules caused by plasma treatment, thixotropy is decreased, indicating that its lower structure is organized by shear force. On the other hand, a slight rheopectic property was observed in the sample treated using helium plasma at 15 kV for 10 and 15 minutes. Rheopexy is time-dependent shear-thickening behavior that involves structure build-up induced by shear flow. This could be due to rougher starch granules and amylopectin leaching after plasma treatment, which promoted the formation of a shear-induced structure. Tattiyakul and Rao (2000) discovered that increasing the temperature caused granules to rupture and release amylopectin, which contributed to the shear-induced structural formation of 6% (w/w) gelatinized crosslinked waxy maize starch.

Two-way ANOVA analysis revealed that the effects of types of the feed gas, voltage levels, and their interactions had a significant influence on the values of  $\sigma_0$ , K, n, and hysteresis area of the treated samples ( $P < 0.05$ ) (see appendixes C.86 to C.89). Nevertheless, the interaction between voltage levels and time had no significant effect on the K value ( $P \geq 0.05$ ).

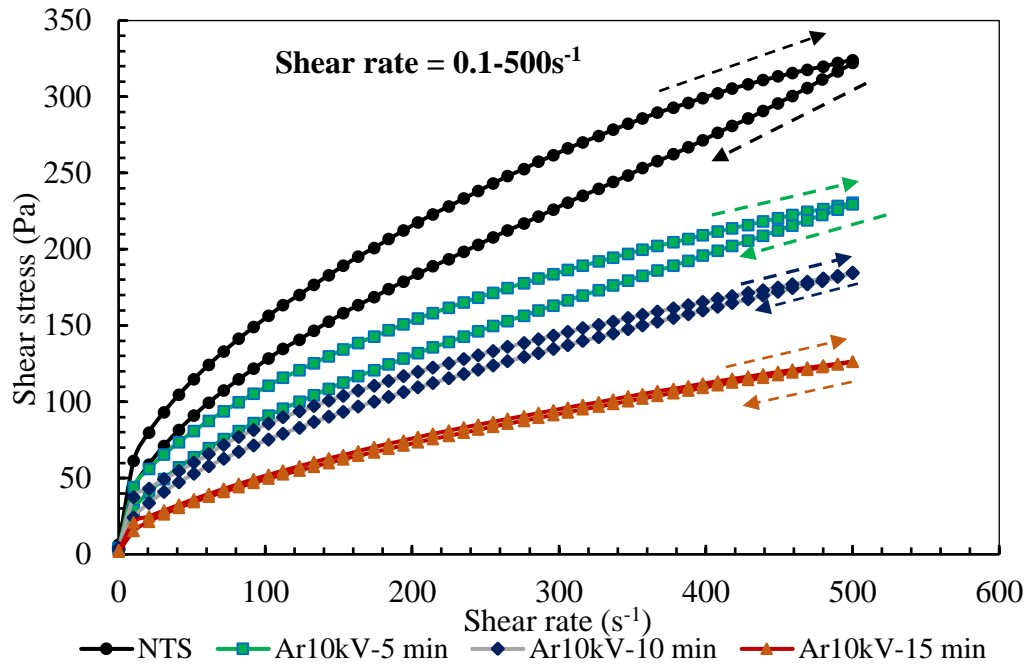


**Figure 4.16** Effect of shear rate on native and argon treated tapioca starch at 10 kV levels and various treatment times (5, 10, 15 min)

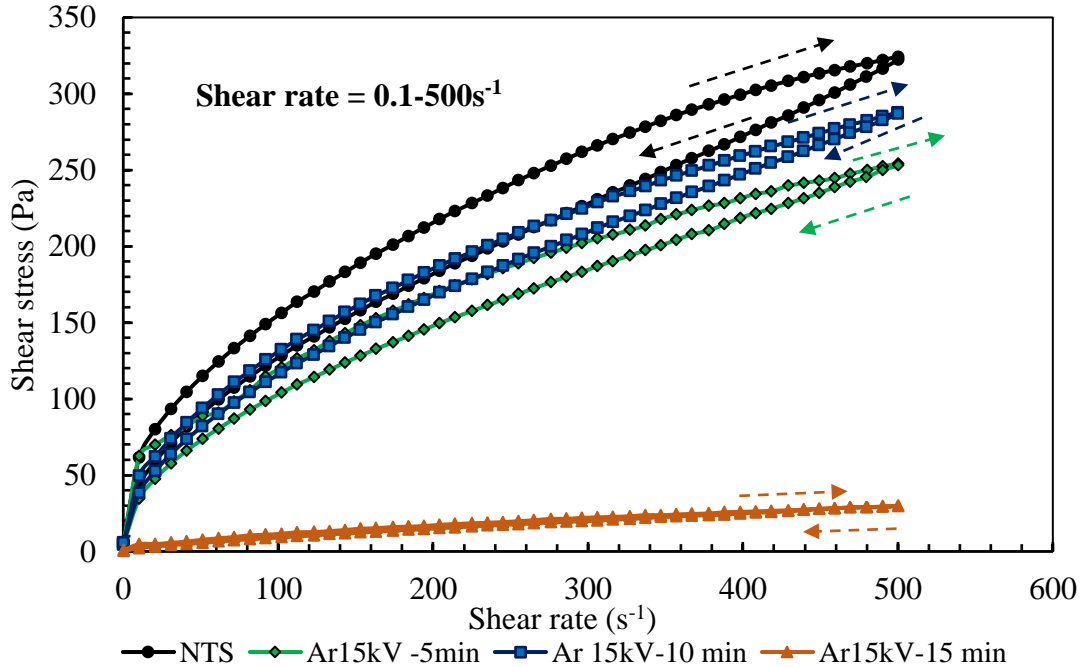


**Figure 4.17** Effect of shear rate on native and argon treated tapioca starch at 15 kV levels and various treatment times (5, 10, 15 min)

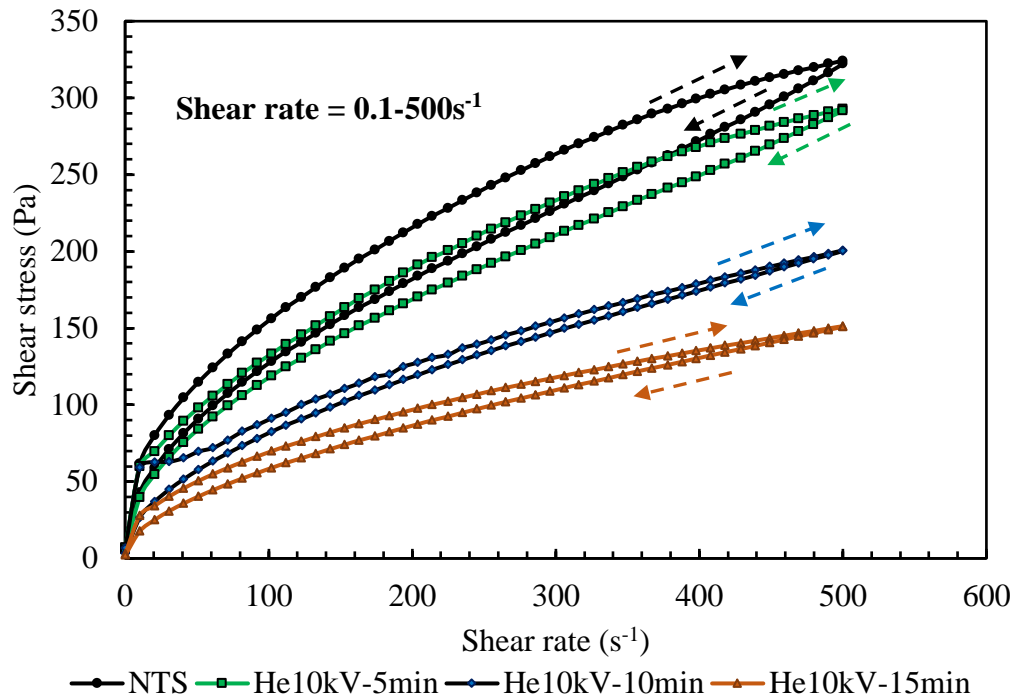


**Figure 4.18** Effect of shear rate on native and helium treated tapioca starch at 10 kV levels and various treatment times (5, 10, 15 min)

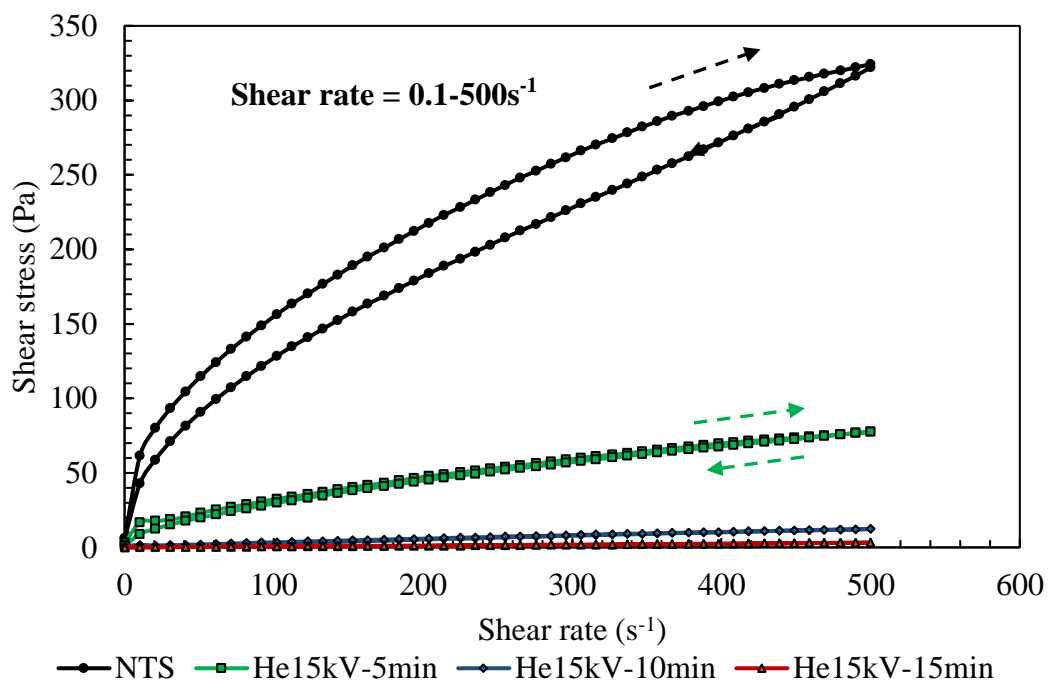


**Figure 4.19** Effect of shear rate on native and helium treated tapioca starch at 15 kV levels and various treatment times (5, 10, 15 min)

**Table 4.9** Parameter of the Herschel-Bulkley model fitted to native and treated tapioca starch during steady shear rate and area of hysteresis

Sample	Herschel-Bulkley				Hysteresis area (Pa / (s·cm <sup>3</sup> ))
	$\sigma_0$ (Pa)	K (Pa·s <sup>n</sup> )	n (-)	R <sup>2</sup>	
NTS	1.26 <sup>c</sup> ± 0.00	8.91 <sup>a</sup> ± 0.25	0.57 <sup>fgh</sup> ± 0.00	0.997	2347.50 <sup>a</sup> ± 70.99
Ar10kV-5min	1.53 <sup>c</sup> ± 0.01	5.99 <sup>bc</sup> ± 0.05	0.58 <sup>def</sup> ± 0.00	0.998	1689.90 <sup>b</sup> ± 172.25
Ar10kV-10min	1.40 <sup>c</sup> ± 0.05	5.43 <sup>c</sup> ± 0.45	0.56 <sup>gh</sup> ± 0.01	0.999	1163.40 <sup>d</sup> ± 44.83
Ar10kV-15min	1.22 <sup>cd</sup> ± 0.10	3.39 <sup>d</sup> ± 0.52	0.59 <sup>def</sup> ± 0.01	1.000	267.03 <sup>f</sup> ± 44.54
Ar15kV-5min	3.16 <sup>a</sup> ± 0.09	6.82 <sup>b</sup> ± 0.24	0.58 <sup>def</sup> ± 0.01	0.999	1581.60 <sup>b</sup> ± 181.16
Ar15kV-10min	2.35 <sup>b</sup> ± 0.42	5.83 <sup>c</sup> ± 0.77	0.61 <sup>cd</sup> ± 0.02	0.999	1354.65 <sup>c</sup> ± 7.71
Ar15kV-15min	0.90 <sup>d</sup> ± 0.03	0.48 <sup>f</sup> ± 0.03	0.64 <sup>c</sup> ± 0.02	0.992	165.15 <sup>f</sup> ± 41.52
He10kV-5min	1.29 <sup>c</sup> ± 0.05	9.49 <sup>a</sup> ± 0.63	0.56 <sup>h</sup> ± 0.01	0.998	1716.50 <sup>b</sup> ± 30.54
He10kV-10min	2.92 <sup>a</sup> ± 0.15	6.00 <sup>bc</sup> ± 0.35	0.57 <sup>fgh</sup> ± 0.02	0.985	776.60 <sup>e</sup> ± 28.11
He10kV-15min	1.45 <sup>d</sup> ± 0.24	3.78 <sup>d</sup> ± 0.18	0.60 <sup>def</sup> ± 0.02	1.000	788.15 <sup>e</sup> ± 45.91
He15kV-5min	0.55 <sup>e</sup> ± 0.64	1.76 <sup>e</sup> ± 0.13	0.60 <sup>de</sup> ± 0.01	1.000	221.31 <sup>f</sup> ± 12.53
He15kV-10min	0.12 <sup>f</sup> ± 0.05	0.06 <sup>f</sup> ± 0.00	0.87 <sup>b</sup> ± 0.04	0.999	-46.39 <sup>g</sup> ± 1.06
He15kV-15min	0.00 <sup>f</sup> ± 0.00	0.01 <sup>f</sup> ± 0.00	0.97 <sup>a</sup> ± 0.01	0.998	-20.60 <sup>g</sup> ± 4.07

Means ± standard deviation (n = 2) with different letters within a column are significantly different (P ≤ 0.05).

$\sigma_0$ : yield stress; K: consistency index; n: the flow behavior index

## Chapter 5 Conclusions

The result confirmed that tapioca starch modification in solid-state using non-thermal dielectric barrier discharge (DBD) plasma could be done. In comparison with native tapioca starch, the structural properties of plasma-treated samples showed dented starch granules without modification of starch birefringence. An unchanged characteristic C-type diffraction pattern of treated samples was observed after plasma treatment, but the relative crystallinity of all samples was reduced. Moreover, the treated samples had higher amylose content and reducing sugar with increasing voltage levels and treatment times, except for the sample treated with helium plasma at 15 kV, which could reduce apparent amylose after increasing treatment times. Both argon and helium plasma treatments had no significant change in functional groups and could lower  $\overline{M}_w$  of amylopectin.

For the functional properties of plasma-treated samples, there was no negative effect on pH and color. Furthermore, there was no significant change in argon-plasma-treated samples' moisture content, while the samples treated with helium plasma had a significantly lower moisture content than native and argon plasma-treated samples. Lower peak viscosity, breakdown percentage, and setback percentage were found when the sample was subjected to short-time argon plasma treatment for 5 minutes. However, increasing treatment time at both power levels and gas types caused the breakdown and setback percentages to increase. Increasing the voltage level and times for argon and helium plasma treatment could reduce the swelling power and enhance the solubility of samples. After plasma treatment, the water-binding capacity of samples was increased. The frequency sweep test revealed that 6% (w/w) starch paste samples had higher  $G'$  than  $G''$ , indicating dominated elastic behavior. Tests on 6% gelatinized modified starch pastes showed lower thixotropy with increasing voltage and treatment times. The argon plasma-modified samples at 15 kV for 5 and 10 minutes and helium plasma at 10 kV for 10 minutes showed a significant increase in the yield stress ( $\sigma_0$ ) value but a decrease in the consistency index (K). The lowest K value was observed after using helium plasma at 15 kV for 15 minutes. It also showed that the helium plasma modification at 15 kV for 15 minutes had the highest flow behavior index (n), which means that the fluid was more likely to be a Newtonian fluid.

To summarize, helium plasma is significantly easier to generate than Argon plasma when higher voltage levels and treatment times are applied. As a result, helium plasma affects tapioca starch's structural, physical, chemical, and functional properties more than argon plasma.

### **Suggestion**

- The uniformity of solid-state plasma modification should be improved
- Other types of feed gas and treatment conditions should be further investigated.
- The plasma modification process should be scaled up for use in the manufacturing of modified starch.
- The plasma-modified samples should be applied to food products and their properties studied. For example, starch gum candy manufacturing. The plasma-treated samples are capable of producing highly concentrated fluid pastes that are solidified into firm gels after cooling and aging. Most manufacturers now use pressurized cooking to prepare starch gum candies.



## REFERENCES

- AACC. (2000). Method 61-02.01. Determination of the pasting properties of rice with the rapid visco analyzer. *AACC International Approved Methods of Analysis*.
- Abd-Allah, M. A., Foda, Y. H., & Hamed, M. G. E. (1974). Characteristics and “Fodal”-Factor of Mango Seed Kernel Starch. *Starch - Stärke*, 26(12), 426-433. <https://doi.org/https://doi.org/10.1002/star.19740261207>
- Abd Allah, Z. (2012). *Non-thermal atmospheric pressure plasma for remediation of volatile organic compounds*. The University of Manchester (United Kingdom).
- Alcázar-Alay, S. C., & Meireles, M. A. A. (2015). Physicochemical properties, modifications and applications of starches from different botanical sources. *Food Science and Technology*, 35, 215-236. <https://doi.org/https://doi.org/10.1590/1678-457X.6749>.
- AOAC. (2000). *Official Methods of Analysis*. Association of Official Analytical Chemists, Maryland, USA
- Ashogbon, A. O., & Akintayo, E. T. (2014). Recent trend in the physical and chemical modification of starches from different botanical sources: A review. *Starch - Stärke*, 66(1-2), 41-57. <https://doi.org/https://doi.org/10.1002/star.201300106>
- Asioli, D., Aschemann-Witzel, J., Caputo, V., Vecchio, R., Annunziata, A., Næs, T., & Varela, P. (2017). Making sense of the “clean label” trends: A review of consumer food choice behavior and discussion of industry implications. *Food Research International*, 99, 58-71. <https://doi.org/https://doi.org/10.1016/j.foodres.2017.07.022>
- Bahrami, N., Bayliss, D., Chope, G., Penson, S., Pehinec, T., & Fisk, I. D. (2016). Cold plasma: A new technology to modify wheat flour functionality. *Food Chemistry*, 202, 247-253. <https://doi.org/https://doi.org/10.1016/j.foodchem.2016.01.113>
- Banura, S., Thirumdas, R., Kaur, A., Deshmukh, R. R., & Annapure, U. S. (2018). Modification of starch using low pressure radio frequency air plasma. *LWT*, 89, 719-724. <https://doi.org/https://doi.org/10.1016/j.lwt.2017.11.056>
- Barretti, B. R. V., Almeida, V. S. d., Ito, V. C., Silva, B. M., Carvalho Filho, M. A. d. S., Sydney, E. B., . . . Lacerda, L. G. (2020). Combination of organic acids and heat-moisture treatment on the normal and waxy corn starch: thermal, structural, pasting properties, and digestibility investigation. *Food Science and Technology*, 42, e33120. <https://doi.org/10.1590/fst.33120>
- BeMiller, J. N. (2019). 6 - Starches: Molecular and Granular Structures and Properties. In J. N. BeMiller (Ed.), *Carbohydrate Chemistry for Food Scientists (Third Edition)* (pp. 159-189). AACC International Press. <https://doi.org/https://doi.org/10.1016/B978-0-12-812069-9.00006-6>
- Bergthaller, W., & Hollmann, J. (2014). Starch☆. In *Reference Module in Chemistry, Molecular Sciences and Chemical Engineering*. Elsevier. <https://doi.org/https://doi.org/10.1016/B978-0-12-409547-2.11374-5>
- Bie, P., Pu, H., Zhang, B., Su, J., Chen, L., & Li, X. (2016). Structural characteristics and rheological properties of plasma-treated starch. *Innovative Food Science & Emerging Technologies*, 34, 196-204. <https://doi.org/https://doi.org/10.1016/j.ifset.2015.11.019>

- Bonechi, C., Consumi, M., Donati, A., Leone, G., Magnani, A., Tamasi, G., & Rossi, C. (2017). Biomass: an overview. In *Bioenergy systems for the future* (pp. 3-42). Elsevier. <https://doi.org/https://doi.org/10.1016/B978-0-08-101031-0.00001-6>
- Breuninger, W. F., Piyachomkwan, K., & Sriroth, K. (2009). Chapter 12 - Tapioca/Cassava Starch: Production and Use. In J. BeMiller & R. Whistler (Eds.), *Starch (Third Edition)* (pp. 541-568). Academic Press. <https://doi.org/https://doi.org/10.1016/B978-0-12-746275-2.00012-4>
- Chaiwat, W., Wongsagonsup, R., Tangpanichyanon, N., Jariyaporn, T., Deeyai, P., Suphantharika, M., . . . Dangtip, S. (2016). Argon Plasma Treatment of Tapioca Starch Using a Semi-continuous Downer Reactor. *Food and Bioprocess Technology*, 9(7), 1125-1134. <https://doi.org/10.1007/s11947-016-1701-6>
- Chaple, S., Sarangapani, C., Jones, J., Carey, E., Causeret, L., Genson, A., . . . Bourke, P. (2020). Effect of atmospheric cold plasma on the functional properties of whole wheat (*Triticum aestivum* L.) grain and wheat flour. *Innovative Food Science & Emerging Technologies*, 66, 102529. <https://doi.org/https://doi.org/10.1016/j.ifset.2020.102529>
- Charles, A. L., Chang, Y. H., Ko, W. C., Sriroth, K., & Huang, T. C. (2005). Influence of Amylopectin Structure and Amylose Content on the Gelling Properties of Five Cultivars of Cassava Starches. *Journal of Agricultural and Food Chemistry*, 53(7), 2717-2725. <https://doi.org/10.1021/jf048376+>
- Chen, C. R., & Ramaswamy, H. S. (1999). Rheology of tapioca starch. *Food Research International*, 32(5), 319-325. [https://doi.org/https://doi.org/10.1016/S0963-9969\(99\)00090-3](https://doi.org/https://doi.org/10.1016/S0963-9969(99)00090-3)
- Chen, H. H., Chen, Y. K., & Chang, H. C. (2012). Evaluation of physicochemical properties of plasma treated brown rice. *Food Chemistry*, 135(1), 74-79. <https://doi.org/https://doi.org/10.1016/j.foodchem.2012.04.092>
- Chhabra, R. P. (2010). Non-Newtonian Fluids: An Introduction. In J. M. Krishnan, A. P. Deshpande, & P. B. S. Kumar (Eds.), *Rheology of Complex Fluids* (pp. 3-34). Springer New York. [https://doi.org/10.1007/978-1-4419-6494-6\\_1](https://doi.org/10.1007/978-1-4419-6494-6_1)
- Chizoba Ekezie, F.-G., Sun, D.-W., & Cheng, J.-H. (2017). A review on recent advances in cold plasma technology for the food industry: Current applications and future trends. *Trends in Food Science & Technology*, 69, 46-58. <https://doi.org/https://doi.org/10.1016/j.tifs.2017.08.007>
- Crosbie, G. B. (1991). The relationship between starch swelling properties, paste viscosity and boiled noodle quality in wheat flours. *Journal of Cereal Science*, 13(2), 145-150. [https://doi.org/https://doi.org/10.1016/S0733-5210\(09\)80031-3](https://doi.org/https://doi.org/10.1016/S0733-5210(09)80031-3)
- Cui, S. W. (2005). *Food Carbohydrates*. CRC press. <https://doi.org/10.1201/9780203485286>
- Dar, M. Z., Deepika, K., Jan, K., Swer, T. L., Kumar, P., Verma, R., . . . Bashir, K. (2018). Modification of structure and physicochemical properties of buckwheat and oat starch by  $\gamma$ -irradiation. *International Journal of Biological Macromolecules*, 108, 1348-1356. <https://doi.org/https://doi.org/10.1016/j.ijbiomac.2017.11.067>
- Dome, K., Podgorbunskikh, E., Bychkov, A., & Lomovsky, O. (2020). Changes in the Crystallinity Degree of Starch Having Different Types of Crystal Structure after Mechanical Pretreatment. *Polymers*, 12(3), 641. <https://www.mdpi.com/2073-4360/12/3/641>

- Domonkos, M., Tichá, P., Trejbal, J., & Demo, P. (2021). Applications of Cold Atmospheric Pressure Plasma Technology in Medicine, Agriculture and Food Industry. *Applied Sciences*, 11(11), 4809. <https://www.mdpi.com/2076-3417/11/11/4809>
- Exarhopoulos, S., & Raphaelides, S. N. (2012). Morphological and structural studies of thermally treated starch-fatty acid systems. *Journal of Cereal Science*, 55(2), 139-152. <https://doi.org/https://doi.org/10.1016/j.jcs.2011.10.011>
- French, D. (1972). Fine Structure of Starch and its Relationship to the Organization of Starch Granules. *Journal of the Japanese Society of Starch Science*, 19(1), 8-25. <https://doi.org/10.5458/jag1972.19.8>
- Gayin, J., Abdel-Aal, E.-S. M., Manful, J., & Bertoft, E. (2016). Unit and internal chain profile of African rice (*Oryza glaberrima*) amylopectin. *Carbohydrate Polymers*, 137, 466-472. <https://doi.org/https://doi.org/10.1016/j.carbpol.2015.11.008>
- Grace, N. C. F., & Jeyakumar Henry, C. (2020). The Physicochemical Characterization of Unconventional Starches and Flours Used in Asia. *Foods*, 9(2), 182. <https://www.mdpi.com/2304-8158/9/2/182>
- Grgić, I., Ačkar, Đ., Barišić, V., Vlainić, M., Knežević, N., & Medverec Knežević, Z. (2019). Nonthermal methods for starch modification—A review. *Journal of Food Processing and Preservation*, 43(12), e14242. <https://doi.org/https://doi.org/10.1111/jfpp.14242>
- Gunaratne, A., & Hoover, R. (2002). Effect of heat–moisture treatment on the structure and physicochemical properties of tuber and root starches. *Carbohydrate Polymers*, 49(4), 425-437. [https://doi.org/https://doi.org/10.1016/S0144-8617\(01\)00354-X](https://doi.org/https://doi.org/10.1016/S0144-8617(01)00354-X)
- Guo, Z., Gou, Q., Yang, L., Yu, Q.-l., & Han, L. (2022). Dielectric barrier discharge plasma: A green method to change structure of potato starch and improve physicochemical properties of potato starch films. *Food Chemistry*, 370, 130992. <https://doi.org/https://doi.org/10.1016/j.foodchem.2021.130992>
- Hizukuri, S. (1986). Polymodal distribution of the chain lengths of amylopectins, and its significance. *Carbohydrate Research*, 147(2), 342-347. [https://doi.org/10.1016/s0008-6215\(00\)90643-8](https://doi.org/10.1016/s0008-6215(00)90643-8)
- Hojnik, N., Cvelbar, U., Tavčar-Kalcher, G., Walsh, J. L., & Križaj, I. (2017). Mycotoxin Decontamination of Food: Cold Atmospheric Pressure Plasma versus “Classic” Decontamination. *Toxins*, 9(5), 151. <https://www.mdpi.com/2072-6651/9/5/151>
- Hoover, R. (2001). Composition, molecular structure, and physicochemical properties of tuber and root starches: a review. *Carbohydrate Polymers*, 45(3), 253-267. [https://doi.org/https://doi.org/10.1016/S0144-8617\(00\)00260-5](https://doi.org/https://doi.org/10.1016/S0144-8617(00)00260-5)
- Hoover, R., Hughes, T., Chung, H. J., & Liu, Q. (2010). Composition, molecular structure, properties, and modification of pulse starches: A review. *Food Research International*, 43(2), 399-413. <https://doi.org/https://doi.org/10.1016/j.foodres.2009.09.001>
- Jae Koo, L., Babaeva, N. Y., Hyun Chul, K., Manuilenko, O. V., & Jong Won, S. (2004). Simulation of capacitively coupled single- and dual-frequency RF discharges. *IEEE Transactions on Plasma Science*, 32(1), 47-53. <https://doi.org/10.1109/TPS.2004.823975>
- Juliano, B. O. (1971). A simplified assay for milled rice amylose. *Cereal Science Today*

- 16, 334-360. <https://ci.nii.ac.jp/naid/10021062690/en/>
- Khorram, S., Zakerhamidi, M. S., & Karimzadeh, Z. (2015). Polarity functions' characterization and the mechanism of starch modification by DC glow discharge plasma. *Carbohydrate Polymers*, 127, 72-78. <https://doi.org/https://doi.org/10.1016/j.carbpol.2015.03.056>
- Klein, B., Vanier, N. L., Moomand, K., Pinto, V. Z., Colussi, R., da Rosa Zavareze, E., & Dias, A. R. G. (2014). Ozone oxidation of cassava starch in aqueous solution at different pH. *Food Chemistry*, 155, 167-173. <https://doi.org/https://doi.org/10.1016/j.foodchem.2014.01.058>
- Kumar, R., & Khatkar, B. S. (2017). Thermal, pasting and morphological properties of starch granules of wheat (*Triticum aestivum* L.) varieties. *Journal of Food Science and Technology*, 54(8), 2403-2410. <https://doi.org/10.1007/s13197-017-2681-x>
- Lagarrigue, S., & Alvarez, G. (2001). The rheology of starch dispersions at high temperatures and high shear rates: a review. *Journal of Food Engineering*, 50(4), 189-202. [https://doi.org/https://doi.org/10.1016/S0260-8774\(00\)00239-9](https://doi.org/https://doi.org/10.1016/S0260-8774(00)00239-9)
- Laroque, D. A., Seo, S. T., Valencia, G. A., Laurindo, J. B., & Carciofi, B. A. M. (2022). Cold plasma in food processing: Design, mechanisms, and application. *Journal of Food Engineering*, 312, 110748. <https://doi.org/https://doi.org/10.1016/j.jfoodeng.2021.110748>
- Li, M., & Lee, T.-C. (1996). Effect of Cysteine on the Functional Properties and Microstructures of Wheat Flour Extrudates. *Journal of Agricultural and Food Chemistry*, 44(7), 1871-1880. <https://doi.org/10.1021/jf9505741>
- Lii, C.-y., Liao, C.-d., Stobinski, L., & Tomasik, P. (2003). Effect of corona discharges on granular starches. *Journal of Food Agriculture and Environment*, 1(2), 143-149.
- Lii, C. Y., Liao, C. D., Stobinski, L., & Tomasik, P. (2002). Effects of hydrogen, oxygen, and ammonia low-pressure glow plasma on granular starches [Article]. *Carbohydrate Polymers*, 49(4), 449-456. [https://doi.org/10.1016/S0144-8617\(01\)00351-4](https://doi.org/10.1016/S0144-8617(01)00351-4)
- Liu, Y., Winter, H. H., & Perry, S. L. (2017). Linear viscoelasticity of complex coacervates. *Advances in Colloid and Interface Science*, 239, 46-60. <https://doi.org/https://doi.org/10.1016/j.cis.2016.08.010>
- Luallen, T. (2018). Chapter 13 - Utilizing Starches in Product Development. In M. Sjöö & L. Nilsson (Eds.), *Starch in Food (Second Edition)* (pp. 545-579). Woodhead Publishing. <https://doi.org/https://doi.org/10.1016/B978-0-08-100868-3.00013-5>
- Lund, D., & Lorenz, K. J. (1984). Influence of time, temperature, moisture, ingredients, and processing conditions on starch gelatinization. *C R C Critical Reviews in Food Science and Nutrition*, 20(4), 249-273. <https://doi.org/10.1080/10408398409527391>
- Masina, N., Choonara, Y. E., Kumar, P., du Toit, L. C., Govender, M., Indermun, S., & Pillay, V. (2017). A review of the chemical modification techniques of starch. *Carbohydrate Polymers*, 157, 1226-1236. <https://doi.org/https://doi.org/10.1016/j.carbpol.2016.09.094>
- Medcalf, D. G. (1965). Wheat starches I. Comparison of physicochemical properties. *Cereal Chemistry*, 42, 558-568. <https://ci.nii.ac.jp/naid/10012126745/en/>
- Miao, M., Jiang, B., Cui, S. W., Zhang, T., & Jin, Z. (2015). Slowly Digestible Starch—

- A Review. *Critical Reviews in Food Science and Nutrition*, 55(12), 1642-1657. <https://doi.org/10.1080/10408398.2012.704434>
- Okyere, A. Y., Bertoft, E., & Annor, G. A. (2019). Modification of cereal and tuber waxy starches with radio frequency cold plasma and its effects on waxy starch properties. *Carbohydrate Polymers*, 223, 115075. <https://doi.org/https://doi.org/10.1016/j.carbpol.2019.115075>
- Pankaj, S. K., Wan, Z., & Keener, K. M. (2018). Effects of Cold Plasma on Food Quality: A Review. *Foods*, 7(1), 4. <https://www.mdpi.com/2304-8158/7/1/4>
- Pérez, S., Baldwin, P. M., & Gallant, D. J. (2009). Chapter 5 - Structural Features of Starch Granules I. In J. BeMiller & R. Whistler (Eds.), *Starch (Third Edition)* (pp. 149-192). Academic Press. <https://doi.org/https://doi.org/10.1016/B978-0-12-746275-2.00005-7>
- Prasertsung, I., Chutinate, P., Watthanaphanit, A., Saito, N., & Damrongsakkul, S. (2017). Conversion of cellulose into reducing sugar by solution plasma process (SPP). *Carbohydrate Polymers*, 172, 230-236. <https://doi.org/https://doi.org/10.1016/j.carbpol.2017.05.025>
- Rickard, J. E., Asaoka, M., & Blanshard, J. M. V. (1991). The physico-chemical properties of cassava starch. *Tropical science.*, 31(2), 189-207. <http://europemc.org/abstract/AGR/IND91031212>
- Robin, J. P. (1974). Lint-nerized starches. Gel filtration and enzymatic studies of insoluble residues from prolonged acid treatment of potato starch. *Cereal Chemistry*, 51, 389-406. <https://ci.nii.ac.jp/naid/80003929647/en/>
- Sánchez, T., Salcedo, E., Ceballos, H., Dufour, D., Mafla, G., Morante, N., . . . Moreno, I. X. (2009). Screening of Starch Quality Traits in Cassava (*Manihot esculenta* Crantz). *Starch - Stärke*, 61(1), 12-19. <https://doi.org/https://doi.org/10.1002/star.200800058>
- Schirmer, M., Jekle, M., & Becker, T. (2015). Starch gelatinization and its complexity for analysis. *Starch - Stärke*, 67(1-2), 30-41. <https://doi.org/https://doi.org/10.1002/star.201400071>
- Schmitz, C. S., De Simas, K. N., Santos, K., João, J. J., De Mello Castanho Amboni, R. D., & Amante, E. R. (2006). Cassava starch functional properties by etherification – hydroxypropylation. *International Journal of Food Science & Technology*, 41(6), 681-687. <https://doi.org/https://doi.org/10.1111/j.1365-2621.2005.01136.x>
- Schoch, T. J. (1964). (28) Swelling Power and solubility of Granular Starches. *Methods in Carbohydrate Chemistry*, 106-108.
- Schweigert, I., Zakrevsky, D., Gugin, P., Yelak, E., Golubitskaya, E., Troitskaya, O., & Koval, O. (2019). Interaction of Cold Atmospheric Argon and Helium Plasma Jets with Bio-Target with Grounded Substrate Beneath. *Applied Sciences*, 9(21), 4528. <https://www.mdpi.com/2076-3417/9/21/4528>
- Shah, N., Mewada, R. K., & Mehta, T. (2016). Crosslinking of starch and its effect on viscosity behaviour. *Reviews in Chemical Engineering*, 32(2), 265-270. <https://doi.org/doi:10.1515/revce-2015-0047>
- Shariffa, Y. N., Karim, A. A., Fazilah, A., & Zaidul, I. S. M. (2009). Enzymatic hydrolysis of granular native and mildly heat-treated tapioca and sweet potato starches at sub-gelatinization temperature. *Food Hydrocolloids*, 23(2), 434-440. <https://doi.org/https://doi.org/10.1016/j.foodhyd.2008.03.009>

- Shen, H., Ge, X., Zhang, B., Su, C., Zhang, Q., Jiang, H., . . . Li, W. (2021). Understanding the multi-scale structure, physicochemical properties and in vitro digestibility of citrate naked barley starch induced by non-thermal plasma [10.1039/D1FO00678A]. *Food & Function*, 12(17), 8169-8180. <https://doi.org/10.1039/D1FO00678A>
- Singh, S., Raina, C. S., Bawa, A. S., & Saxena, D. C. (2005). Effect of Heat-Moisture Treatment and Acid Modification on Rheological, Textural, and Differential Scanning Calorimetry Characteristics of Sweetpotato Starch. *Journal of Food Science*, 70(6), e373-e378. <https://doi.org/https://doi.org/10.1111/j.1365-2621.2005.tb11441.x>
- Sriroth, K., Santisopasri, V., Petchalanuwat, C., Kurotjanawong, K., Piyachomkwan, K., & Oates, C. G. (1999). Cassava starch granule structure–function properties: influence of time and conditions at harvest on four cultivars of cassava starch. *Carbohydrate Polymers*, 38(2), 161-170. [https://doi.org/https://doi.org/10.1016/S0144-8617\(98\)00117-9](https://doi.org/https://doi.org/10.1016/S0144-8617(98)00117-9)
- Steffe, J. F. (1996). *Rheological methods in food process engineering*. Freeman press.
- Tattiyakul, J., & Rao, M. A. (2000). Rheological behavior of cross-linked waxy maize starch dispersions during and after heating. *Carbohydrate Polymers*, 43(3), 215-222. [https://doi.org/https://doi.org/10.1016/S0144-8617\(00\)00160-0](https://doi.org/https://doi.org/10.1016/S0144-8617(00)00160-0)
- Tattiyakul, J., Rao, M. A., & Datta, A. K. (2002). Heat transfer to a canned corn starch dispersion under intermittent agitation. *Journal of Food Engineering*, 54(4), 321-329. [https://doi.org/https://doi.org/10.1016/S0260-8774\(01\)00218-7](https://doi.org/https://doi.org/10.1016/S0260-8774(01)00218-7)
- Thirumdas, R., Kadam, D., & Annapure, U. S. (2017). Cold Plasma: an Alternative Technology for the Starch Modification. *Food Biophysics*, 12(1), 129-139. <https://doi.org/10.1007/s11483-017-9468-5>
- Thirumdas, R., Trimukhe, A., Deshmukh, R. R., & Annapure, U. S. (2017). Functional and rheological properties of cold plasma treated rice starch. *Carbohydrate Polymers*, 157, 1723-1731. <https://doi.org/https://doi.org/10.1016/j.carbpol.2016.11.050>
- Trela, V. D., Ramallo, A. L., & Albani, O. A. (2020). Synthesis and Characterization of Acetylated Cassava Starch with Different Degrees of Substitution. *Brazilian Archives of Biology and Technology*, 63. <https://doi.org/10.1590/1678-4324-2020180292>
- Trithavisup, K., Krusong, K., & Tananuwong, K. (2019). In-depth study of the changes in properties and molecular structure of cassava starch during resistant dextrin preparation. *Food Chemistry*, 297, 124996. <https://doi.org/https://doi.org/10.1016/j.foodchem.2019.124996>
- Villa Zabala, C. C. (2020). An overview on starch structure and chemical nature. *Starch-based Nanomaterials*, 3-9. [https://doi.org/https://doi.org/10.1007/978-3-030-42542-5\\_2](https://doi.org/https://doi.org/10.1007/978-3-030-42542-5_2)
- Wang, S., Chao, C., Cai, J., Niu, B., Copeland, L., & Wang, S. (2020). Starch–lipid and starch–lipid–protein complexes: A comprehensive review. *Comprehensive Reviews in Food Science and Food Safety*, 19(3), 1056-1079. <https://doi.org/https://doi.org/10.1111/1541-4337.12550>
- Wang, S., & Copeland, L. (2013). Molecular disassembly of starch granules during gelatinization and its effect on starch digestibility: a review. *Food Funct*, 4(11), 1564-1580. <https://doi.org/10.1039/c3fo60258c>

- Wongsagonsup, R., Deeyai, P., Chaiwat, W., Horrungsawat, S., Leejariensuk, K., Suphantharika, M., . . . Dangtip, S. (2014). Modification of tapioca starch by non-chemical route using jet atmospheric argon plasma. *Carbohydrate Polymers*, *102*, 790-798.  
<https://doi.org/https://doi.org/10.1016/j.carbpol.2013.10.089>
- Yan, S.-L., Chen, G.-Y., Hou, Y.-J., & Chen, Y. (2020). Improved solubility of banana starch by dielectric barrier discharge plasma treatment. *International Journal of Food Science & Technology*, *55*(2), 641-648.  
<https://doi.org/https://doi.org/10.1111/ijfs.14318>
- Yoo, S.-H., & Jane, J.-I. (2002). Molecular weights and gyration radii of amylopectins determined by high-performance size-exclusion chromatography equipped with multi-angle laser-light scattering and refractive index detectors. *Carbohydrate Polymers*, *49*(3), 307-314. [https://doi.org/https://doi.org/10.1016/S0144-8617\(01\)00339-3](https://doi.org/https://doi.org/10.1016/S0144-8617(01)00339-3)
- Yu, L., & Christie, G. (2005). Microstructure and mechanical properties of orientated thermoplastic starches. *Journal of Materials Science*, *40*(1), 111-116.  
<https://doi.org/10.1007/s10853-005-5694-1>
- Zavareze, E. d. R., & Dias, A. R. G. (2011). Impact of heat-moisture treatment and annealing in starches: A review. *Carbohydrate Polymers*, *83*(2), 317-328.  
<https://doi.org/https://doi.org/10.1016/j.carbpol.2010.08.064>
- Zhang, B., Chen, L., Li, X., Li, L., & Zhang, H. (2015). Understanding the multi-scale structure and functional properties of starch modulated by glow-plasma: A structure-functionality relationship. *Food Hydrocolloids*, *50*, 228-236.  
<https://doi.org/https://doi.org/10.1016/j.foodhyd.2015.05.002>
- Zhang, B., Xiong, S., Li, X., Li, L., Xie, F., & Chen, L. (2014). Effect of oxygen glow plasma on supramolecular and molecular structures of starch and related mechanism. *Food Hydrocolloids*, *37*, 69-76.  
<https://doi.org/https://doi.org/10.1016/j.foodhyd.2013.10.034>
- Zhu, F. (2015). Composition, structure, physicochemical properties, and modifications of cassava starch. *Carbohydrate Polymers*, *122*, 456-480.  
<https://doi.org/https://doi.org/10.1016/j.carbpol.2014.10.063>
- Zou, J.-J., Liu, C.-J., & Eliasson, B. (2004). Modification of starch by glow discharge plasma. *Carbohydrate Polymers*, *55*(1), 23-26.  
<https://doi.org/https://doi.org/10.1016/j.carbpol.2003.06.001>

## **Appendix A**

### **Analytical methods**

#### **A.1 Color ( $L^*$ $a^*$ $b^*$ )**

##### Instrument

1. Chroma meter (Konica Minolta model CR-400, Osaka, Japan)

##### Methods

1. Place the sample on the granular material attachment and compact.
2. Insert the Minolta Chroma meter was into a granular material attachment.
3. Measure And record the following parameters  
L\* value for lightness (100 white, 0 black)  
a\* value for red or green color (positive values are red color, negative values are green color)  
b\* value for yellow or blue color (positive values are yellow color, negative values are blue color)

#### **A.2 Surface morphology (Scientific and Technological Research Equipment Centre (STREC), Chulalongkorn University)**

##### Instrument

1. Scanning electron microscope (Model IT5R, JEOL Co., Ltd. Japan)

##### Methods

1. 1. Mount the sample on aluminum stubs using double-sided tape and spitter-coat with gold.
2. Investigate using SEM at an accelerated voltage of 15 kV.



### **A.3 Birefringence pattern**

#### Instrument

1. The Olympus BX51 light microscope (Melville, NY., USA)

#### Chemical reagent

1. 50% glycerol solution

#### Methods

1. Drop 1-2 drops of 50% glycerol solution on a glass slide.
2. Suspend the starch sample in the solution.
3. View under a light microscope equipped with a polarizer and a camera set.

### **A.4 X-ray diffraction pattern** (Scientific and Technological Research Equipment Centre (STREC), Chulalongkorn University)

#### Instrument

1. X-ray diffractometer (Model D8 Discover, Bruker AXS, Germany)

#### Methods

1. Place the starch sample into the sample plate
2. Put the sample in a sample holder in the X-ray diffractometer
3. Set up conditions for XRD analysis following Table A.1
4. Compare XRD pattern with the peak characteristic of theoretical diffractogram ( $2\theta$ , d-spacing, and intensity) given by Zobel (1964) (Table A.2)
5. Calculate the degree of crystallinity using Equation A.1

$$\% \text{ Crystallinity} = \frac{\text{Crystalline area}}{\text{Total area}} \times 100 \quad (\text{A.1})$$

**Table A.1** Conditions of XRD analysis

Target	Cu
Voltage	40 kV
Current	40 mA
Angle (2 $\theta$ )	2-40 degree
Step	0.0229 degree
Step time	197 sec
Detector	VÅNTEC-1 Detector (Super Speed Detector)

### **A.5 Moisture content (AOAC, 2000)**

#### Instruments

1. Hot air oven (Mettler, DO6062, Germany)
2. Desiccator
3. Weighing machine 4 digit (Denver Instrument, SI-234, Germany)

#### Methods

1. Weigh an aluminum pan that has been dried, weighed to a constant value, and kept in a desiccator.
2. Fill the aluminum pan with 3 g of the sample.
3. Dry the sample to constant weight in a hot air oven set to 105 °C.
4. Bring the sample pan out of the oven. Cool the pan in a desiccator to room temperature before weighing the sample.
5. Calculate moisture content following Equation A.2

$$\% \text{ Moisture content (wb)} = \frac{W_1 - W_2}{W_1}$$

Where  $W_1$  is g of sample before drying

$W_2$  is g of sample after drying

## A.6 Ash content (AOAC, 2000)

### Instruments

1. Hot air oven (Memmert, DO 6062, Germany)
2. Hotplate Stirrer (MS-H280-Pro, USA)
3. Muffle Furnace, Model CWF1200 (Carbolite, Hope Valley, U.K.)

### Method

1. Weigh a crucible that was previously ignited at 550 °C and cooled in a desiccator.
2. Accurately weigh 3 g of dried sample into the crucible.
3. Heat the sample using a hotplate stirrer until it is charred.
4. Put the sample in a muffle furnace at 550 °C for 4 hours or until grayish-white ash is obtained.
5. Cool to room temperature in a desiccator and weigh
6. Calculate ash content using Equation A.3

$$\%Ash (wb) = \frac{g \text{ of ash}}{g \text{ of sample}} \times 100 \quad A.3$$

## A.7 Protein content (AOAC, 2000)

### Instruments

1. Kjeldahl digestion unit (Bushi digestion unit K-424, USA)
2. Kjeldahl distillation unit (Buchi distillation unit K-350, USA)
3. Scrubber (Buchi scrubber K-415, USA)

### Chemical reagents

1. Kjeldahl catalyst: 9 parts of potassium sulfate ( $K_2SO_4$ ) with 1 part of copper sulphate ( $CuSO_4$ )
2. Concentrated Sulfuric acid ( $H_2SO_4$ ) (96.5%, w/w)
3. Sodium hydroxide pellet (NaOH) (45%, w/v)
4. Hydrochloric acid (HCl), 0.1 N
5. Boric acid ( $H_3BO_3$ ), 4% (w/w)
6. Indicator (0.1% methylene blue + 0.2% methyl red)

### Methods

1. Place 2.0 g of sample on a Whatman No.1 filter paper in the sample tube.
2. Add 20 mL of concentrated H<sub>2</sub>SO<sub>4</sub> and the Kjeldahl catalyst.
3. Put the rack holding the sample tubes into the Kjeldahl digestion unit. Turn on the water pump and connect the fume exhaust unit to the tubes. Set the thermostat to 400 °C and digest the sample until it turns clear brown solution.
4. Remove the sample tubes from the digestion unit. Leave the water pump on and the fume exhaust unit connected. Allow for cooling of the sample tube and add 20 mL of water.
5. Remove the exhaust unit from the sample tube and place the tube in the Kjeldahl distillation unit. Add 60-70 mL of 45 % NaOH
6. Place a conical flask containing 50 mL of 4% H<sub>3</sub>BO<sub>3</sub> and 4 drops of indicator
7. Run the distillation unit according to the instrument manual.
8. Remove the flask from the distillation unit. Titrate ammonia in the solution with 0.1 N HCl until the purplish color is obtained
9. Calculate protein content using Equation A.3:

$$\% \text{ Nitrogen} = \frac{(\text{mL HCl} - \text{mL blank}) \times \text{N of HCl} \times 1.4 \times \text{conversion factor}}{\text{g of sample}} \quad (\text{A.4})$$

**Note:** Conversion factor = 5.7 for flour or starch

### **A.8 Fat content (AOAC, 2000)**

#### Instruments

1. Soxhlet extractor (Gerhardt, Bonn, Germany)
2. Hot air oven (Mettler, DO 6062, Germany)
3. Rotary Evaporator (Buchi Rotavapor R-200, USA)
4. Hot air oven (Mettler, DO 6062, Germany)

#### Chemical reagent

1. Petroleum ether

#### Method

1. Place a round bottom flask in the hot air oven at 105 °C to ensure that the weight of the bottle is stable.
2. Weigh a dried round bottom and cooled to room temperature.

3. Weigh 3-5 g of dried sample onto Whatman No.1 filter paper and place into extraction thimble. Place the thimble into the Soxhlet extractor.
4. Add 250 mL of petroleum ether into a round bottom flask.
5. Heat the solvent and allow the extraction process to proceed for 3-4 hours (heat rate of 150 drops/min)
6. Evaporate the solvent by using a rotary evaporator.
7. Dry the remaining liquid in the hot air oven at 60°C for 30 minutes and then keep it in a desiccator for cooling. Weight the fat obtained.
8. Calculate fat content following Equation A.5

$$\text{Fat content (\%)} = \frac{\text{g of fat}}{\text{g of sample}} \times 100 \quad (\text{A.5})$$

### **A.9 Crude fiber (AOAC, 2000)**

#### Instruments

1. Hot air oven (Memmert, DO 6062, Germany)
2. Muffle Furnace, Model CWF1200 (Carbolite, Hope Valley, U.K.)
3. Hotplate Stirrer (MS-H280-Pro, USA)

#### Chemical reagents

1. Sulfuric acid (H<sub>2</sub>SO<sub>4</sub>), 1.25 % (v/v)
2. Sodium hydroxide pellet (NaOH), 1.25 % (w/w)
3. Ethanol, 95% (w/w)

#### Method

1. Put the dried defatted sample (5g) in a dried fiber bag (constant weight) and place it into a beaker
2. Add 200 mL of 1.25 % H<sub>2</sub>SO<sub>4</sub> and boil for 30 minutes in a hotplate stirrer
3. Rinse with hot water to neutralize the residue
4. Transfer the residue to a beaker. Add 200 mL of 1.25 % NaOH and boil for 30 minutes
5. Rinse with hot water to neutralize the residue
6. Rinse the residue with 95% Ethanol
7. Dry the residue in a hot air oven to a constant weight and keep it in a desiccator.

8. Weight a crucible that was previously ignited at 550 °C and cooled to room temperature in a desiccator.
9. Transfer the residue into a crucible. Heat the residue using a hot plate until it is charred. And then incinerate the residue in a muffle furnace at 550 °C until grayish-white ash is obtained.
10. Cool to room temperature in a desiccator and weigh
11. Obtain the amount of crude fiber by subtracting the weight after incineration from the weight before incineration (g of crude fiber)
12. Calculate crude fiber content using Equation A.6

$$\text{Crude fiber (\%wb)} = \frac{\text{g of crude fiber}}{\text{g of defatted sample}} \times 100$$

(A.6)

#### **A.10 Carbohydrate (AOAC, 2000)**

The carbohydrate content is calculated by difference following the equation below.

$$\text{Carbohydrate (\%db)} = 100 - \% (\text{Protein} + \text{Ash} + \text{Crude Fiber} + \text{Fat})$$

#### **A.11 Apparent amylose contents (Modified from Juliano (1971))**

##### Instruments

1. Spectrophotometer (Thermo Spectronic, Genesys 10 UV, USA)
2. Weighing machine 4 digits (Denver Instrument, SI-234, Germany)

##### Chemical reagents

1. Amylose from potatoes (Sigma-ALDRICH, Germany)
2. Sodium hydroxide (NaOH), 1 N
3. Ethanol, 95% (w/w)
4. Acetic acid, 1 N
5. Iodine solution (The mixture of iodine (0.2g) and potassium iodine (2.0g) is adjusted the volume of 100 mL with distillation water)

## Methods

### Preparation standard amylose curve

1. Weigh 0.0400 g of amylose from potatoes and transfer to 100 mL volumetric flask
2. Add 1 mL of 95% ethanol and 9 mL of 1N NaOH, mix thoroughly
3. Boil sample in water bath for 10 minutes and cool down to room temperature
4. Transfer to 100 mL volumetric flask, dilute to volume with water, and mix well.
5. Use the stock solution to prepare the standard amylose solution of 0.4, 0.8, 1.2, 1.4, 1.6, and 2.0 mg/100mL
6. Dilute the stock solution and add chemicals following Table A.3

**Table 6.1** Reaction mixture for standard amylose curve

Flask No.	Acetic acid (mL)	Iodine solution (mL)	Standard solution (mL)	Water to adjust volume (mL)	Amylose equivalence (mg/100mL)
1	0.2	2	1	100	0.4
2	0.4	2	2	100	0.8
3	0.6	2	3	100	1.2
4	0.8	2	4	100	1.6
5	1.0	2	5	100	2.0

7. Mix well and stand for 20 minutes.
8. Read absorbance at 620 nm against the blank.
9. The standard curve of potato amylose was constructed for the calculation of amylose content (Figure A.1)

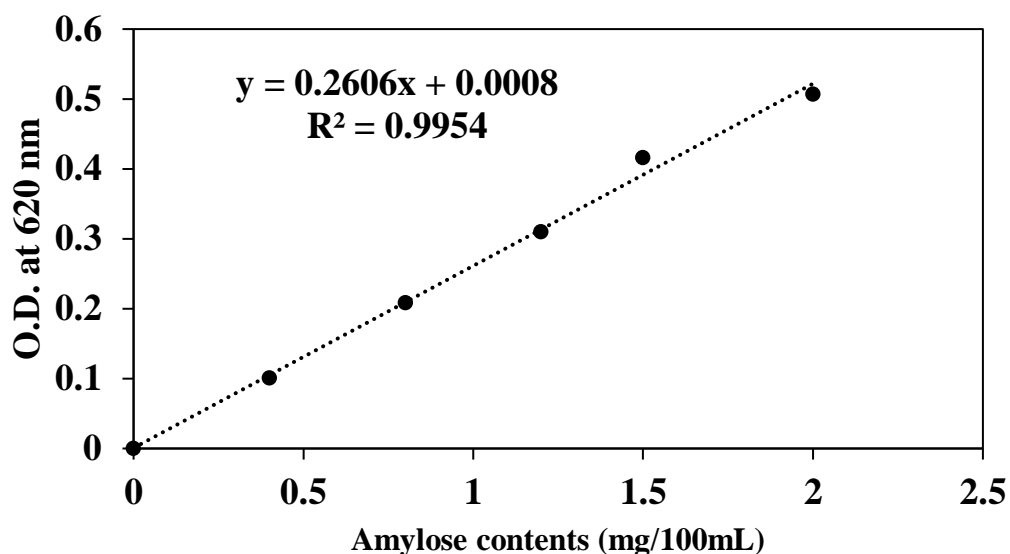


**Figure 6.1** Standard curve for determining amylose content

#### Determination of amylose content in the starch sample

1. Weigh 100 mg of sample and transfer to a 100 mL flask.
2. Add 100 mL of 95% ethanol and 9 mL of 1N NaOH, mix thoroughly
3. Boil sample in a water bath with 10 minutes to gelatinize the starch, and cool down to room temperature,
4. Transfer sample into 100 mL volumetric flask, dilute to volume with distilled water, and mix well.
5. Pipette 5 mL aliquot into 100 mL volumetric flask
6. Add 1 N acetic acid solution and 2 mL iodine solution, dilute to volume with water, and mix well
7. Mix well and incubate at room temperature for 20 minutes.
8. Read absorbance 620 nm.
9. The amylose content was determined from a previous standard curve of potato amylose. (Equation A.7)

$$\text{Apparent amylose content (\%)} = \frac{A \times 10}{5 \times W} \quad (\text{A.7})$$

A: Amylose content (mg/100 mL) from standard curve (X-axis)

W: Weight (g) of sample



## A.12 Reducing sugar (Trithavisup et al., 2019)

### Instruments

1. Spectrophotometer (Thermo Spectronic, Genesys 10 UV, USA)
2. Weighing machine 4 digit (Denver Instrument, SI-234, Germany)
3. Hot plate

### Chemical reagents

1. Ammonium molybdate tetrahydrate
2. Copper (II) sulfate
3. D-glucose
4. Disodium arsenate heptahydrate
5. Potassium sodium tartrate tetrahydrate
6. Sodium carbonate (anhydrous)
7. Sodium hydrogen carbonate
8. Sodium sulfate (anhydrous)
9. Sulfuric acid

### Methods

#### Reagent preparation for analysis

1. Copper reagent A: weigh the reagents including
  - 25g of Sodium carbonate (anhydrous)
  - 25g of Potassium sodium tartrate tetrahydrate
  - 20g of hydrogen carbonate
  - 200g of sodium sulfate

Dissolve reagents in 800 mL of distilled water and dilute to 1000 mL. Filter with a Whatman No.1 filter paper and keep it in an amber reagent glass bottle at cool temperature (below 20°C).

2. Copper reagent B: Dissolve 9.6 g of Copper (II) sulfate in 100 mL of distilled water and add one or two drops of Sulfuric acid.
3. Arsenomolybdate color reagent: dissolve 25 g of Ammonium molybdate in 450 mL of distilled water. Then, add 21 mL of Sulfuric acid and mix thoroughly. Add 3g of Disodium arsenate heptahydrate dissolved in 25mL of distilled water. Place in an

incubator at 37°C for 24 to 48 hours of heat to 55°C for 25 minutes. Keep the color reagent in an amber reagent glass bottle.

#### Preparation of standard glucose solution curve

1. Prepare 20, 40, 60, 80, 100 µg/mL glucose solutions.mL
2. Pitter 1 mLmL of glucose solution (20-100 µg/mL) in mL25 mL of volumetric flasks at each glucose concentration.
3. Mix Copper reagent A and Copper reagent B in a ratio of 25 to 1 (Nelson's copper reagent) and then add 1 mL of Nelson's copper reagent into each glucose concentration.
4. Boil in hot water using a hot plate for 20 minutes and cooling in cool water for 3 – 5 minutes.
5. Add 1 mL of Arsenomolybdate color reagent and mix thoroughly.
6. Adjust volume to 25mL with distilled water and mix well.
7. Read absorbance 745 nm against blank.
8. Standard curve of glucose solution was construction for the calculation of reducing sugar content (Figure A.2)

#### Determination reducing sugar content in the starch sample

1. Mix 1 mL of the sample solution (30% solid content) with 1 mL of Nelson's copper reagent.
2. Boil in hot water using a hot plate for 20 minutes and cool in cool water for 3 – 5 minutes.
3. Add 1 mL of Arsenomolybdate color reagent and mix thoroughly
4. Adjust volume to 25 mL with distilled water and mix well
5. Read absorbance 745 nm against blank.
6. The reducing sugar content was determined from a previous standard curve and was calculated following Equation A.8

$$\text{Reducing sugar}(\mu\text{g/g dry starch}) = \frac{A \times V}{W} \quad (\text{A.8})$$

A: reducing sugar content (µg/mL) from the standard curve (X-axis)

V: Volume of sample solution

W: Weight (g) of sample on dry basis

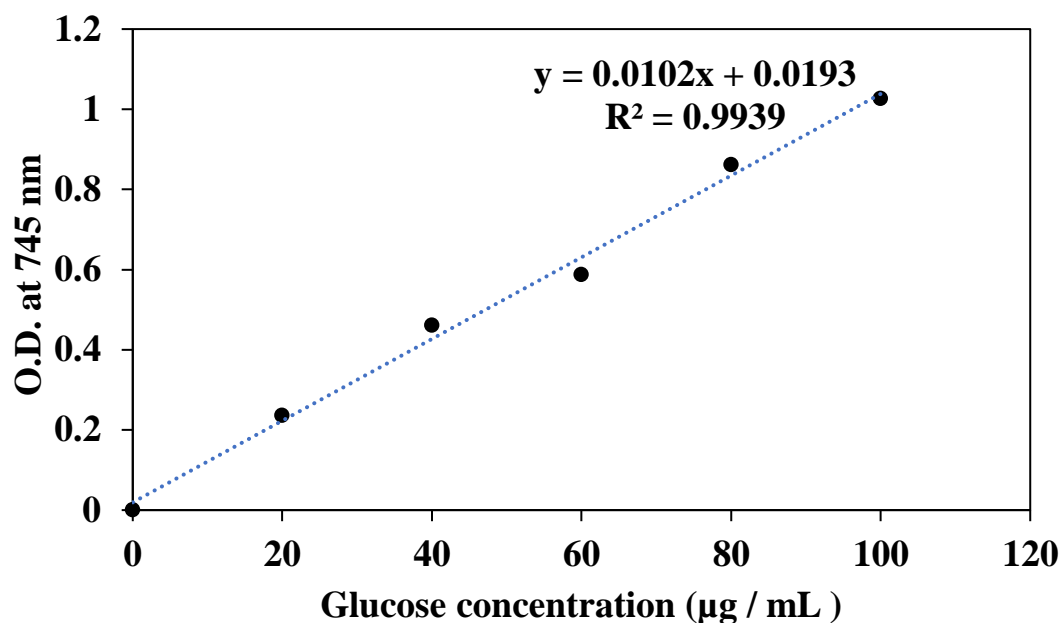


**Figure 6.2** Standard curve for determining reducing sugar content

### A.13 Fourier transform infrared (FTIR) spectroscopy (Yan et al., 2020)

#### Instrument

1. Fourier Transform Infrared Spectrometer (Thermo scientific, model Nicolet 6700, USA)

#### Method

1. Mix 1 mg of starch sample and 150 mg of FTIR- grade potassium bromide (KBr)
2. Grind the sample with an agate pestle and mortar under an infrared lamp.
3. Press the power into 13-mm-diameter discs under 15 tons of pressure for 30 seconds.
4. Transfer the pellet into the FTIR spectrometer, and spectra were obtained in transmittance mode from 4000 to 400  $\text{cm}^{-1}$ .
5. Convert to absorbance mode using Equation A.9

$$\text{Absorbance} = 2 - \log(\% \text{ Transmittance}) \quad (\text{A.9})$$

#### **A.14 Molecular weight of amylose and amylopectin (modified from Yoo and Jane (2002))**

##### Instruments

1. High-performance size-exclusion chromatography (Water e2695, Separations module, Waters Corporation, USA)
2. Centrifuge
3. Hot plate stirrer
4. Multi angle laser light scattering detector (MALLS, DAWN HELEOS, Wyatt Technology Corp., Santa Barbara, CA)
5. Waters 2414 RI detector (Waters Corporation, USA)

##### Chemical reagents

1. Dimethyl sulfoxide (DMSO)
2. Ethanol, 95% (w/w)
3. Standard dextra

##### Methods

###### Preparation of starch aqueous dispersions for HPSEC

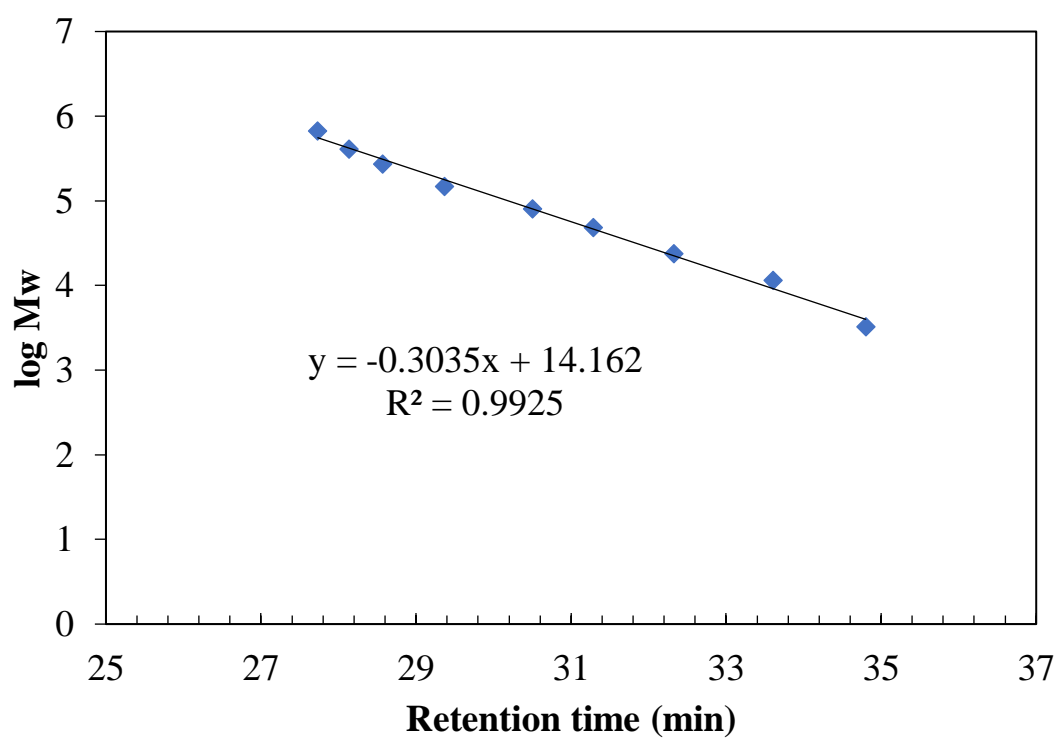
1. Mix 0.2 g of sample and 1.2 mL of water and then disperse in 10.8 mL of DMSO.
2. Stir a starch suspension while heating in a boiling water for 1 hour.
3. Stir the suspension for 24 hours at 25°C
4. Mix 0.4 mL of an aliquot of starch dispersion (1.0 % w/v) with 2 mL of Ethanol.
5. Centrifuge at 6750×g for 20 minutes for separating the ethanol-precipitated starch
6. Add 1.5 ml of water and then boil the starch pellet in boiling water for 10 minutes
7. Filter the solution through a nylon membrane filter (8 µm) and then inject into HPSEC equipped with Multi angle laser light scattering and Waters 2414 RI detector.
8. Inject the starch solution (20 mg/mL) and use Ultrahydrogel linear (exclusion limit =  $7 \times 10^6$  Da) and guard column (Waters Corporation, USA) for size separation at 40°C

9. Add membrane-filtered water (0.025  $\mu\text{m}$ , Millipore, Bedford, MA) for the mobile phase and set flow rate to 0.3 mL/min.
10. Analyze the data by using Astra software (Version 5.3.4, Wyatt Tech. Corp., Santa Barbara, CA)
11. Normalize by Dextran 25000 ( $M_w = 2.56 \times 10^4$  g/mol) for weight average molecular weight ( $M_w$ ) of amylopectin that is calculated by using second order berry plot and  $dn/dc$  (0.146 mg/mL).
12. Use dextran standards ( $M_w$  range 3.26 to 667.8 KDa) for calculated  $M_w$  of amylose



**Table 6.2** Molecular weight of standard dextran for construction standard curve

Standard dextran	Mw (Da)
5K	3260
12K	11600
25K	23800
50K	48600
80K	80900
150K	147600
270K	273000
410K	409800
670K	667800

**Figure 6.3** Standard curve for calculating molecular weight of amylose and amylopectin

### A.15 Pasting properties (AACC, 2000)

#### Instruments

1. RVA (Rapid Visco analyzer) (Newport Scientific Instrument & Engineer, RVA-4, Australia).
2. Weighing machine 4 digits (Denver Instrument, SI-234, Germany)

#### Method

1. Mix 3 g of starch sample (14% moisture content) with 25 g of distilled water in the canister.
2. Measure immediately by using RVA following testing profile (Table A.5)
3. Viscosity parameters (peak, trough, final, breakdown, and setback viscosity) were expressed in centipoise (cP) by Thermocline software, version 3.11.

**Table 6.3** Testing profile for RVA

Stage	Temperature/ speed	Time
1	50°C	0 min, 0 sec
2	960 rpm	0 min, 0 sec
3	160 rpm	0 min, 0 sec
4	50°C	1 min, 0 sec
5	95°C	4 min, 42 sec
6	95°C	7 min, 12 sec
7	50°C	11 min, 0 sec
End of test		13 min, 0 sec
Time between readings		4 sec

## A.16 Swelling power and solubility (Schoch, 1964)

### Instruments

1. Centrifuge (Hettich zentrifugen 19, Germany)
2. Shaker water bath (Thermo Scientific, model NESLAB EX 10, USA)
3. Weighing machine 4 digits (Denver Instrument, SI-234, Germany)
4. Hot-air oven (Mettler, model W350, Germany)

### Method

1. Weigh 0.5 g of sample ( $W_1$ ) and transfer to centrifuge tube.
2. Add 15 mL distilled water and vortex.
3. Incubate in a shaker water bath at 60°C, 70°C, 80°C, and 90°C at 174 rpm for 30 minutes
4. Cool to room temperature and centrifuge at  $6000 \times g$  at 4°C for 20 minutes
5. The supernatant was decanted carefully and kept, and the residue was weighed ( $W_2$ ).
6. The supernatant was poured out from the tube to an aluminum dish.
7. The dish was dried at 105°C in a hot-air oven to constant and weighed ( $W_3$ )
8. Calculate swelling power and solubility of the sample by using Equation A.9-A.10

$$\text{Swelling power } \left(\frac{g}{g}\right) = \frac{W_2 \times 100}{W_1 \times (100 - \% \text{ solubility})} \quad (\text{A.9})$$

$$\% \text{ Solubility} = \frac{W_2 \times 100}{W_1 \times (100 - \% \text{ solubility})} \quad (\text{A.10})$$

$W_1$  : g of sample before analyst

$W_2$  : g of the wet sediment

$W_3$  : g of the dried supernatant



### A.17 Water-binding capacity (Medcalf, 1965)

#### Instruments

1. Centrifuge (Hettich zentrifugen 19, Germany)
2. Shaker water bath (Thermo Scientific, model NESLAB EX 10, USA)
3. Weighing machine 4 digits (Denver Instrument, SI-234, Germany)
4. Hot-air oven (Mettler, model W350, Germany)

#### Method

1. Weigh 1 g of sample ( $W_1$ ) and transfer to a centrifuge tube.
2. Add 15 mL distilled water and vortex.
3. Incubate in a shaker water bath at  $30^\circ\text{C}$  at 174 rpm for 30 minutes.
4. Centrifuge at  $5000 \times g$  for 20 minutes.
5. The supernatant was decanted carefully and the residue was weighed ( $W_2$ )
6. Calculate water-binding capacity of the sample by using Equation A.11

$$\text{Water binding capacity} = \frac{W_2 - W_1}{W_1} \quad (\text{A.11})$$

$W_1$  : g of sample before analyst

$W_2$  : g of sample after analyst

## **A.18 Viscoelastic properties** (modified from Wongsagonsup et al. (2014))

### Instrument

1. Rheometer with geometry (MCR102, Anton Paar, Graz, Austria)

### Method

1. Starch suspensions (6% w/w) was prepared at room temperature
2. Install a measuring geometry (parallel plate 50 mm diameter) onto the rheometer
3. Set zero and set gap at 1 mm
4. Set mode oscillation
  - Temperature sweep test
    - Shear Stress 1 Pa
    - Angular frequency 6.28 rad/s
    - Temperature  
20 °C – 75 °C for 15 min
  - Frequency sweep test
    - Shear Stress 1 Pa
    - Minimum frequency 0.1 Hz
    - Maximum frequency 100 Hz
    - Isothermal 25 °C
5. Load the sample into the rheometer plate and adjust the parallel plate into the gap size.
6. Drop immersion oil to prevent evaporation and cover with closure.
7. Start to run the temperature sweep test to gelatinized starch and continue to the frequency sweep test.
8. Storage modulus ( $G'$ ), loss modulus ( $G''$ ), and loss tangent ( $\tan \delta$ ) were recorded with RheoCompass<sup>TM</sup> software.

## A.19 Flow properties (modified from Chaiwat et al. (2016))

### Instrument

1. Rheometer with geometry (MCR102, Anton Paar, Graz, Austria)

### Method

1. Carry on with a steady shear test of 6 % fully gelatinized starch from A.17
2. Set mode steady flow test
  - Ramp up with shear rates of 1 to 500 s<sup>-1</sup>
  - Ramp down with shear rates of 500 to 1 s<sup>-1</sup>
  - Isothermal 25 °C
3. Load the sample into the rheometer plate and adjust the parallel plate into the gap size and start to run a steady flow test.
4. The data of shear stress and shear rate of the second cycle was used to characterize the flow behavior of the sample and was fitted to the Herschel-Bulkley model (Equation A.12)

$$\sigma = \sigma_0 + K(\dot{\gamma}^n) \quad (\text{A.12})$$

$\sigma$ : Shear stress

$\sigma_0$ : yield stress

$\dot{\gamma}$ : the shear rate (s<sup>-1</sup>)

K: the consistency index (Pa.s<sup>n</sup>)

n: the flow behavior index (n=1 Newtonian, <1 for shear-thinning, and >1 for shear-thickening), which was obtained from linear regression of the square root of shear rate-shear stress data.

---

## Appendix B

### Additional Data

**Table 7.1** Swelling power of native and plasma modified tapioca starch with different conditions.

Samples	Swelling power (g/g)			
	60°C	70°C	80°C	90°C
NTS	3.86 <sup>a</sup> ± 0.15	6.84 <sup>a</sup> ± 0.12	8.61 <sup>a</sup> ± 0.16	11.29 <sup>a</sup> ± 0.21
Ar10kV-5min	3.76 <sup>a</sup> ± 0.04	6.82 <sup>a</sup> ± 0.10	8.16 <sup>ab</sup> ± 0.21	11.07 <sup>a</sup> ± 0.13
Ar10kV-10min	3.42 <sup>b</sup> ± 0.16	6.56 <sup>a</sup> ± 0.12	7.68 <sup>bc</sup> ± 0.07	9.12 <sup>b</sup> ± 0.57
Ar10kV-15min	3.56 <sup>ab</sup> ± 0.27	6.52 <sup>a</sup> ± 0.23	6.33 <sup>de</sup> ± 0.21	8.86 <sup>b</sup> ± 0.08
Ar15kV-5min	3.74 <sup>a</sup> ± 0.14	6.69 <sup>a</sup> ± 0.06	7.99 <sup>b</sup> ± 0.27	10.64 <sup>a</sup> ± 0.74
Ar15kV-10min	3.73 <sup>a</sup> ± 0.05	6.75 <sup>a</sup> ± 0.06	7.57 <sup>bc</sup> ± 0.18	9.57 <sup>b</sup> ± 0.23
Ar15kV-15min	3.79 <sup>a</sup> ± 0.09	6.46 <sup>a</sup> ± 0.07	6.39 <sup>de</sup> ± 0.53	8.84 <sup>b</sup> ± 0.41
He10kV-5min	2.99 <sup>c</sup> ± 0.15	6.65 <sup>a</sup> ± 0.64	7.87 <sup>bc</sup> ± 0.26	6.70 <sup>c</sup> ± 0.58
He10kV-10min	2.63 <sup>de</sup> ± 0.14	5.82 <sup>b</sup> ± 0.25	5.93 <sup>e</sup> ± 0.27	5.99 <sup>d</sup> ± 0.42
He10kV-15min	2.38 <sup>ef</sup> ± 0.20	4.70 <sup>d</sup> ± 0.39	5.12 <sup>f</sup> ± 0.05	5.38 <sup>d</sup> ± 0.34
He15kV-5min	2.74 <sup>cd</sup> ± 0.12	5.27 <sup>c</sup> ± 0.20	6.47 <sup>d</sup> ± 0.45	5.84 <sup>d</sup> ± 0.49
He15kV-10min	2.34 <sup>f</sup> ± 0.28	3.99 <sup>e</sup> ± 0.17	4.38 <sup>g</sup> ± 0.28	4.38 <sup>de</sup> ± 0.28
He15kV-15min	2.17 <sup>f</sup> ± 0.14	3.39 <sup>f</sup> ± 0.36	3.66 <sup>h</sup> ± 0.16	3.88 <sup>f</sup> ± 0.37

Means ± standard deviation (n = 3) with different letters within a column are significantly different (P < 0.05)

**Table 7.2** Solubility of native and plasma modified tapioca starch with different conditions.

Samples	Solubility (%)			
	60°C	70°C	80°C	90°C
NTS	0.84 <sup>g</sup> ± 0.10	1.69 <sup>f</sup> ± 0.12	3.12 <sup>d</sup> ± 0.15	8.37 <sup>e</sup> ± 0.60
Ar10kV-5min	0.97 <sup>fg</sup> ± 0.08	1.99 <sup>ef</sup> ± 0.10	3.14 <sup>d</sup> ± 0.02	8.68 <sup>e</sup> ± 0.77
Ar10kV-10min	1.16 <sup>ef</sup> ± 0.09	2.30 <sup>de</sup> ± 0.12	4.41 <sup>e</sup> ± 0.05	9.05 <sup>ec</sup> ± 0.56
Ar10kV-15min	1.87 <sup>b</sup> ± 0.08	3.61 <sup>c</sup> ± 0.23	4.54 <sup>e</sup> ± 0.08	12.64 <sup>d</sup> ± 0.29
Ar15kV-5min	1.05 <sup>fg</sup> ± 0.15	2.69 <sup>d</sup> ± 0.06	3.50 <sup>d</sup> ± 0.19	9.17 <sup>e</sup> ± 0.55
Ar15kV-10min	1.33 <sup>de</sup> ± 0.04	2.06 <sup>ef</sup> ± 0.06	3.61 <sup>d</sup> ± 0.18	9.51 <sup>e</sup> ± 0.34
Ar15kV-15min	1.83 <sup>b</sup> ± 0.04	3.67 <sup>c</sup> ± 0.07	4.50 <sup>e</sup> ± 0.03	12.02 <sup>d</sup> ± 0.25
He10kV-5min	1.31 <sup>e</sup> ± 0.08	2.69 <sup>d</sup> ± 0.23	4.40 <sup>e</sup> ± 0.38	18.39 <sup>c</sup> ± 1.01
He10kV-10min	1.66 <sup>bc</sup> ± 0.15	3.37 <sup>c</sup> ± 0.30	8.40 <sup>c</sup> ± 0.47	22.35 <sup>b</sup> ± 1.86
He10kV-15min	2.30 <sup>a</sup> ± 0.19	4.50 <sup>b</sup> ± 0.16	9.52 <sup>b</sup> ± 0.28	22.68 <sup>b</sup> ± 1.09
He15kV-5min	1.71 <sup>bc</sup> ± 0.27	3.38 <sup>c</sup> ± 0.34	5.95 <sup>d</sup> ± 0.75	22.94 <sup>b</sup> ± 2.14
He15kV-10min	1.54 <sup>cd</sup> ± 0.13	4.84 <sup>b</sup> ± 0.35	11.83 <sup>a</sup> ± 0.48	21.67 <sup>b</sup> ± 0.86
He15kV-15min	2.18 <sup>a</sup> ± 0.14	7.48 <sup>a</sup> ± 0.37	12.08 <sup>a</sup> ± 0.83	25.19 <sup>a</sup> ± 2.36

Means ± standard deviation (n = 3) with different letters within a column are significantly different (P < 0.05)

## Appendix C

### Analysis of Variance

**Table C.1** Analysis of variance for L\* value of native and plasma-treated starch

Source	SS	df	Mean Square	F	Sig.
Treatments	155.434	12	12.953	135.410	.000
Error	2.487	26	.096		
Total	157.921	38			

**Table C.2** Comparison of means for L\* value of native and plasma-treated starch by using Duncan's Multiple Range test (DMRT) at 95 % confidence interval

Treatments	Subset				
	1	2	3	4	5
NTS	98.5100				
Ar10kV-10min	98.5500	98.5500			
Ar15kV-10min	99.0500	99.0500	99.0500		
Ar10kV-5min		99.0733	99.0733		
Ar15kV-5min			99.1533		
Ar10kV-15min			99.1967		
Ar15kV-15min			99.3100		
He10kV-5min				102.5167	
He15kV-10min				102.8533	102.8533
He15kV-5min				102.8900	102.8900
He10kV-15min					103.1167
He10kV-10min					103.1300
He15kV-15min					103.1733

**Table C.3** Analysis of variance for a\* value of native and plasma-treated starch

Source	SS	df	Mean Square	F	Sig.
Treatments	.155	12	.013	14.709	.000
Error	.023	26	.001		
Total	.178	38			

Treatments	Subset					
	1	2	3	4	5	6
Ar10kV-5min	.1200					
Ar10kV-10min	.1300	.1300				
Ar10kV-15min	.1533	.1533	.1533			
He15kV-15min	.1600	.1600	.1600			
Ar15kV-5min	.1633	.1633	.1633			
Ar15kV-10min		.1833	.1833	.1833		
Ar15kV-15min		.1833	.1833	.1833		
NTS			.1967	.1967		
He10kV-10min			.2033	.2033		
He10kV-5min				.2200	.2200	
He10kV-15min					.2600	
He15kV-10min						.3100
He15kV-5min						.3367

**Table C.4** Comparison of means for a\*value of native and plasma-treated starch by using Duncan's Multiple Range test (DMRT) at 95% confidence interval

**Table C.5** Analysis of variance for b\*value of native and plasma-treated starch

Source	SS	df	Mean Square	F	Sig.
Treatments	12.166	12	1.014	50.478	.000
Error	.522	26	.020		
Total	12.688	38			

Treatments	Subset					
	1	2	3	4	5	6
NTS	1.3600					
Ar15kV-5min		1.6500				
Ar15kV-10min		1.6500				
Ar10kV-15min		1.7067	1.7067			
Ar10kV-5min		1.7333	1.7333			
Ar15kV-15min		1.7767	1.7767			
Ar10kV-10min			1.9567			
He10kV-5min				2.4600		
He10kV-10min				2.5967	2.5967	
He15kV-5min				2.6367	2.6367	
He10kV-15min				2.6500	2.6500	
He15kV-10min					2.7800	
He15kV-15min						3.2500

**Table C.6** Comparison of means for b\* value of native and plasma-treated starch by using Duncan's Multiple Range test (DMRT) at 95% confidence interval

**Table C.7** Analysis of variance for whiteness index of native and plasma-treated starch

Source	SS	df	Mean Square	F	Sig.
Treatments	394.700	12	32.892	70.230	.000
Error	12.177	26	.468		
Total	406.877	38			

**Table C.8** Comparison of means for whiteness index of native and

Treatments	Subset			
	1	2	3	4
He15kV-15min	89.6409			
He10kV-15min		91.5676		
He10kV-10min		91.6955		
He15kV-10min		91.9790		
He15kV-5min		92.2542		
He10kV-5min			93.6621	
Ar10kV-10min				96.9669
NTS				97.9442
Ar15kV-10min				98.0097
Ar10kV-5min				98.0540
Ar10kV-15min				98.1620
Ar10kV-15min				98.2070
Ar15kV-5min				98.2612

plasma-treated starch by using Duncan's Multiple Range test (DMRT) at 95% confidence interval

**Table C.9** Analysis of variance for pH value of native and plasma-treated starch

Source	SS	df	Mean Square	F	Sig.
Treatments	4.150	12	.346	72.666	.000
Error	.124	26	.005		
Total	4.274	38			



**Table C.10** Comparison of means for pH value of native and plasma-treated starch by using Duncan's Multiple Range test (DMRT) at 95% confidence interval

Treatments	Subset						
	1	2	3	4	5	6	7
He15kV-15min	4.5433						
He10kV-15min		4.7367					
He15kV-10min		4.8467					
Ar10kV-10min			5.0367				
He10kV-10min			5.0667				
He15kV-5min			5.0767				
Ar15kV-10min				5.1967			
Ar10kV-15min				5.2300			
Ar15kV-5min				5.2467			
He15kV-5min				5.2967			
Ar10kV-5min					5.4867		
Ar15kV-15min						5.6200	
NTS							5.7467

**Table C.11** Analysis of variance for relative crystallinity of native and plasma-treated starch

Source	SS	df	Mean Square	F	Sig.
Treatments	174.976	12	14.581	44.134	.000
Error	4.295	13	.330		
Total	179.271	25			

**Table C.12** Comparison of means for relative crystallinity of native and plasma-treated starch by using Duncan's Multiple Range test (DMRT) at 95% confidence interval

Treatment	Subset				
	1	2	3	4	5
He15kV-10min	27.3000				
He10kV-15min	27.3000				
He10kV-5min	27.4500	27.4500			
He15kV-5min	27.9500	27.9500	27.9500		
He10kV-10min		28.7000	28.7000		
He15kV-15min			29.2000		
Ar15kV-5min				32.1500	
Ar15kV-15min				32.2500	
Ar10kV-15min				32.7500	
Ar15kV-10min				32.9500	
Ar10kV-5min				33.0000	
Ar10kV-10min				33.2500	
NTS					34.5000

**Table C.13** Analysis of variance for moisture content of native and plasma-treated starch

Source	SS	df	Mean Square	F	Sig.
Treatments	28.523	12	2.377	16.017	.000
Error	3.858	26	.148		
Corrected Total	32.382	38			

**Table C.14** Comparison of means for moisture content of native and plasma-treated starch by using Duncan's Multiple Range test (DMRT) at 95% confidence interval

Treatments	Subset		
	1	2	3
He15kV-10min	8.5888		
He15kV-15min	8.6710		
He15kV-5min	9.0513	9.0513	
He10kV-10min	9.2112	9.2112	
He10kV-15min		9.4071	
He10kV-5min		9.7328	
Ar15kV-10min			10.5068
Ar10kV-10min			10.6299
Ar15kV-15min			10.6350
Ar10kV-15min			10.7365
Ar10kV-5min			10.7815
Ar15kV-5min			10.8085
NTS			10.9730

**Table C.15** Analysis of variance for apparent amylose of native and plasma-treated starch

Source	SS	df	Mean Square	F	Sig.
Treatments	107.956	12	8.996	32.753	.000
Error	7.141	26	.275		
Total	115.097	38			

**Table C.16** Comparison of means for apparent amylose of native and plasma-treated starch by using Duncan's Multiple Range test (DMRT) at 95% confidence interval

Treatments	Subset					
	1	2	3	4	5	6
NTS	22.6338					
He15kV-15min	23.0081	23.0081				
He10kV-5min		23.7381	23.7381			
Ar10kV-5min			24.3690	24.3690		
Ar15kV-5min			24.6001	24.6001	24.6001	
He15kV-15min			24.6395	24.6395	24.6395	
He10kV-10min				24.8884	24.8884	
He10kV-10min				25.0719	25.0719	
Ar10kV-10min				25.2531	25.2531	
He10kV-15min				25.3594	25.3594	
Ar15kV-10min					25.4128	
Ar15kV-15min						28.2387
Ar10kV-15min						28.6504

**Table C.17** Analysis of variance for reducing sugar of native and plasma-treated starch

Source	SS	df	Mean Square	F	Sig.
Treatments	9352939.985	12	779411.665	5771.454	.000
Error	3511.195	26	135.046		
Total	9356451.181	38			

**Table C.18** Comparison of means for reducing sugar of native and plasma-treated starch by using Duncan's Multiple Range test (DMRT) at 95% confidence interval

Treatments	Subset									
	1	2	3	4	5	6	7	8	9	10
NTS	26.340									
He10kV-5min	34.9467	34.9467								
Ar10kV-5min	35.2133	35.2133	35.2133							
Ar15kV-5min	51.8500	51.8500	51.8500	51.8500						
Ar10kV-10min	63.3233	63.3233	63.3233	63.3233	63.3233					
Ar15kV-10min	74.1433	74.1433	74.1433	74.1433	74.1433	74.1433				
He15kV-5min	85.2067	85.2067	85.2067	85.2067	85.2067	85.2067	139.0667			
He10kV-10min	143.1700	143.1700	143.1700	143.1700	143.1700	143.1700	143.1700	194.1000		
Ar10kV-15min	241.6967	241.6967	241.6967	241.6967	241.6967	241.6967	241.6967	241.6967	1214.8933	
Ar15kV-15min	1636.2767	1636.2767	1636.2767	1636.2767	1636.2767	1636.2767	1636.2767	1636.2767	1636.2767	1636.2767

**Table C.19** Analysis of variance for ratio between 1047 and 1022  $\text{cm}^{-1}$  of native and plasma-treated starch

Source	SS	df	Mean Square	F	Sig.
Treatments	.012	12	.001	1.098	.402
Error	.024	26	.001		
Total	.036	38			

**Table C.20** Comparison of means for ratio between 1047 and 1022 cm<sup>-1</sup> of native and plasma-treated starch by using Duncan's Multiple Range test (DMRT) at 95% confidence interval

Treatment	Subset	
	1	2
Ar10kV-15min	.8906	
Ar15kV-10min	.9009	.9009
Ar10kV-10min	.9028	.9028
Ar15kV-5min	.9034	.9034
NTS	.9034	.9034
Ar15kV-15min	.9077	.9077
Ar10kV-5min	.9087	.9087
He15kV-15min	.9160	.9160
He15kV-5min	.9200	.9200
He10kV-5min	.9207	.9207
He10kV-15min	.9321	.9321
He15kV-10min	.9393	.9393
He10kV-10min		.9579

**Table C.21** Analysis of variance for pasting properties of native and plasma-treated starch

Source	SS	df	Mean Square	F	Sig.
Treatments	53705240.308	12	4475436.692	145.724	.000
Error	798504.667	26	30711.718		
Total	54503744.974	38			

**Table C.22** Comparison of means for peak viscosity of native and plasma-treated starch by using Duncan's Multiple Range test (DMRT) at 95% confidence interval

Treatments	Subset								
	1	2	3	4	5	6	7	8	9
He15kV-15min	340.6667								
He15kV-10min		787.6667							
Ar15kV-15min			1677.6667						
Ar10kV-15min			1823.0000						
He15kV-5min			1979.3333	1979.3333					
Ar15kV-10min				2248.3333	2248.3333				
He10kV-15min					2329.0000				
He10kV-10min						2687.6667			
Ar10kV-10min						2731.3333			
Ar10kV-15min							3202.3333		
He10kV-5min								3871.3333	
Ar10kV-5min								4106.0000	
NTS									4442.3333

**Table C.23** Analysis of variance for trough viscosity of native and plasma-treated starch

Source	SS	df	Mean Square	F	Sig.
Treatments	50822156.564	12	4235179.714	217.667	.000
Error	505885.333	26	19457.128		
Total	51328041.897	38			











**Table C.31** Analysis of variance for pasting temperature of native and plasma-treated starch

Source	SS	df	Mean Square	F	Sig.
Treatments	5.229	12	.436	2.618	.019
Error	4.328	26	.166		
Total	9.557	38			

**Table C.32** Comparison of means for pasting temperature of native and plasma-treated starch by using Duncan's Multiple Range test (DMRT) at 95% confidence interval

Treatments	Subset		
	1	2	3
Ar10kV-15min	70.4333		
Ar15kV-10min	70.5333		
Ar15kV-5min	70.7833	70.7833	
Ar15kV-15min	70.7833	70.7833	
Ar10kV-5min	70.8667	70.8667	
He15kV-5min	71.0667	71.0667	71.0667
Ar10kV-10min	71.0833	71.0833	71.0833
He10kV-5min	71.0833	71.0833	71.0833
NTS	71.1167	71.1167	71.1167
He10kV-10min	71.1500	71.1500	71.1500
He10kV-15min		71.4000	71.4000
He15kV-10min		71.5667	71.5667
He15kV-15min			71.7667

**Table C.33** Analysis of variance for breakdown percentage of native and plasma-treated starch

Source	SS	df	Mean Square	F	Sig.
Treatments	4247.878	12	353.990	168.361	.000
Error	54.667	26	2.103		
Total	4302.544	38			

**Table C.34** Comparison of means for breakdown percentage of native and plasma-treated starch by using Duncan's Multiple Range test (DMRT) at 95% confidence interval

Treatments	Subset						
	1	2	3	4	5	6	7
Ar15kV-5min	52.2133						
Ar10kV-5min		54.8000					
Ar10kV-10min			60.2367				
He10kV-5min			60.3433				
NTS			61.2200	61.2200			
Ar15kV-10min			62.4833	62.4833			
He15kV-5min			63.3433	63.3433			
He10kV-10min			63.4033	63.4033			
He10kV-15min					66.2767		
Ar10kV-15min					67.0867		
Ar15kV-15min					68.3000		
He15kV-10min						80.3300	
He15kV-15min							93.8500

**Table C.35** Analysis of variance for setback percentage of native and plasma-treated starch

Source	SS	df	Mean Square	F	Sig.
Treatments	81707.383	12	6808.949	85.709	.000
Error	2065.519	26	79.443		
Total	83772.902	38			

**Table C.36** Comparison of means for breakdown percentage of native and plasma-treated starch by using Duncan's Multiple Range test (DMRT) at 95% confidence interval

Treatments	Subset					
	1	2	3	4	5	6
He10kV-10min	38.1667					
He10kV-5min	38.2500					
He10kV-15min	38.6200	38.6200				
Ar10kV-5min	39.3400	39.3400				
Ar15kV-5min	39.4767	39.4767				
Ar10kV-10min	45.7000	45.7000	45.7000			
He15kV-5min	55.0433	55.0433	55.0433	55.0433		
Ar15kV-10min	55.1267	55.1267	55.1267	55.1267		
Ar10kV-15min	55.5033	55.5033	55.5033	55.5033		
Ar15kV-15min			59.7700	59.7700	70.7600	
NTS				70.7600	70.7600	
He15kV-10min					78.7567	
He15kV-15min						216.3300

**Table C.37** Analysis of variance for swelling power at 60°C of native and plasma-treated starch

Source	SS	df	Mean Square	F	Sig.
Treatments	14.702	12	1.225	47.487	.000
Error	.671	26	.026		
Total	15.373	38			

**Table C.38** Comparison of means for swelling power at 60°C of native and plasma-treated starch by using Duncan's Multiple Range test (DMRT) at 95% confidence interval

Treatments	Subset					
	1	2	3	4	5	6
He15kV-15min	2.1700					
He15kV-10min	2.3400					
He10kV-15min	2.3767	2.3767				
He10kV-10min		2.6267	2.6267			
He15kV-5min			2.7333	2.7333		
He10kV-5min				2.9867		
Ar10kV-10min					3.4200	
Ar10kV-15min					3.5633	3.5633
Ar15kV-10min						3.7333
Ar15kV-5min						3.7433
Ar10kV-5min						3.7567
Ar15kV-15min						3.7867
NTS						3.8600

**Table C.39** Analysis of variance for swelling power at 70°C of native and plasma-treated starch

Source	SS	df	Mean Square	F	Sig.
Treatments	49.621	12	4.135	56.649	.000
Error	1.898	26	.073		
Total	51.519	38			

**Table C.40** Comparison of means for swelling power at 70°C of native and plasma-treated starch by using Duncan's Multiple Range test (DMRT) at 95% confidence interval

Treatments	Subset					
	1	2	3	4	5	6
He15kV-15min	3.3900					
He15kV-10min		3.9933				
He10kV-15min			4.7033			
He15kV-5min				5.2700		
He10kV-10min					5.8200	
Ar15kV-15min						6.4633
Ar10kV-15min						6.5233
Ar10kV-10min						6.5600
He10kV-5min						6.6533
Ar15kV-5min						6.6900
Ar15kV-10min						6.7467
Ar10kV-5min						6.8200
NTS						6.8367

**Table C.41** Analysis of variance for swelling power at 80°C of native and plasma-treated starch

Source	SS	df	Mean Square	F	Sig.
Treatments	85.266	12	7.105	96.619	.000
Error	1.912	26	.074		
Corrected Total	87.178	38			



**Table C.42** Comparison of means for swelling power at 80°C of native and plasma-treated starch by using Duncan's Multiple Range test (DMRT) at 95% confidence interval

Treatments	Subset							
	1	2	3	4	5	6	7	8
He15kV-15min	3.6633							
He15kV-10min		4.3767						
He10kV-15min			5.1233					
He10kV-10min				5.9267				
Ar10kV-15min				6.3233	6.3233			
Ar15kV-15min				6.3900	6.3900			
He15kV-5min					6.4633			
Ar15kV-10min						7.5633		
Ar10kV-10min						7.6833	7.6833	
He10kV-5min						7.8633	7.8633	
Ar15kV-5min						7.9900	7.9900	
Ar10kV-5min							8.1600	8.1600
NTS								8.6067

**Table C.43** Analysis of variance for swelling power at 90°C of native and plasma-treated starch

Source	SS	df	Mean Square	F	Sig.
Treatments	229.134	12	19.095	111.312	.000
Error	4.460	26	.172		
Total	233.594	38			

**Table C.44** Comparison of means for swelling power at 90°C of native and plasma-treated starch by using Duncan's Multiple Range test (DMRT) at 95% confidence interval

Treatments	Subset					
	1	2	3	4	5	6
He15kV-15min	3.8800					
He15kV-10min		4.8300				
He10kV-15min		5.3733	5.3733			
He15kV-5min			5.8400			
He10kV-10min			5.9900			
He10kV-5min				6.7000		
Ar15kV-15min					8.8400	
Ar10kV-15min					8.8567	
Ar10kV-10min					9.1267	
Ar15kV-10min					9.5733	
Ar15kV-5min						10.6367
Ar10kV-5min						11.0633
NTS						11.2933

**Table C.45** Analysis of variance for solubility at 60°C of native and plasma-treated starch

Source	SS	df	Mean Square	F	Sig.
Treatments	7.569	12	.631	36.474	.000
Error	.450	26	.017		
Total	8.018	38			

**Table C.46** Comparison of means for solubility at 60°C of native and plasma-treated starch by using Duncan's Multiple Range test (DMRT) at 95% confidence interval

Treatments	Subset						
	1	2	3	4	5	6	7
NTS	.8367						
Ar10kV-5min	.9700	.9700					
Ar15kV-5min	1.0500	1.0500					
Ar10kV-10min		1.1633	1.1633				
He10kV-5min			1.3100				
Ar15kV-10min			1.3300	1.3300			
He15kV-10min				1.5433	1.5433		
He10kV-10min					1.6600	1.6600	
He15kV-5min					1.7067	1.7067	
Ar15kV-15min						1.8300	
Ar10kV-15min						1.8733	
He15kV-15min							2.1800
He10kV-15min							2.3033

**Table C.47** Analysis of variance for solubility at 70°C of native and plasma-treated starch

Source	SS	df	Mean Square	F	Sig.
Treatments	86.910	12	7.242	146.525	.000
Error	1.285	26	.049		
Total	88.195	38			

**Table C.48** Comparison of means for solubility at 70°C of native and plasma-treated starch by using Duncan's Multiple Range test (DMRT) at 95% confidence interval

Treatments	Subset					
	1	2	3	4	5	6
NTS	1.6900					
Ar10kV-5min	1.9900	1.9900				
Ar15kV-10min	2.0633	2.0633				
Ar10kV-10min		2.3033	2.3033			
Ar15kV-5min			2.6900			
He10kV-5min			2.6900			
He10kV-10min				3.3667		
He15kV-5min				3.3833		
Ar10kV-15min				3.6133		
Ar15kV-15min				3.6667		
He10kV-15min					4.4933	
He15kV-10min					4.8400	
He15kV-15min						7.4833

**Table C.49** Analysis of variance for solubility at 80°C of native and plasma-treated starch

Source	SS	df	Mean Square	F	Sig.
Treatments	380.663	12	31.722	203.402	.000
Error	4.055	26	.156		
Total	384.718	38			

**Table C.50** Comparison of means for solubility at 80°C of native and plasma-treated starch by using Duncan's Multiple Range test (DMRT) at 95% confidence interval

Treatments	Subset					
	1	2	3	4	5	6
NTS	3.1167					
Ar10kV-5min	3.1433					
Ar15kV-5min	3.4967					
Ar15kV-10min	3.6067					
He10kV-5min		4.3967				
Ar10kV-10min		4.4133				
Ar15kV-15min		4.4967				
Ar10kV-15min		4.5400				
He15kV-5min			5.9500			
He10kV-10min				8.3967		
He10kV-15min					9.5200	
He15kV-10min						11.8267
He15kV-15min						12.0767

**Table C.51** Analysis of variance for solubility at 90°C of native and plasma-treated starch

Source	SS	df	Mean Square	F	Sig.
Treatments	1588.029	12	132.336	93.587	.000
Error	36.765	26	1.414		
Total	1624.794	38			

**Table C.52** Comparison of means for solubility at 90°C of native and plasma-treated starch by using Duncan's Multiple Range test (DMRT) at 95% confidence interval

Treatments	Subset				
	1	2	3	4	5
NTS	8.3633				
Ar10kV-5min	8.6800				
Ar10kV-10min	9.0533				
Ar15kV-5min	9.1633				
Ar15kV-10min	9.5133				
Ar15kV-15min		12.0167			
Ar10kV-15min		12.6400			
He10kV-5min			18.3967		
He15kV-10min				21.6700	
He10kV-10min				22.3500	
He10kV-15min				22.6800	
He15kV-5min				22.9367	
He15kV-15min					25.1900

**Table C.53** Analysis of variance for water-binding capacity of native and plasma-treated starch

Source	SS	df	Mean Square	F	Sig.
Treatments	.054	12	.005	3.225	.006
Error	.036	26	.001		
Total	.091	38			

**Table C.54** Comparison of means for water-binding capacity of native and plasma-treated starch by using Duncan's Multiple Range test (DMRT) at 95% confidence interval

Treatments	Subset	
	1	2
NTS	.7300	
He15kV-15min		.8200
He15kV-5min		.8233
He10kV-15min		.8300
He15kV-10min		.8333
Ar10kV-5min		.8400
Ar10kV-10min		.8400
He10kV-5min		.8400
Ar15kV-10min		.8500
Ar15kV-15min		.8533
He10kV-10min		.8667
Ar15kV-5min		.8767
Ar10kV-15min		.8933

**Table C.55** Analysis of variance for yield stress of native and plasma-treated starch

Source	SS	df	Mean Square	F	Sig.
Treatments	21.990	12	1.833	83.296	.000
Error	.286	13	.022		
Total	22.276	25			

**Table C.56** Comparison of means for yield stress of native and plasma-treated starch by using Duncan's Multiple Range test (DMRT) at 95 % confidence interval

Treatment	Subset					
	1	2	3	4	5	6
He15kV-15min	.0000					
He15kV-10min	.1150					
He15kV-5min		.5500				
Ar15kV-15min			.9050			
Ar10kV-15min			1.2150	1.2150		
NTS				1.2600		
He10kV-5min				1.2850		
Ar10kV-10min				1.4050		
He10kV-15min				1.4550		
Ar10kV-5min				1.5350		
Ar15kV-10min					2.3500	
He10kV-10min						2.9200
Ar15kV-5min						3.1650

**Table C.57** Analysis of variance for consistency index of native and plasma-treated starch

Source	SS	df	Mean Square	F	Sig.
Treatment	228.988	12	19.082	141.435	.000
Error	1.754	13	.135		
Total	230.742	25			



**Table C.58** Comparison of means for consistency index of native and plasma-treated starch by using Duncan's Multiple Range test (DMRT) at 95% confidence interval

Treatment	Subset						
	1	2	3	4	5	6	7
He15kV-10min	.0550						
Ar15kV-15min	.4850	.4850					
He15kV-15min		.9660					
He15kV-5min			1.7600				
Ar10kV-15min				3.3850			
He10kV-15min				3.7850			
Ar10kV-10min					5.4250		
Ar15kV-10min					5.8250		
Ar10kV-5min					5.9950	5.9950	
He10kV-10min					6.0000	6.0000	
Ar15kV-5min						6.8200	
NTS							8.9100
He10kV-5min							9.4950

**Table C.59** Analysis of variance for the flow behavior index of native and plasma-treated starch

Source	SS	df	Mean Square	F	Sig.
Treatments	.825	12	.069	288.476	.000
Error	.003	13	.000		
Total	.829	25			

**Table C.60** Comparison of means for the flow behavior index of native and plasma-treated starch by using Duncan's Multiple Range test (DMRT) at 95% confidence interval

Treatment	Subset							
	1	2	3	4	5	6	7	8
He15kV-15min	.0082							
He10kV-5min		.5550						
Ar10kV-10min		.5600	.5600					
He10kV-10min		.5650	.5650	.5650				
NTS		.5700	.5700	.5700	.5700			
Ar10kV-5min		.5800	.5800	.5800	.5800	.5800		
Ar15kV-5min		.5800	.5800	.5800	.5800	.5800		
Ar10kV-15min			.5950	.5950	.5950	.5950		
He10kV-15min			.6000	.6000	.6000	.6000		
He15kV-5min				.6050	.6050	.6050		
Ar15kV-10min						.6100		
Ar15kV-15min							.6450	
He15kV-10min								.8650

**Table C.61** Analysis of variance for hysteresis area of native and plasma-treated starch

Source	SS	df	Mean Square	F	Sig.
Treatment	14577774.570	12	1214814.547	205.374	.000
Error	76896.632	13	5915.126		
Total	14654671.201	25			



**Table C.63** Two-way ANOVA analysis for L\* value of native and plasma-treated starch at 95% confidence interval

Source	SS	df	Mean Square	F	Sig.
Gas	136.267	1	136.267	1319.100	.000
Voltage	.179	1	.179	1.735	.200
Time	.707	2	.354	3.422	.049
Gas * Voltage	.073	1	.073	.706	.409
Voltage * Time	.034	2	.017	.165	.849
Gas * Time	.543	2	.272	2.628	.093
Gas * Voltage * Time	.446	2	.223	2.161	.137
Error	2.479	24	.103		
Total	140.729	35			

**Table C.64** Two-way ANOVA analysis for a\* value of native and plasma-treated starch at 95% confidence interval

Source	SS	df	Mean Square	F	Sig.
Gas	.077	1	.077	82.268	.000
Voltage	.016	1	.016	16.593	.000
Time	.003	2	.002	1.596	.224
Gas * Voltage	.000	1	.000	.003	.957
Voltage * Time	.026	2	.013	14.044	.000
Gas * Time	.014	2	.007	7.313	.003
Gas * Voltage * Time	.019	2	.009	10.003	.001
Error	.023	24	.001		
Total	.178	35			

**Table C.65** Two-way ANOVA analysis for b\* value of native and plasma-treated starch at 95% confidence interval

Source	SS	df	Mean Square	F	Sig.
Gas	8.703	1	8.703	401.037	.000
Voltage	.102	1	.102	4.719	.040
Time	.307	2	.154	7.082	.004
Gas * Voltage	.410	1	.410	18.876	.000
Voltage * Time	.252	2	.126	5.811	.009
Gas * Time	.229	2	.115	5.277	.013
Gas * Voltage * Time	.032	2	.016	.734	.491
Error	.521	24	.022		
Total	10.556	35			

**Table C.66** Two-way ANOVA analysis for whiteness index of native and plasma-treated starch at 95% confidence interval

Source	SS	df	Mean Square	F	Sig.
Gas	339.694	1	339.694	670.950	.000
Voltage	.852	1	.852	1.683	.207
Time	8.908	2	4.454	8.797	.001
Gas * Voltage	4.528	1	4.528	8.944	.006
Voltage * Time	4.464	2	2.232	4.409	.023
Gas * Time	9.594	2	4.797	9.475	.001
Gas * Voltage * Time	.516	2	.258	.509	.607
Error	12.151	24	.506		
Total	380.708	35			

**Table C.67** Two-way ANOVA analysis for pH value of plasma-treated starch at 95% confidence interval

Source	SS	df	Mean Square	F	Sig.
Gas	1.266	1	1.266	249.658	.000
Voltage	.026	1	.026	5.156	.032
Time	.469	2	.234	46.252	.000
Gas * Voltage	.222	1	.222	43.884	.000
Gas * Time	.757	2	.379	74.668	.000
Voltage * Time	.164	2	.082	16.202	.000
Gas * Voltage * Time	.141	2	.071	13.940	.000
Error	.122	24	.005		
Total	3.167	35			

**Table C.68** Two-way ANOVA analysis for relative crystallinity of plasma-treated starch at 95% confidence interval

Source	SS	df	Mean Square	F	Sig.
Gas	127.420	1	127.420	402.910	.000
Voltage	12.760	1	12.760	40.349	.000
Time	10.491	2	5.245	16.586	.000
Gas * Voltage	1.450	1	1.450	4.586	.053
Gas * Time	1.776	2	.888	2.808	.100
Voltage * Time	11.191	2	5.595	17.693	.000
Gas * Voltage * Time	5.186	2	2.593	8.199	.006
Error	3.795	12	.316		
Total	174.070	23			

**Table C.69** Two-way ANOVA analysis for moisture content of plasma-treated starch at 95% confidence interval

Source	SS	df	Mean Square	F	Sig.
Gas	22.259	1	22.259	141.049	.000
Voltage	1.252	1	1.252	7.932	.010
Time	.796	2	.398	2.522	.101
Gas * Voltage	.849	1	.849	5.377	.029
Voltage * Time	.013	2	.006	.040	.961
Gas * Time	.130	2	.065	.413	.666
Gas * Voltage * Time	.017	2	.008	.053	.948
Error	3.788	24	.158		
Total	29.103	35			

**Table C.70** Two-way ANOVA analysis for apparent amylose of plasma-treated starch at 95% confidence interval

Source	SS	df	Mean Square	F	Sig.
Gas	24.101	1	24.101	86.523	.000
Voltage	.127	1	.127	.455	.506
Time	18.743	2	9.372	33.643	.000
Gas * Voltage	.112	1	.112	.404	.531
Voltage * Time	7.049	2	3.524	12.653	.000
Gas * Time	35.082	2	17.541	62.971	.000
Gas * Voltage * Time	3.509	2	1.755	6.299	.006
Error	6.685	24	.279		
Total	95.409	35			

**Table C.71** Two-way ANOVA analysis for reducing sugar of plasma-treated starch at 95% confidence interval

Source	SS	df	Mean Square	F	Sig.
Gas	1946424.921	1	1946424.921	13309.967	.000
Voltage	1688769.557	1	1688769.557	11548.078	.000
Time	1551319.246	2	775659.623	5304.085	.000
Gas * Voltage	1491182.900	1	1491182.900	10196.949	.000
Gas * Time	944613.384	2	472306.692	3229.709	.000
Voltage * Time	767311.919	2	383655.960	2623.501	.000
Gas * Voltage * Time	714390.889	2	357195.444	2442.560	.000
Error	3509.716	24	146.238		
Total	9107522.532	35			

**Table C.72** Two-way ANOVA analysis for ratio between 1047 and 1022  $\text{cm}^{-1}$  of plasma-treated starch at 95% confidence interval

Source	SS	df	Mean Square	F	Sig.
Gas	.007	1	.007	7.342	.012
Voltage	.000	1	.000	.163	.690
Time	.001	2	.001	.662	.525
Gas * Voltage	.001	1	.001	.508	.483
Gas * Time	.002	2	.001	.816	.454
Voltage * Time	.000	2	.000	.090	.915
Gas * Voltage * Time	.001	2	.000	.267	.768
Error	.024	24	.001		
Total	.036	35			



**Table C.73** Two-way ANOVA analysis for pasting temperature of plasma-treated starch at 95% confidence interval

Source	SS	df	Mean Square	F	Sig.
Gas	3.151	1	3.151	20.128	.000
Voltage	.058	1	.058	.373	.547
Time	.157	2	.078	.501	.612
Gas * Voltage	.276	1	.276	1.761	.197
Gas * Time	.796	2	.398	2.543	.100
Voltage * Time	.348	2	.174	1.110	.346
Gas * Voltage * Time	.429	2	.214	1.370	.273
Error	3.757	24	.157		
Total	181705.138	36			
Corrected Total	8.971	35			

**Table C.74** Two-way ANOVA analysis for peak viscosity of plasma-treated starch at 95% confidence interval

Source	SS	df	Mean Square	F	Sig.
Gas	3596712.250	1	3596712.250	108.608	.000
Voltage	13367554.694	1	13367554.694	403.654	.000
Time	19047194.889	2	9523597.444	287.580	.000
Gas * Voltage	4512084.028	1	4512084.028	136.250	.000
Gas * Time	212066.667	2	106033.333	3.202	.059
Voltage * Time	167676.222	2	83838.111	2.532	.101
Gas * Voltage * Time	273921.556	2	136960.778	4.136	.029
Error	794792.000	24	33116.333		
Total	41972002.306	35			

**Table C.75** Two-way ANOVA analysis for breakdown percentage of plasma-treated starch at 95% confidence interval

Source	SS	df	Mean Square	F	Sig.
Gas	974.272	1	974.272	442.449	.000
Voltage	584.995	1	584.995	265.666	.000
Time	1580.888	2	790.444	358.967	.000
Gas * Voltage	543.512	1	543.512	246.827	.000
Gas * Time	24.449	2	12.224	5.551	.010
Voltage * Time	312.350	2	156.175	70.924	.000
Gas * Voltage * Time	162.661	2	81.330	36.935	.000
Error	52.848	24	2.202		
Total	4235.974	35			

**Table C.76** Two-way ANOVA analysis for setback percentage of plasma-treated starch at 95% confidence interval

Source	SS	df	Mean Square	F	Sig.
Gas	7246.266	1	7246.266	86.059	.000
Voltage	15490.706	1	15490.706	183.974	.000
Time	16145.005	2	8072.502	95.872	.000
Gas * Voltage	12239.366	1	12239.366	145.359	.000
Gas * Time	7737.420	2	3868.710	45.946	.000
Voltage * Time	11437.143	2	5718.571	67.916	.000
Gas * Voltage * Time	11259.025	2	5629.513	66.858	.000
Error	2020.818	24	84.201		
Total	83575.749	35			

**Table C.77** Two-way ANOVA analysis for swelling power at 60°C of plasma-treated starch at 95% confidence interval

Source	SS	df	Mean Square	F	Sig.
Gas	11.458	1	11.458	439.855	.000
Voltage	.012	1	.012	.479	.496
Time	.753	2	.376	14.449	.000
Gas * Voltage	.403	1	.403	15.479	.001
Voltage * Time	.042	2	.021	.799	.462
Gas * Time	.398	2	.199	7.643	.003
Gas * Voltage * Time	.049	2	.024	.934	.407
Error	.625	24	.026		
Total	13.740	35			

**Table C.78** Two-way ANOVA analysis for swelling power at 70°C of plasma-treated starch at 95% confidence interval

Source	SS	df	Mean Square	F	Sig.
Gas	24.867	1	24.867	314.637	.000
Voltage	5.123	1	5.123	64.817	.000
Time	7.116	2	3.558	45.020	.000
Gas * Voltage	5.108	1	5.108	64.626	.000
Voltage * Time	.027	2	.013	.169	.846
Gas * Time	4.132	2	2.066	26.143	.000
Gas * Voltage * Time	.289	2	.144	1.827	.183
Error	1.897	24	.079		
Total	1260.758	36			
Corrected Total	48.558	35			

**Table C.79** Two-way ANOVA analysis for swelling power at 80°C of plasma-treated starch at 95% confidence interval

Source	SS	df	Mean Square	F	Sig.
Gas	28.587	1	28.587	368.744	.000
Voltage	5.367	1	5.367	69.229	.000
Time	30.314	2	15.157	195.510	.000
Gas * Voltage	4.382	1	4.382	56.524	.000
Voltage * Time	.029	2	.015	.190	.828
Gas * Time	3.798	2	1.899	24.495	.000
Gas * Voltage * Time	.034	2	.017	.221	.803
Error	1.861	24	.078		
Total	74.372	35			

**Table C.80** Two-way ANOVA analysis for swelling power at 90°C of plasma-treated starch at 95% confidence interval

Source	SS	df	Mean Square	F	Sig.
Gas	134.986	1	134.986	225.958	.000
Voltage	5.752	1	5.752	9.629	.005
Time	31.747	2	15.873	26.571	.000
Gas * Voltage	5.768	1	5.768	9.655	.005
Voltage * Time	1.944	2	.972	1.627	.217
Gas * Time	.553	2	.277	.463	.635
Gas * Voltage * Time	.169	2	.085	.142	.869
Error	14.337	24	.597		
Total	2355.492	36			
Corrected Total	195.257	35			

**Table C.81** Two-way ANOVA analysis for solubility at 60°C of plasma-treated starch at 95% confidence interval

Source	SS	df	Mean Square	F	Sig.
Gas	1.546	1	1.546	86.055	.000
Voltage	.032	1	.032	1.804	.192
Time	4.140	2	2.070	115.219	.000
Gas * Voltage	.001	1	.001	.030	.863
Voltage * Time	.161	2	.080	4.473	.022
Gas * Time	.034	2	.017	.933	.407
Gas * Voltage * Time	.140	2	.070	3.888	.034
Error	.431	24	.018		
Total	6.483	35			

**Table C.82** Two-way ANOVA analysis for solubility at 70°C of plasma-treated starch at 95% confidence interval

Source	SS	df	Mean Square	F	Sig.
Gas	24.651	1	24.651	470.543	.000
Voltage	8.037	1	8.037	153.415	.000
Time	30.072	2	15.036	287.003	.000
Gas * Voltage	5.390	1	5.390	102.887	.000
Voltage * Time	1.506	2	.753	14.374	.000
Gas * Time	4.408	2	2.204	42.070	.000
Gas * Voltage * Time	3.280	2	1.640	31.300	.000
Error	1.257	24	.052		
Total	78.601	35			

**Table C.83** Two-way ANOVA analysis for solubility at 80°C of plasma-treated starch at 95% confidence interval

Source	SS	df	Mean Square	F	Sig.
Gas	202.635	1	202.635	1211.329	.000
Voltage	12.402	1	12.402	74.139	.000
Time	79.664	2	39.832	238.111	.000
Gas * Voltage	16.147	1	16.147	96.525	.000
Voltage * Time	.223	2	.112	.668	.522
Gas * Time	37.676	2	18.838	112.610	.000
Gas * Voltage * Time	3.465	2	1.733	10.357	.001
Error	4.015	24	.167		
Total	356.227	35			

**Table C.84** Two-way ANOVA analysis for solubility at 90°C of plasma-treated starch at 95% confidence interval

Source	SS	df	Mean Square	F	Sig.
Gas	1301.646	1	1301.646	866.892	.000
Voltage	11.189	1	11.189	7.452	.012
Time	72.164	2	36.082	24.030	.000
Gas * Voltage	9.151	1	9.151	6.094	.021
Voltage * Time	10.442	2	5.221	3.477	.047
Gas * Time	2.237	2	1.119	.745	.485
Gas * Voltage * Time	11.530	2	5.765	3.839	.036
Error	36.036	24	1.502		
Total	1454.395	35			

**Table C.85** Two-way ANOVA analysis for water-binding capacity of plasma-treated starch at 95% confidence interval

Source	SS	df	Mean Square	F	Sig.
Gas	.005	1	.005	3.607	.070
Voltage	.001	1	.001	.524	.476
Time	.000	2	.000	.039	.962
Gas * Voltage	.001	1	.001	.818	.375
Voltage * Time	.002	2	.001	.689	.512
Gas * Time	.004	2	.002	1.589	.225
Gas * Voltage * Time	.003	2	.002	1.143	.336
Error	.033	24	.001		
Total	.049	35			

**Table C.86** Two-way ANOVA analysis for yield stress of plasma-treated starch at 95% confidence interval

Source	SS	df	Mean Square	F	Sig.
Gas	3.010	1	3.010	126.311	.000
Voltage	1.242	1	1.242	52.118	.000
Time	3.194	2	1.597	67.003	.000
Gas * Voltage	8.785	1	8.785	368.585	.000
Voltage * Time	2.446	2	1.223	51.310	.000
Gas * Time	1.574	2	.787	33.021	.000
Gas * Voltage * Time	1.699	2	.849	35.639	.000
Error	.286	12	.024		
Total	22.236	23			

**Table C.87** Two-way ANOVA analysis for consistency index of plasma-treated starch at 95% confidence interval

Source	SS	df	Mean Square	F	Sig.
Gas	5.751	1	5.751	40.854	.000
Voltage	55.049	1	55.049	391.079	.000
Time	59.975	2	29.988	213.036	.000
Gas * Voltage	36.625	1	36.625	260.192	.000
Voltage * Time	.552	2	.276	1.961	.183
Gas * Time	9.348	2	4.674	33.205	.000
Gas * Voltage * Time	20.144	2	10.072	71.554	.000
Error	1.689	12	.141		
Total	189.134	23			

**Table C.88** Two-way ANOVA analysis for the flow behavior index of plasma-treated starch at 95% confidence interval.

Source	SS	df	Mean Square	F	Sig.
Gas	.023	1	.023	89.172	.000
Voltage	.003	1	.003	12.968	.004
Time	.144	2	.072	279.398	.000
Gas * Voltage	.019	1	.019	75.362	.000
Voltage * Time	.206	2	.103	398.533	.000
Gas * Time	.210	2	.105	407.095	.000
Gas * Voltage * Time	.219	2	.109	423.809	.000
Error	.003	12	.000		
Total	.829	23			



**Table C.89** Two-way ANOVA analysis for hysteresis area of plasma-treated starch at 95% confidence interval

Source	SS	df	Mean Square	F	Sig.
Gas	1293321.582	1	1293321.582	215.984	.000
Voltage	1647838.542	1	1647838.542	275.188	.000
Time	4018840.398	2	2009420.199	335.572	.000
Gas * Voltage	1609441.579	1	1609441.579	268.776	.000
Voltage * Time	250842.951	2	125421.475	20.945	.000
Gas * Time	1248527.754	2	624263.877	104.252	.000
Gas * Voltage * Time	115819.702	2	57909.851	9.671	.003
Error	71856.552	12	5988.046		
Total	10256489.060	23			



## VITA

**NAME** Natchanon Srangsomjit

**DATE OF BIRTH** 11 December 1995

**PLACE OF BIRTH** Phang nga

**INSTITUTIONS ATTENDED** Prince of Songkla Univeristy

**HOME ADDRESS** 25/2 Moo 1 Tombon Thungkangok Amphoe Muang Phang nga 82000

**PUBLICATION** Srangsomjit, N., Bovornratanaraks, T., and Anuntagool, J. (2021). Effect of voltage level and treatment time on properties of tapioca starch subjected to modification using nonthermal dielectric barrier discharge plasma. Proceedings of the 23rd Food Innovation Asia Conference 2021, June 17-18, 2021, BITEC, Bangkok, Thailand. pp. 187-194.

**AWARD RECEIVED**

1. First prize winner in the ASEAN Innovation Challenge June 2021(ProVeg International 2021) Winning Topic: The international plant-based food innovation concept contest
2. First prize winner of graduate student poster competition June 2021 in Food Innovation Asia Conference 2021.